PRODUCTION AND ENGINEERING OF THERAPEUTIC PROTEIN NANOPARTICLES

A Dissertation
Presented to
The Academic Faculty

by

Lina Herrera Estrada

In Partial Fulfillment
of the Requirements for the Degree
Doctor of Philosophy in the
School of Chemical & Biomolecular Engineering

Georgia Institute of Technology
December 2014

PRODUCTION AND ENGINEERING OF THERAPEUTIC PROTEIN NANOPARTICLES

Approved by:

Dr. Julie Champion, Advisor
School of Chemical & Biomolecular Engineering
Georgia Institute of Technology

Dr. Andreas Bommarius
School of Chemical & Biomolecular Engineering
Georgia Institute of Technology

Dr. Christine Payne
School of Chemistry and Biochemistry
Georgia Institute of Technology

Dr. Lakeisha Taite
School of Chemical & Biomolecular Engineering
Georgia Institute of Technology

Dr. Melissa Kemp
School of Biomedical Engineering
Georgia Institute of Technology

Date Approved: October, 31, 2014

ACKNOWLEDGMENTS

First and foremost, I would like to thank my husband, family and Heavenly Father for their unconditional love, years of encouragement and continuous support. Words are not enough to express my gratitude to them.

I also wish to thank my thesis advisor, Dr. Julie Champion for her constant support, patience, and guidance. Her enthusiasm and encouragement kept me motivated during the course of this research; the freedom and valuable insights she provided while I conducted this research, allowed me to grow scientifically. I also express gratitude to my committee members, Dr. Christine Payne, Dr. Andreas Bommarius, Dr. Lakeisha Taite and Dr. Melissa Kemp, for their patience, advice and feedback.

I also wish to thank the members of the Champion Lab, Won Min Park, Trudy Padmore, Anusha Garapaty, Kevin Ling, Tim Chang and Bradley Silverman, for their friendship and assistance that made the sweet and bitter moments more enjoyable. We shared many hours working in the lab, debating the state of the world and planning pranks.

Finally, I want to acknowledge my friends, who were always there for me and became my family during the past five years. Cami, Loice, Michael, Jose, Swetha, Aritra, Ambarish, Tanu, Juliana, Bessy, Gabriel, Christina, Kathy, Keith, Greg and many other friends, we have shared many birthdays together, movies, meals and trips. I hope we can share many more moments together.

TABLE OF CONTENTS

LIST OF FIGURES

LIST OF SYMBOLS AND ABBREVIATIONS

6xHis	Hexahistidine tag
AvrA	Avirulence factor A
AvrA-GST	AvrA and GST fusion protein
β-gal	β-galactosidase
BMP-2	Bone morphogenic protein-2
BSA	Bovine serum albumin
BS^3	Bis[sulfosuccinimidyl] suberate
c-Myc	c-Myc protooncogene transcription factor activated by MAPK
c-Myb	c-Myb protooncogene member of the myeloblastosis transcription factors
DTSSP	3,3'-Dithiobis(sulfosuccinimidylpropionate)
eGFP	Enhanced green fluorescent protein
eGFP+β-gal	eGFP and β-gal nanoparticles
eGFP+AvrA	eGFP and AvrA nanoparticles
ELP	Elastin polypeptide
ERK 1/2	Extracellular signal-regulated kinases 1/2
FBS	Fetal bovine serum
FDA	Food and drug administration
GFP	Green fluorescent protein
GST	Glutathione S-tranferase
GTA	Glutaraldehyde
HER-2	Human epidermal growth factor receptor-2, also known as ErbB2
IBD	Inflammatory bowel disease

ICAM-1	Intercellular adhesion molecule 1
IP6	Inositol hexakisphosphate
JNK	c-Jun N-terminal kinase
MAPK	Mitogen-activated protein kinases
MEK 1/2	Mitogen-activated protein kinase kinase 1/2
MKK4/7	Mitogen-activated protein kinase kinase 4/7
mRFP	Monomeric red fluorescent protein
mRFP+YopJ-HIS-TAT	mRFP and YopJ-HIS-TAT nanoparticles
NF-κB	Nuclear factor κB
p38	MAP kinase p38 protein
SAPK	Stress-activated protein kinases
sulfo-NHS	sulfo(N-hydroxysulfosuccinimide)
TAT	Transactivator of transcription peptide
TNFα	Tumor necrosis factor α
YopJ	Yersinia outer protein J
YopJ-GST	YopJ and GST fusion protein nanoparticles
YopJ-HIS-TAT	YopJ, GST and 6His-TAT-6His fusion protein
YopP	Yersinia outer protein P

SUMMARY

Proteins and enzymes are dynamic and versatile macromolecules that have the capacity to perform a complex set of functions while being highly specific. This grants them an advantage over small molecules and has led to a dramatic increase in their use for therapeutic purposes over the past couple of decades. Intracellular delivery of therapeutic proteins or enzymes has the potential to restore normal cellular function by substitution of deficient proteins or regulation of intracellular signaling pathways.

Bacterial pathogens have evolved mechanisms by which they can control the fate of host cells during infection. Some Gram-negative bacteria inject effector proteins directly into the cytoplasm of eukaryotic host cells. These effector proteins have high potential as therapeutic agents because they are capable of efficiently subverting a variety of eukaryotic signaling pathways by regulating protein factors involved in signal transduction. However, bacterial delivery of effector proteins for therapeutic purposes is not a viable option.

Effectors and other therapeutic proteins and enzymes require modification, encapsulation or immobilization to improve their stability and limited distribution. Hence, there is a critical need to develop delivery systems that will improve accessibility of enzymatic drugs to intracellular compartments. The production of protein-enzyme nanoparticles was investigated in this thesis with the goal of developing a protein carrier for active enzyme delivery.

In Chapter 4 of this thesis, β-galactosidase –a model enzyme– is incorporated into enhanced green fluorescent protein (eGFP) nanoparticles prepared via desolvation. Particle size is shown to be sensitive to type of cross-linker, cross-linking time, and the presence of imidazole. Enzymatic activity is shown to be highly retained after particle fabrication and high protein encapsulation yields are demonstrated. Protein-enzyme

nanoparticles are shown to effectively deliver the enzyme to multiple cell lines *in vitro*. More importantly, delivered enzymes are shown to retain their biological activity. This data demonstrates that protein nanoparticles are a biocompatible, high efficiency alternative for intracellular delivery of active enzyme therapeutics. Thus, the potential of protein nanoparticles for therapeutic protein and enzyme delivery is studied in two diseases models: inflammatory bowel disease (IBD) and breast cancer.

AvrA an acetyltransferase effector from *Salmonella*, suppresses acute inflammatory responses such as those observed in inflammatory bowel disease. Bacterial delivery of this effector is substituted in Chapter 5 with protein nanoparticles made directly from AvrA and a carrier protein, eGFP. eGFP+AvrA nanoparticle size is shown to be controlled by imidazole concentration during particle fabrication. These nanoparticles are shown to effectively deliver AvrA to model intestinal epithelial and immune cells. Furthermore, *in vivo* studies performed by an Emory collaborator reveal that eGFP+AvrA nanoparticles inhibit inflammatory signaling and confer cytoprotection *in vitro*, and in murine colitis models decrease clinical and histological indices of inflammation.

In Chapter 6, the use of YopJ –an effector from Yersinia pestis– is evaluated for the treatment of breast cancer. YopJ is known to down-regulate the MAPK and NF-κB pathways to induce apoptosis in specific cell types. In this chapter YopJ is produced in *E. coli* as a fusion protein with glutathione S-transferase (GST), forming self-assembled protein nanoparticles. YopJ-GST nanoparticles are shown to efficiently deliver proteins to breast cancer cells. These nanoparticles are also shown to induce dose and time-dependent death in SKBR-3 breast cancer cells, more effective than the same molar dose of doxorubicin. More importantly, the results of treatment with sub-lethal doses of nanoparticles exhibit decreased cell migration *in vitro* and down-regulated the MAPK ERK 1/2 pathway, which has been correlated to metastasis. Moreover, YopJ-GST nanoparticles are shown to induce cell death in a panel of breast cancer cell lines, but are not cytotoxic to healthy fibroblasts or cervical cancer cells. Consequently, YopJ-GST

nanoparticles demonstrate the potential of effector proteins as breast cancer therapeutics with selective cytotoxicity and the capacity to decrease metastatic predictive-behaviors.

Finally, in Chapter 7, conclusions are reported and protein particles are discussed as an interesting and potentially useful strategy for delivery of protein and enzyme therapeutics. Bacterial effector proteins are presented as novel therapeutic agents and future direction for research are also discussed.

CHAPTER 1: INTRODUCTION

In the past decades, the mechanisms and causes of many diseases have been elucidated. This knowledge made the design and discovery of new therapies possible. For years the pharmaceutical industry focused its efforts in the development of small molecule drugs that would target cell receptors, enzymes and proteins. With the development of protein chemistry and recombinant techniques the identification, isolation, purification and engineering of large proteins as drugs became possible. Protein-based drugs now represent an increasing share of the pharmaceutical sector and have become highly successful in the clinic, enjoying unprecedented recognition of their potential [1]. Currently, there are more than 130 biological drugs in the market, which include monoclonal antibodies, peptides, proteins and enzymes.

Enzyme therapeutics offer multiple advantages over small molecule drugs. Enzymes, like many other proteins, can bind to their targets with high affinity and act with high specificity [2]. Most importantly, an enzyme's catalytic activity allows it to rapidly convert multiple target molecules into products, which significantly amplifies its effect compared to small molecules and binding proteins [3, 4]. These unique properties make enzymes promising therapeutic agents, and an important and growing segment of pharmaceuticals.

Although most targets of FDA approved enzymatic drugs are extracellular, there are many diseases for which treatment requires intracellular delivery [5]. Intracellular enzyme therapy has the potential to restore normal cellular function by substitution of defective or deficient enzymes, regulation of intracellular signaling pathways and/or proteolysis. Effective enzyme replacement for treatment of genetic diseases such as Pompe and Krappe, two types of lysosomal storage diseases, requires intracellular delivery to lysosomal compartments [3, 6]. More therapeutic applications of intracellular

enzymes are expected to emerge, including inhibition or reversal of ubiquitination for cancer [7], phosphorylation of Tau protein for Alzheimer's disease [8] and regulation of specific intracellular pathways that contribute to disease pathogenesis. For example, in chronic inflammatory diseases, such as rheumatoid arthritis and systemic lupus erymathosus, alterations in the Ras family of small GTPases contribute to the observed dysfunctions [9]. Similarly, in multiple autoimmune diseases, reactivation of the Notch-signaling pathway is at the center of abnormal behavior [10]. In many types of cancer the Ras family of oncogenes, Notch, TGF-β, WNT, MAPK and NF-κB are common aberrant pathways [11-13]. Enzymes can effectively inhibit or modify many of these pathways [14-17] and thus, could be used as a new generation of intracellular therapeutics.

Bacterial pathogen evolution has produced a broad spectrum of enzymes that subvert and control normal cellular functions during infection [18]. These enzymes, known as effectors, actively regulate host cell cycle, inflammation, immune signaling, apoptosis, and the actin cytoskeleton by manipulating intracellular signaling pathways [19-22]. Some effectors interfere with phosphorylation cascades or ubiquitinylation processes [23], while others mimic the functions of protein kinases and phosphatases. These hijacking mechanisms have been proven to be highly efficient [20] and therefore, bacterial effectors have high potential as therapeutic enzymes.

The YopJ family of effectors is an example of enzymes of bacterial origin with therapeutic potential. These are homologue acetyltransferases capable of simultaneously down-regulating nuclear factor κB (NF-κB) and mitogen activated protein kinase (MAPK) pathways by preventing phosphorylation of key kinases. These pathways are critical for the development of diseases such as inflammatory bowel disease (IBD) and breast cancer. YopJ, from *Yersinia*, simultaneously blocks several MAPK cascades and NFκB signaling to induce apoptosis. Whereas AvrA, from *Salmonella,* modifies and inactivates only MAPK JNK and NF-κB pathways to reduce immune response and

inflammation, without inducing cell death [24]. These functions make YopJ and AvrA ideal therapeutic agents for breast cancer and IBD, respectively.

However, effectors and other potential therapeutic enzymes require modification, encapsulation or immobilization on biocompatible matrices to improve their stability and limited distribution [2, 3, 25]. Thus, there is a critical need to develop delivery systems that will improve accessibility of enzymatic drugs to intracellular compartments. There are many challenges associated with the delivery and retention of activity, given the large size of enzymes and their complex tertiary or quaternary structure that can be highly sensitive to the environment [3]. Delivery vehicle fabrication conditions must be gentle enough for activity retention and be small enough to penetrate tissues and be internalized by cells [26, 27]. In general, enzymes packaged in a delivery vehicle possess several advantages over soluble formulations, such as higher stability, lower immune response and targeting capabilities [25, 26, 28-32]. Most current delivery systems immobilize enzymes on the surface of another material or encapsulate them in polymeric, lipid or mesoporous materials [3, 5, 33-38]. Other methods involve fusion of an enzyme to other proteins or peptides [39]. However, some challenges remain, such as low encapsulation efficiencies, reduction in activity from fabrication conditions, or undesirable degradation products [40].

It is possible to address these delivery challenges and engineer a completely biodegradable enzyme delivery method by using protein particles. Protein particles offer multiple advantages over their polymeric, inorganic and liposomal counterparts. Some of the most striking advantages are their high loading capacity, ease of production, surrounding protein environment, and amino acid degradation products [41, 42]. Currently, most protein particles are studied for intracellular delivery of small molecule drugs [42-48] and little is known about the production or function of enzyme nanoparticles.

The present work shows a comprehensive picture of the use of bacterial effector proteins as therapeutic agents. It first focuses on recombinant production and solubilization of bacterial effectors that have potential as therapeutic agents for breast cancer and inflammatory bowel disease (Chapter 3). This is followed by production and detailed optimization of enzyme carrier particles and investigation of intracellular active enzyme delivery (Chapter 4). Finally, two candidate bacterial effectors, YopJ and AvrA are evaluated in breast cancer and inflammatory bowel disease models (Chapter 5-6). This thesis presents an innovative approach for the development of novel potent therapeutics using effector proteins and establishes an effective delivery method.

1-1 References

1. Dimitrov, D.S., *Therapeutic Proteins.* Methods Molec. Biol., 2012. **899**.

2. Holcenberg, J.S. and J. Roberts, *Enzymes as drugs.* Ann. Rev. Pharm., 1977. **17**: p. 97-116.

3. Holcenberg, J.S., *Enzyme therapy: problems and solutions.* Ann. Rev. Biochem., 1982. **51**: p. 795-812.

4. Vellard, M., *The enzyme as drug: application of enzymes as pharmaceuticals.* Curr. Opin. Biotech., 2003. **14**: p. 444-450.

5. Torchilin, V., *Intracellular delivery of protein and peptide therapeutics.* Drug Discov. Today: Technol., 2008. **5**(2-3): p. e95-e103.

6. Richard, E., G. Douillard-Guilloux, and C. Cailaud, *New insights into therapeutic options for Pompe diseases.* Life, 2011. **63**(11): p. 979-986.

7. Yang, Y. and e. al., *Inhibitors of ubiquitin-activating enzyme (E1), a new class of potential cancer therapeutics.* Am. Assoc. Cancer Res. , 2013. **67**: p. 9472-9481.

8. Cutler, N.R., *Review of the next generation of Alzheimer's disease therapeutics: challenges for drug development.* Prog. Neuro-Psychopharm. Biol. Psych., 2001. **25**(1): p. 27-57.

9. Reedquist, K.A. and P.P. Tak, *Signal transduction pathways in chronic inflammatory autoimmune disease: small GTPases.* Open Rheumatol. J., 2012. **6**: p. 259-272.

10. Ma, D., et al., *Targeting the Notch signaling pathway in autoimmune diseases.* Expert. Opin. Ther. Targets., 2010. **14**(5): p. 553-565.

11. Karin, M., *NF-κB as a Critical Link Between Inflammation and Cancer.* Cold Spring Harb. Perpect. Biol., 2009. **1**.

12. McCleary-Wheeler, A.L., R. McWilliams, and M.E. Fernandez-Zapico, *Aberrant signaling pathways in pancreatic cancer: a two compartment view.* Molec. Carcinogenesis, 2011. **51**(1): p. 25-39.

13. Dhillon, A.S., et al., *MAP kinase signalling pathways in cancer.* Oncogene, 2007. **26**: p. 3279-3290.

14. Sowa, M.E., et al., *Defining the human deubiquitinating enzyme interaction landscape.* Cell, 2009. **138**(2): p. 389-403.

15. Borodovsky, A., et al., *Chemistry-based functional proteomics reveals novel members of the deubiquitinating enzyme family.* Chem. Biol. , 2002. **9**: p. 1149-1159.

16. Ludlow, J.W., et al., *Specific enzymatic dephosphorylation of the retinoblastoma protein.* Molec. Cell Biol. , 1993. **13**(1): p. 367-372.

17. Winkler, S., D. Wilson, and D.L. Kaplan, *Controlling β-sheet assembly in genetically engineered silk by enzymatic phosphorylation/dephosphorylation.* Biochem., 2000. **39**(41): p. 12739-12746.

18. Grassme, H., V. Jendrossek, and E. Gulbins, *Molecular mechanisms of bacteria induced apoptosis.* Apoptosis, 2001. **6**: p. 441-445.

19. Mattoo, S., Y.M. Lee, and J.E. Dixon, *Interaction of bacterial effector proteins with host proteins.* Curr Opin Immunol, 2007. **19**: p. 392-401.

20. Shames, S.R., S.D. Auweter, and B.B. Finlay, *Co-evolution and exploitation of host cell signaling pathways by bacterial pathogens.* Int J Biochem Cell Biol, 2009. **41**: p. 380-389.

21. Yoshida, S. and C. Sasakawa, *Exploting host microtubule dynamics: a new aspect of bacterial invasion.* TRENDS Microb., 2003. **11**(3): p. 139-143.

22. Lubran, M.M., *Bacterial toxins.* Ann Clin Lab Sci, 1988. **18**(1): p. 58-71.

23. Bhavsar, A.P., J.A. Guttman, and B.B. Finlay, *Manipulation of host-cell pathways by bacterial pathogens.* Nature, 2007. **449**(827-834).

24. Collier-Hyams, L.S., et al., *Cutting Edge: Salmonella AvrA effector inhibits the key proinflammatory, anti-apoptotic NF-κB pathway.* The Journal of Immunology, 2002. **169**: p. 2846-2850.

25. Gu, Z., et al., *Tailoring nanocarriers for intracellular protein delivery.* Chem. Soc. Rev., 2011. **40**: p. 3638-3655.

26. Farokhzad, O.C. and R. Langer, *Impact of Nanotechnology on Drug Delivery.* ACS Nano, 2009. **3**(1): p. 16-20.

27. Win, K.Y. and S.S. Feng, *Effects of particle size and surface coating on cellular uptakeof polymeric nanoparticles for oral delivery of anticancer drugs.* Biomat., 2005. **26**: p. 2713-2722.

28. LaVan, D.A., T. McGuire, and R. Langer, *Small-scale systems for in vivo delivery.* Nat. Biotech., 2003. **21**(10): p. 1188-1191.

29. Shi, J., et al., *Nanotechnology in drug delivery and tissue engineering: from discovery to applications.* Nano Lett., 2010. **10**: p. 3223-3230.

30. Zhao, M., et al., *Redox-resopnsive nanocapsules for intracellular protein delivery.* Biomat., 2011. **32**: p. 5223-5230.

31. Koo, O.M., I. Rubinstein, and H. Onyuksel, *Role of nanotechnology in targeted drug delivery and imaging: a concise review.* Nanomed.: Nanotech. Biol. Med., 2005. **1**: p. 193-212.

32. Ganta, S., et al., *A review of stimuli-responsive nanocarriers for drug and gene delivery.* J. Control. Release, 2008. **126**: p. 187-204.

33. Slowing, I.I., et al., *Mesoporous silica nanoparticles for drug delivery and biosensing applications.* Adv. Funct. Mat., 2007. **17**: p. 1225-1236.

34. Chen, Y.P., et al., *A new strategy for intracellular delivery of enzyme using mesoporous silica nanoparticles: Superoxide Dismutase.* JACS, 2013. **135**: p. 1516-1523.

35. Simone, E.A., et al., *Effect of polymer amphiphilicity on loading of therapeutic enzyme into protective filamentous and spherical polymer nanocarriers.* Biomacromol., 2007. **8**(12): p. 3914-3921.

36. Boado, R.J., et al., *Genetic engineering of a lysosomal enzyme fusion protein for targeted delivery across the human blood-brain barrier.* Biotech. Bioeng., 2008. **99**(2): p. 475-484.

37. Karajanagi, S.S., et al., *Structure and function of enzyme adsorbed onto single-walled carbon nanotubes.* Langmuir, 2004. **20**: p. 11594-11599.

38. Biswas, A., et al., *Endoprotease-mediated intracellular protein delivery using nanocapsules.* ACS Nano, 2011. **5**(5): p. 1385-1394.

39. Cronican, J.J., et al., *Potent delivery of functional proteins into mammalian cells in vitro and in vivo using a supercharged protein.* ACS Chem. Biol. , 2010. **5**(8): p. 747-752.

40. Stolnik, S. and K. Shakesheff, *Formulations for delivery of therapeutic proteins.* Biotech. Lett., 2009. **31**: p. 1-11.

41. Rubino, O.P., R. Kowalsky, and J. Swarbrick, *Albumin microspheres as a drug delivery system: Relation among turbidity ratio, degree of cross-linking, and drug release.* Pharm Res, 1993. **10**(7): p. 1059-1065.

42. Hawkins, M.J., P. Soon-Shiong, and N. Desai, *Protein nanoparticles as drug carriers in clinical medicine.* Adv. Drug Deliv. Rev., 2008. **60**: p. 876-885.

43. Langer, K., et al., *Optimization of the preparation process for human serum albumin (HSA) nanoparticles.* Int. J. Pharm, 2003. **257**: p. 169-180.

44. Gunasekaran, S., K. Sanghoon, and L. Xiao, *Use of whey proteins for encapsulation and controlled delivery applications.* J. Food Eng. , 2007. **83**: p. 31-40.

45. Biman, B.M. and S.C. Kundu, *Self assembled silk sericin/poloxamer nanoparticles as nanocarriers of hydrophobic and hydrophilic drugs for targeted delivery.* Nanotech., 2009. **20**(35): p. 355101.

46. Ren, D., F. Kratz, and S.W. Wang, *Protein nanocapsules containing doxorubicin as a pH-responsive delivery system.* Small, 2011. **7**(8): p. 1051-1060.

47. Kratz, F., *Albumin as a drug carrier: Design of prodrugs, drug conjugates and nanoparticles* J. Control. Rel., 2008. **132**: p. 171-183.

48. Elzohghby, A.O., W.M. Samy, and N.A. Elgindy, *Albumin-based nanoparticles as potential controlled release drug delivery systems.* J. Control. Rel., 2012. **157**: p. 168-172.

CHAPTER 2: BACKGROUND

Many diseases are triggered and sustained by molecular alterations within the cell. Enzymes have the potential to restore normal cellular function by reversing molecular changes through activation or deregulation of intracellular pathways. As described in the previous chapter, bacterial pathogens produce a variety of enzymes that target multiple eukaryotic signaling pathways and could potentially be used for therapeutic purposes. In the following sections the molecular treatment of breast cancer and IBD, a discussion on bacterial effector proteins and intracellular enzyme delivery are presented. Eventhough these two diseases and the therapeutic goals associated to each of them are significantly different, dysregulated signaling pathways are common between them.

2-1 Molecular treatment of cancer

Cancer has been described as a disease in which alterations in the genetic material deregulate the circuits that govern normal cell proliferation and homeostasis, leading to uncontrolled proliferation, abnormal functions and alterations in cell morphology [1-3]. An accumulation of defects in DNA leads to transformation of the cell and cellular functions. In general, there are two main types of genes involved in this transformation: oncogenes and onco-suppressors. Oncogenes have been described as overexpressed or mutated genes that promote abnormal cell behavior. While onco-suppressor genes are a diverse set of genes whose normal function is to suppress oncogenic phenotype and whose inactivity is necessary for cancer development [4].

Together these damaged genes constitute the molecular basis for the exaggerated behaviors and pathway alterations observed in cancer. Some oncogenes or damaged onco-suppressor genes are translated into proteins that participate in key signaling pathways and thus, lead to mutated signaling molecules that in turn yield constitutive

activation, up-regulation or deregulation of entire signaling pathways [2]. These alterations in signaling allow cancer cells to acquire distinctive and complementary traits that enable tumor growth, metastatic propagation and drug resistance. These traits, now known as the hallmarks of cancer, include: sustaining proliferative signaling, evading growth suppressors, enabling replicative immortality, activating invasion and metastasis, resisting cell death, inducing angiogenesis, avoiding immune destruction, tumor promoting inflammation, genome instability and mutation, and deregulating cellular energetics[3].

The past three decades of research have yielded a better understanding of each of these traits and the mechanisms through which the malignant behavior is supported. In consequence, molecularly targeted therapies have emerged. These therapies were designed to interfere with a specific molecular target (typically a protein) associated with tumor growth and progression [5]. Various targeted therapies have been approved by the Food and Drug Administration (FDA) to treat specific types of cancer and many others are currently being studied. These therapies target growth factor receptors, signaling molecules, cell-cycle proteins, modulators of apoptosis and molecules involved in invasion and angiogenesis. To date, the more than 20 FDA-approved targeted therapies, which include monoclonal antibodies, fusion proteins and small molecules, have had substantial success in the market and their projected sales grow everyday [6].

The small molecule kinase inhibitor imatinib mesylate (Gleevec) is an example of this success. Imatinib established a paradigm for treatment of tumors whose growth is dependent on specific kinase targets. It has shown remarkable clinical success for the treatment of myeloid leukemia and gastrointestinal stromal tumors [7]. Similarly, monoclonal antibody drugs like trastuzumab (Herceptin) have been shown in the clinic to effectively block the ability of HER-2 positive breast cancer cells to grow [8].

In general, the main advantage of these molecular-targeted drugs lies in their highly specific action that, in principle, leads to relatively fewer off-target effects.

Currently, reported side effects of targeted therapeutics tend to be less severe than those of traditional chemotherapeutics [5]. Unfortunately, clinical responses to these drugs have been observed to be transitory and relapses are common. Experimental data suggests that this occurs because these drugs have been developed to target only one specific molecule, despite the fact that multiple signaling pathways control each hallmark capability. Therefore, the parallel nature of the signaling cascades allows cancer cells to recover and reestablish the hallmark trait through a pathway different than the one targeted by the drug [3]. Such considerations suggest that more effective therapeutics would require selective and simultaneous targeting of multiple pathways to prevent adaptive resistance.

2-1-1 Molecular targets for breast cancer therapy

Genetic alterations can affect one or multiple signaling pathways in tumor cells, but the precise identity of the pathways, level and type of alteration varies among cancer types. Several oncogenes, proteins and signaling pathways have been implicated in the development and progression of breast cancer. For example, the cell cycle progression regulator protein, Cyclin D1, and its binding partners have been found to affect cell migration, stem-like cell activity and breast cancer cell growth [9]. Half of triple-negative and inflammatory breast cancer cases overexpress EGFR [10] and 30% of all breast cancers cases overexpress HER-2 [8]. Vascular endothelial growth factor (VEGF) has been observed to be uniquely influenced by female sex steroid hormones to induce protumorigenic behavior [11]. Overexpression of cyclooxygenases (COX), c-Jun, c-Myc and matrix metalloproteinases was found to contribute to breast cancer development, cell proliferation and regulation of cell migration [12-15]. The nuclear factor–kappa B (NF-κB) and mitogen activated protein kinase (MAPK) transduction pathways are at the center of multiple cellular processes and are related to several of these proteins and oncogenes known to promote and sustain breast cancer [16, 17].

The NF-κB pathway controls expression of hundreds of human genes involved in key cellular processes such as innate immunity, inflammation, angiogenesis, proliferation and cell survival [18-20]. Mis-regulation of this signaling cascade, either by mutation or epigenetic mechanisms, has been observed in diseases associated with inflammation, immunodeficiency or cancer. NF-κB has been directly linked to cell cycle progression through cyclin D1, correlated to induction of growth promoter genes (such as c-Myc and c-Myb) and is considered a major apoptotic regulator [18, 19]. Aberrant sustained activation of NF-κB has been reported in multiple types of mammary tumors [19, 21] and has been considered a main target for breast cancer molecular therapy [22].

NF-κB is an attractive molecular target for multiple reasons. Its anti-apoptotic properties abrogate the effectiveness of many chemotherapeutic agents, which have been shown to activate the pathway [19]. Furthermore, it has been established that cancer cells up-regulate or constitutively activate NF-κB as a protective mechanism. This abnormal activation, commonly found in breast cancer, leads to extensive angiogenesis, metastasis and can even confer resistance to cancer therapies [20, 23, 24]. For these reasons, NF-κB plays a main role in cancer cell survival.

Although NF-κB is an attractive molecular target for treatment of breast cancer, inhibition of NF-κB alone can only induce limited cell death [17]. Therefore, it has been deemed necessary to inhibit additional pathways in order induce apoptosis, stop proliferation and block growth signaling [18, 23]. As previously mentioned, the MAPK signaling network has also been shown to be up-regulated in breast cancer cells and multiple oncogenes are known to be related to it [1, 25]. The MAPK signaling cascade is known to play a central role in cell growth, cycle, differentiation and proliferation; it also interferes in cell survival/death signaling and cross talks with NF-κB [26].

The mammalian MAPK pathway consists of extracellular signal regulated kinases (ERK), p38 and stress-activated protein kinases (SAPK or JNK). Each of these kinases exists in several isoforms, and controls multiple cell processes. The activated ERK

pathway up-regulates MMP expression and prevents cancer cells from anoikis, another form of programmed cell death, providing cell protection and invasion capabilities [26]. The phosphorylated JNK pathway has been implicated in promoting cellular transformation through the oncogenes *c-fos, c-Jun, Ras, Met* and *BCR-Abl [27]*. High levels of JNK and c-Jun have been documented in breast cancer tumor cells [28]. There is little understanding on the role of p38 in tumorigenesis, but evidence suggests p38 might be a tumor suppressor [11].

In summary, an effective molecularly targeted therapy for breast cancer requires inhibition of the NF-κB pathway to sensitize cells to apoptosis, but additional pathways must be targeted. The MAPK pathway is an ideal co-target and simultaneous inhibition of it could lead to induction of apoptosis, as well as prevention of metastasis and resistance.

2-2 Molecular therapy of IBD

Inflammatory bowel disease (IBD), which encompasses ulcerative colitis and Crohn's disease, represents a lifelong chronic and debilitating inflammatory disorder of the intestinal tract. Though the precise pathogenesis of IBD remains to be elucidated, the prevailing theory supports an abnormal immune response to the complex commensal flora in the gut [29]. However, environmental factors, altered commensal intestinal bacteria and genetic susceptibility combined with disease-precipitating events have not been completely excluded [30].

Evidence suggests that dysregulated immune responses strongly contribute to the progression of the disease. Activation of innate cells in the intestinal mucosa leads to overproduction of chemokines and proinflammatory cytokines that in turn activate further immune response [31]. This results in uncontrolled inflammation and intestinal tissue damage [32]. Downregulation of immune response and hence, decrease in production of proinflammatory cytokines has been shown to ameliorate IBD [33, 34]. Current nonsurgical IBD treatments involve immune or inflammatory suppression with local 5-

aminosalicylate preparations, systemic corticosteroids or cytotoxic immunosuppressants, like azathioprine. However, only 50 % of patients achieve sustained remission [31], and these approaches are fraught with the complications of systemic immunosuppression and other toxicities[35, 36].

Recently, therapies that target immune and inflammatory pathways have emerged as new treatments for IBD. These include vaccines, monoclonal antibodies (mAbs) and nanobodies against cytokines and cell trafficking, as well as small molecule agents that inhibit signaling pathways related to cytokine production and activity [37]. To date, several molecules have been studied and evaluated as molecular targets for IBD treatment.

Since IBD is characterized by an imbalance in pro-inflammatory and inhibitory cytokines, with pro-inflammatory cytokines dominating, these have become the main target for therapy. Tumor necrosis factor α (TNF-α) is an important proinflammatory cytokine that has been correlated to the development of IBD. This cytokine is known to modulate immune cell proliferation, regulation of adhesion molecules and induction of apoptosis [31]. In addition, high levels of TNF-α have been found in intestinal tissue during active IBD and thus, it has become a prevalent target for IBD therapeutics. For over a decade, anti-TNF-α mAbs have been shown to be effective in counteracting cell mediated inflammatory damage [38]. Given their success, MAPK p38 and transcription blocking agents are also being studied for inhibition of TNF-α production. Interleukin-10 (IL-10) and IL-11 are inhibitory cytokines whose deficiency is correlated to IBD. Delivery of these cytokines through different methods has been evaluated and shown to be beneficial for IBD patients [31].

Other molecular targets are IL-17, interferon gamma (IFN-γ), IL-6 and IL-12/23p40, which are inflammatory products of activated T cells and can direct development of inflammatory T cells that participate in the development and progression of IBD [39]. Furthermore, intercellular adhesion molecule-1 (ICAM-1), chemokine

receptor 9, α4β1 and α4β7 integrins have been studied and evaluated as targets for inhibition of lymphocyte trafficking. Unfortunately, while these strategies are based on biologic observations, in clinical applications patients are genetically diverse which leads to varied results.

Despite these significant advances in therapeutic strategies, the need for effective therapeutics remains unmet. Since many of the receptors, chemokines and cytokines correlated to IBD are connected to the NF-κB and MAPK pathways, these have become interesting and more generalized targets for new molecular therapeutics. These two pathways are central to recruitment of immune cells in IBD and contribute to the pathology of the disease [40]. For this reason, simultaneous down-regulation of these pathways could lead to reduction of inflammation and immune response during IBD.

2-3 Bacterial Effector Proteins

Bacterial pathogens have evolved mechanisms to subvert and control normal cellular functions during infection. These pathogens produce a broad spectrum of proteins and enzymes capable of interfering with key signaling pathways, inhibiting protein synthesis, forming pores on cell membranes or activating the death machinery of host cells [41]. A single bacterial protein can attack multiple signaling pathways at several points, ensuring an override in important cellular functions [42]. These proteins, known as bacterial effectors, are secreted through diverse systems that have been classified in six distinct categories (types I-VI) [43].

Many pathogenic bacteria have acquired sophisticated strategies to breach the cell membrane and deliver these effectors. Some Gram-negative bacterial pathogens such *Escherichia coli, Salmonella, Yersinia, Vibrio* and *Shigella*, use the type III secretion system (T3SS) to inject multiple effector proteins directly into the cytoplasm of host cells [44]. The T3SS is a needle-like organelle that spans both bacterial membranes and creates a pore in the membrane of host cells, through which semi-unfolded bacterial protein

effectors are translocated [45, 46]. In the bacteria, effector proteins are often silenced by keeping the protein in an unfolded state that is accomplished by association with a chaperone or lack of an activator substrate [47, 48]. In general, effectors remain in a quiescent state until they are translocated to the cytoplasm of the host [49].

Once in the cytoplasm of the host cell, effectors bind to their activator substrate or separate from the chaperone that accompanied them, becoming active and able to alter the signaling circuitry [50]. Many protein effectors manipulate host cell processes by attenuating signaling mediated by post-translational modification of proteins [48]. Some effectors have been observed to interfere with phosphorylation cascades by mimicking the function of kinases and phosphatases [51]. Other effectors are known to interfere by ribosylating target molecules, preventing transfer of ubiquitin, or degrading signaling molecules [45, 48]. In order to accomplish complete subversion of host cells, bacterial pathogens inject an array of effectors that exert different actions. Together these effectors contribute to efficient immune system evasion and proliferation of the bacteria [45].

Several bacterial protein effectors are known to specifically target the NF-κB and MAPK pathways that are central to the development and progression of breast cancer and IBD. One such effector is the acetyltransferase *Yersinia* outer protein J (YopJ), one of the six virulence factors used by *Yersinia pestis* the causal agent of plague. Two other *Yersinia* species, *Yersinia pseudotuberculosis* and *Yersinia enterocolitica* that are known to cause gastrointestinal disorders, produce a homologue effector protein called YopP [47, 52-54]. YopJ and YopP have been shown to inhibit innate immune response and selectively induce apoptosis by disrupting activation of ERK, JNK and p38 MAPK cascades, while simultaneously blocking the NF-κB pathway (Figure 2.1) [42, 45, 47, 53, 55, 56].

Studies on the mechanism of action used by YopJ have revealed that the protein downregulates MAPK signaling by acetylating serine and threonine residues of all MAP kinase kinases (MKKs) and thus, prevents phosphorylation required for activation of

these pathways [45, 50, 53]. Similarly, YopJ has been shown to inhibit the NF-κB pathway by acetylation of the serine and threonine residues on the activation loop of IKKβ, which prevents activation of the IKK complex and phosphorylation of IκB [52]. In addition, recent evidence suggests that YopJ may also have de-ubiquitinating activity, acting on TRAF6, TRAF2 and IκBα; and the capacity to hydrolyze the SUMO1 ubiquitin-like protein [41, 43]. Furthermore, YopJ is likely capable of directly activating some, not yet identified, caspases to induce host cell death [41].

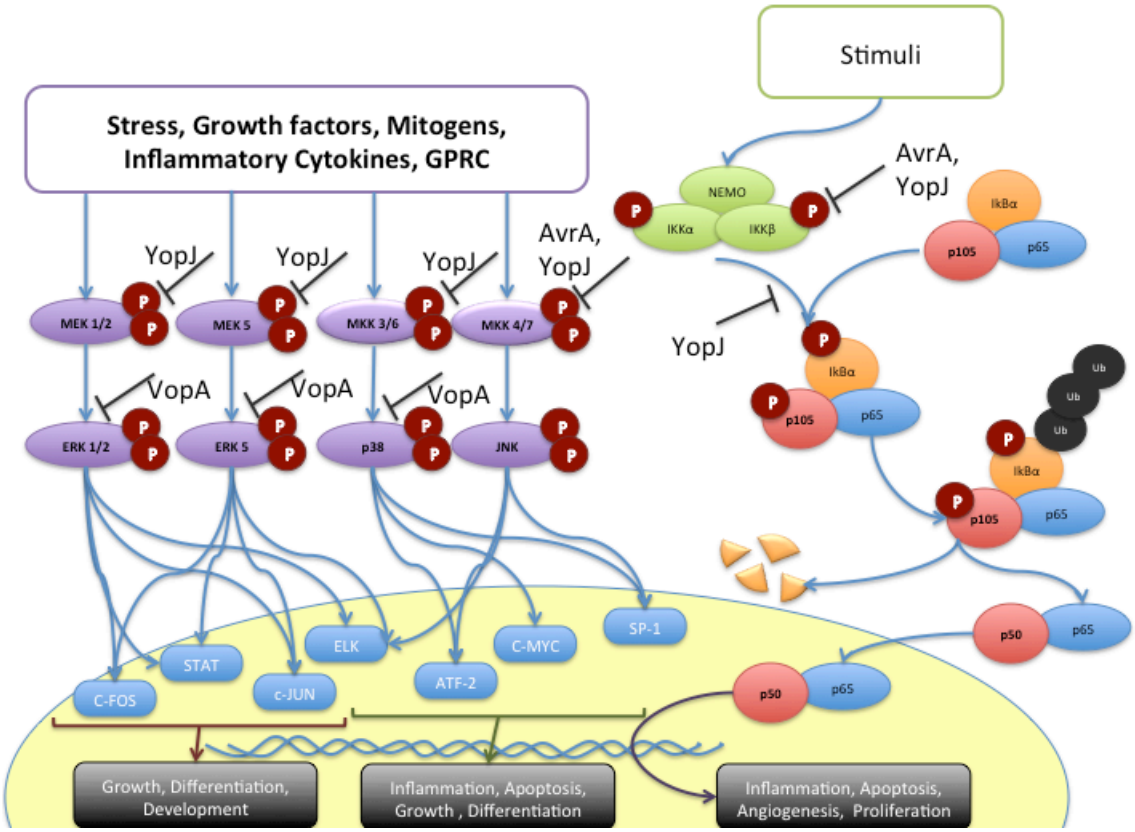

Figure 2.1. Inactivation of MAPK and NF-κB signaling pathways by bacterial protein effectors: YopJ, AvrA and VopA. Effectors acetylate the serine and/or threonine residues of the kinase loops of MAPK signaling molecules preventing their phosphorylation. The specific mechanism of action of these effectors on the NF-κB pathway remains to be elucidated.

It is predicted that YopJ uses a two-substrate, ping-pong mechanism to acetylate serine, lysine or threonine residues [47]. In this mechanism YopJ transfers the acetyl group from acetyl-CoA to the residue, forming an intermediate from which water is then removed to render the final product [48]. Further studies performed on YopJ/P structure and mechanism of action have identified the catalytic triad responsible for MAPK and NF-κB inhibition to be the histidine, cysteine and glutamate or aspartate residues located at positions 109, 172 and 128, respectively [54]. Mutations of the histidine or cysteine residues have been found to yield a version of YopJ (mYopJ) incapable of inhibiting MAPK and NF-κB activation [47, 54, 56]. Similarly, the acetyltransferase activity of YopJ depends on the availability of inositol hexakisphosphatase (IP_6), which acts as an allosteric activator of enzymatic activity [50].

Interestingly, YopJ has been found to induce death in some types of cells and not in others. For instance, neutrophils and endothelial cells have been found to be resistant to YopJ mediated apoptosis, whereas macrophages and dendritic cells are not [41, 57, 58]. This indicates that the outcome of intervention with this effector is cell type dependent. It is plausible that pathogen-mediated delay or decreased apoptosis in certain cell types is the result of a relative required resolution of infection to facilitate *Yersinia* pathogenesis [58].

Orthologs of YopJ are found in other enteric pathogens such as *Vibrio parahemaly* (VopA) [59] and *Aeromonas salmonicida* (AopP) [60]. Another member of this family is avirulence factor A (AvrA), an effector from *Salmonella typhimurium* [45]. AvrA has been shown to have potent and diverse effects on a wide variety of eukaryotic growth, survival and immune pathways [61]. Evidence has demonstrated that AvrA, when overexpressed in transfected cells[62] or in a *Drosophila* transgenic model[63], blocks activation of NF- κB, MAPK JNK, and transcriptional activation of a range of inflammatory effector genes. AvrA has been shown to acetylate MAPKK MKK4/7, accounting for the blockade of JNK activation [64]. This effector has also been shown to

inhibit NF- κB nuclear translocation, but the exact mechanisms remains to be elucidated [65]. Remarkably, AvrA-mediated signaling disruption in MAPK and NF-κB occurs without induction of the apoptotic cell death [66].

Other examples of effectors that target the MAPK and NF-κB pathways are OspF and OspG (Figure 2.1). OspF is a *Shigella* effector protein that actively suppresses activation of MAPK, and indirectly blocks NF-κB activity. This effector directly dephosphorylates MKKs at the threonine residue and simultaneously removes a water molecule, leading to a modified threonine residue that cannot be re-phosphorylated [45, 48]. OspG, also a *Shigella* effector, shares sequence similarity to mammalian serine/threonine protein kinases. This atypical kinase binds to ubiquitin, which activates its kinase activity and leads to attenuation of host innate NF-κB signaling [67].

In summary, bacterial effector proteins can hijack intracellular signaling of eukaryotic cells. The activity of these effectors is under tight regulation and has been proven to manipulate host processes efficiently and effectively. Thus, effector proteins are potent enzymes that could be used to induce cell death in breast cancer cell and reduce inflammatory signals in IBD.

2-4 Delivery of Therapeutic Proteins

In the past few decades, the potential of protein-based therapeutics has been recognized. Many protein drugs have been approved and successfully used in the clinic, and significantly more are under investigation. Their research, production and market have grown significantly in the past years and are expected to continue growing [68].

The shift towards biological drugs is the result of their specific recognition of targets and better mimicking of the complex cellular processes and functions [68, 69]. However, protein drugs pose multiple challenges due to their complexity and fragility, in terms of production, storage and administration. Therapeutic proteins are required to have

high chemical and conformational purity, good stability and a shelf-life of 18-24 months for economic viability [69].

The main challenges involved in the successful application of proteins as therapeutic agents are related to their administration, due to relatively low stability and short *in vivo* half-life. Multiple studies have been conducted on improving protein half-life and preventing early denaturation. Protein engineering has produced multiple options to increase stability. Some examples are chemical changes such as PEGylation or glycosylation, genetic engineering-rational design in which some residues are changed to increase activity or stability, and the creation of fusion proteins to improve the properties of the protein [68, 70, 71].

However, these strategies are not enough for effective intracellular-targeted protein drug delivery. At a cellular level, the delivery of macromolecules *in vivo* is hindered by their three-dimensional structure, size and hydrophobicity, as well as degradation due to the presence of enzymes and proteases [72, 73]. These factors cause proteins to be fragile and highly vulnerable and hence, their delivery in a carrier is an ideal option. Drug delivery vehicles not only offer protection for the protein but also show several other advantages, such as controlled release, improved biodistribution and targeting capabilities. The current methods and developments for peptide and protein delivery include the use of liposomes, polymer particles and protein capsules [72-76].

Although there are multiple protein drug formulations on the market for cancer and IBD therapy, there are no examples of therapeutic protein delivery in nanoparticles. Nonetheless, there are multiple examples of small molecule drug delivery in nanoparticle formulations. Common chemotherapeutic agents such as doxorubicin and daunorubicin have been encapsulated in liposomal vehicles, which are now commercially available under the names of Caelyx®/Doxil® and DaunoXome®. However, few formulations of protein drugs in liposomal carriers have been proposed and analyzed for cancer and IBD therapy. One attempt to use liposomes to deliver pro-apoptotic membrane proteins to

human colorectal carcinoma cells was successfully carried out *in vitro* [77]. Other examples of therapeutic protein delivery have recently become available. For instance, perfluorocarbon nanoparticles have been studied for the delivery of the Nemo binding domain peptide for controlling NF-κB signaling in cancer and inflammation [75]. Hydrophobically modified glycol chitosan has been used to deliver RGD peptides with anti-angiogenic properties to solid tumor models [72]. Schluep et al. conjugated a thyol derivate of tubulysin, a powerful antiproliferative and apoptosis inducer peptide, to a β-cyclodextrin based polymer and produced nanoparticles [78]. These drug carriers were effective in transporting their cargo inside target cells and showed equal or greater efficacy to that of conventional small drugs, but with reduced off-target toxicity.

Despite the success demonstrated by some of the developed protein and peptide carriers, significant limitations remain [72]. Future protein and peptide delivery vehicles should have: (1) safety and biocompatibility of the carrier, (2) high encapsulation efficiency, (3) high retention of protein bioactivity, (4) simple and reproducible production, (5) easy administration options, (6) economic feasibility, (7) controlled release profiles, (8) long circulation times and (9) biodegradability. Protein nanoparticles are a feasible alternative that can offer many of these requirements. Particles derived from proteins are biodegradable, metabolizable, and due to the primary structure of these macromolecules, offer multiple possibilities for the conjugation of drugs, imaging agents or peptides [79, 80]. To date, two main groups of protein nanoparticles are being studied and developed, self-assembled structures and desolvated particles. Self-assembled structures, are naturally occurring, functional macromolecular assemblies that can be manipulated for biomedical applications [81]. An example is the dodecahedral protein cage formed by the dihydrolipolyl acyltransferase (E2) subunit from pyruvate dehydrogenase which has been engineered to encapsulate doxorubicin [81]. Other examples of self-assembled delivery vehicles are elastin polypeptide (ELP) particles that have been developed to encapsulate small molecules, peptides, cytokines and proteins for

extracellular delivery. *In vivo* delivery of keratinocyte growth factor was accomplished by fusing the growth factor to ELPs and inducing thermoresponsive self-assembly into ~240 nm particles[82]. Other thermoresponsive ELP particles have been used to physically encapsulate and deliver bioactive bone morphogenetic proteins [83] The main advantage of this type of protein nanoparticles is simplicity of production and reproducibility of their properties.

Desolvated protein particles are produced by adding a desolvent to a protein solution while stirring. This method produces wider particle size distributions than self-assembly but offers the possibility of tuning particle size and properties [84]. In addition, particles produced by this method require stabilization through covalent cross-linking of the proteins [79]. Multiple studies have been conducted on the production and optimization of protein nanoparticles made of human serum albumin (HSA), bovine serum albumin (BSA) and gelatin [79, 84-86]. Particle size has been found to depend on the amount of desolvation agent used, initial protein solution concentration, pH and temperature [87].

Most protein particles are studied for intracellular delivery of small molecule drugs [81, 85, 86, 88-91] though a few protein drugs have been investigated [92, 93]. An example of a commercially available product based on protein particles for small molecule drug delivery is the 130 nm albumin bound-paclitaxel (Abraxane®), approved by the FDA in January 2005 for the treatment of metastatic breast cancer. Some proteins and enzymes have also been encapsulated in albumin microspheres [94, 95] or crystallized and cross-linked aggregates [96, 97] but the large size of these particles hinders efficient delivery and intracellular uptake. BSA particles have also been used to encapsulate and deliver BMP-2, but particles were stabilized with a polymeric coating and did not require cellular internalization [81, 98]. Recently, particles made directly with glucose oxidase have been shown to be more efficient as biosensors than immobilized enzyme on the surface of gold nanoparticles [99]. This suggests that proteins in protein

particles can retain activity, but more studies on the production of protein particles for delivery of active enzymes are required.

2-5 References

1. Tsatsanis, C.A. and D.A. Spandidos, *Signal Transduction pathways in cancer cells; novel targets for therapeutic intervention.* Gene Therapy and Molecular Biology, 2000. **5**: p. 111-120.

2. Hanahan, D. and R.A. Weinberg, *The hallmarks of cancer.* Cell, 2000. **100**: p. 57-70.

3. Hanahan, D. and R.A. Weinberg, *Hallmarks of cancer: The next generation.* Cell, 2011. **144**: p. 646-674.

4. Spandidos, D. and J.A. Lang, *The role of oncogenes and onco-suppresor genes in carcinogenesis.* Chinese J. Cancer Res., 1989. **1**(2): p. 70-74.

5. Widakowich, C., et al., *Review: Side effects of approved molecular therapies in solid cancers* The Oncologist, 2007. **12**(12): p. 1443-1455.

6. Aggarwal, S., *Targeted cancer therapies.* Nat. Rev. Drug Discov., 2010. **9**: p. 427-428.

7. Sawyers, C., *Targeted cancer therapy.* Nature, 2004. **432**: p. 294-297.

8. Mitri, Z., T. Constantine, and R. O'Regan, *The HER2 receptor in breast cancer: pathophysiology, clinical use, and new advances in therapy.* Chemother. Res. Parct., 2012. **2012**: p. 1-7.

9. Lamb, R., et al., *Cell cycle regulators cyclin D1 and CDK4/6 have estrogen receptor-dependent divergent functions in breast cancer migration and stem cell-like activity.* Cell Cycle, 2013. **12**(15): p. 2384-2394.

10. Masuda, H., et al., *Role of epidermal growth factor receptor in breast cancer.* Breast Cancer Res. Treat., 2012. **136**(2): p. 331-345.

11. Carpini, J.D., A.K. Karam, and L. Montgomery, *Vascular endothelial growth factor and its relationship to the prognosis and treatment of breast, ovarian, and cervical cancer.* Angiogenesis, 2010. **13**(1): p. 43-58.

12. Howe, L.R., *Inflammation and breast cancer. Cyclooxygenase/prostaglandin signaling and breast cancer.* Breast Cancer Res., 2007. **9**(4): p. 210-231.

13. Jiao, X., et al., *c-Jun induces mammary epithelial cellular invasion and breast cancer stem cell expansion.* J. Biol. Chem., 2010. **285**: p. 8218-8226.

14. Bartsch, J.E., E.D. Staren, and H.E. Appert, *Matrix metalloproteinase expression in breast cancer.* J. Surg. Res., 2003. **110**(2): p. 383-392.

15. Liao, D.J. and R.B. Dickson, *c-Myc in breast cancer.* Endocrine-related Cancer, 2000. **7**: p. 143-164.

16. Hoesel, B. and J.A. Schmid, *The complexity of NF-κB signaling in inflammation and cancer.* Molec. Cancer, 2013. **12**(86).

17. Giltnane, J.M. and J.M. Balko, *Rationale for targeting the Ras/MAPK pathway in triple-negative breast cancer.* Discovery Med., 2014. **17**(95): p. 275-283.

18. Karin, M., *Nuclear factor-κB in Cancer development and progression.* Nature 2006. **441**: p. 431-436.

19. Amit, S. and Y. Ben-Neriah, *NF-κB activation in cancer: a challenge for ubiquitination- and proteasome- based therapeutic approach.* Seminars in Cancer Biology, 2003. **13**: p. 15-28.

20. Courtois, G. and T.D. Gilmore, *Mutations in the NF-κB signaling pathway: implications for human disease.* Oncogene, 2006. **25**: p. 6831-6843.

21. Nakshatri, H., et al., *Constitutive activation of NF-κB during progression of breast cancer to hormone-independent growth.* Molecular and Cellular Biology, 1997: p. 3629-3639.

22. Mann, D.A. and F. Oakley, *NF-κB: a signal for cancer.* Journal of Hepatology, 2005. **42**: p. 610-611.

23. Baldwin, A.S., *Control of oncogenesis and cancer therapy resistance by the transcription factor NF-κB.* The Journal of Clinical Investigation, 2001. **107**(3): p. 241-246.

24. Gilmore, T.D., et al., *Rel/NF-κB/IκB signal transduction in the generation and treatment of human cancer.* Cancer Letters, 2002. **181**: p. 1-9.

25. Kohno, M. and J. Pouyssegur, *Targeting the ERK signalig pathway in cancer therapy.* Annals of Medicine, 2006. **38**: p. 200-211.

26. Kim, E.K., *Pathological roles of MAPK signaling pathways in human diseases.* Biochimica et Biophysica Acta, 2010. **1802**: p. 396-405.

27. Whitmarsh, A.J. and R.J. Davis, *Role of mitogen-activated protein kinase kinase 4 in cancer.* Oncogene, 2007. **26**: p. 3172-3184.

28. Brosseau, C.M., G. Pirianov, and K.W. Colston, *Involvement of stress activated protein kinases (JNK and p38) in 1,25 dihydroxyvitamin D3-induced breast cell death.* Steroids, 2010. **75**: p. 1082-1088.

29. McGuckin, M.A., et al., *Intestinal Barrier Dysfunction in Inflammatory Bowel Diseases.* Inflammatory Bowel Diseases, 2009. **15**(1): p. 100-113.

30. Ghosh, S. and R. Panaccione, *Anti-adhesion molecule therapy for inflammatory bowel disease.* Ther. Adv. Gastroenterology. **3**(4): p. 239-258.

31. Bai, A. and Z. Peng, *Biological therapies of inflammatory bowel disease.* Immunotherapy, 2010. **2**(5): p. 727-742.

32. Mahida, Y.R., *The key role of macrophages in the immunopathogenesis of inflammatory bowel disease* Inflamm. Bowel Dis. , 2000. **6**(1): p. 21-33.

33. Andou, A., et al., *Dietary histidine ameliorates murine colitis by inhibition of proinflammatory cytokine production from macrophages.* Gastroenterology, 2009. **136**(2): p. 564-574.

34. Kamada, N., et al., *Unique CD14 intestinal macrophages contribute to the pathogenesis of Crohn disease via IL-23/IFN-gamma axis.* J. Clin. Invest. , 2008. **118**(6): p. 2269-2280.

35. Burger, D. and S. Travis, *Conventional medical management of inflammatory bowel disease.* Gastroenterology, 2011. **140**(6): p. 1827-1837 e2.

36. Plevy, S.E. and S.R. Targan, *Future therapeutic approaches for inflammatory bowel diseases.* Gastroenterology, 2011. **140**(6): p. 1838-46.

37. Malik, T. and P. Mannon, *Inflammatory bowel diseases: emerging therapies and promising molecular targets.* Frontiers Bioscience, 2012. **S4**: p. 1172-1189.

38. Sands, B.E., *Inflammatory bowel disease: past, present, and future.* J. Gastroenterol., 2007. **42**(1): p. 16-25.

39. Peyrin-Biroulet, L., et al., *Crohn's disease: beyond antagonists of tumor necrosis factor.* The Lancet, 2008. **372**: p. 67-81.

40. Xavier, R.J. and D.K. Podolsky, *Unravelling the pathogenesis of inflammatory bowel disease.* Nature, 2007. **448**: p. 427-434.

41. Grassme, H., V. Jendrossek, and E. Gulbins, *Molecular mechanisms of bacteria induced apoptosis.* Apoptosis, 2001. **6**: p. 441-445.

42. Bhavsar, A.P., J.A. Guttman, and B.B. Finlay, *Manipulation of host-cell pathways by bacterial pathogens.* Nature, 2007. **449**(827-834).

43. Mattoo, S., Y.M. Lee, and J.E. Dixon, *Interaction of bacterial effector proteins with host proteins.* Curr Opin Immunol, 2007. **19**: p. 392-401.

44. Raymond, B., et al., *Subversion of trafficking, apoptosis, and innate immunity by type III secretion system effectors.* Trends Microbiol., 2013. **21**(8): p. 430-441.

45. Shames, S.R., S.D. Auweter, and B.B. Finlay, *Co-evolution and exploitation of host cell signaling pathways by bacterial pathogens.* Int J Biochem Cell Biol, 2009. **41**: p. 380-389.

46. Tosi, T., et al., *Structural basis of eukaryotic cell targeting by type III secretion system (T3SS) effectors.* Res. Microbiol., 2013. **164**(6): p. 605-619.

47. Hao, Y., et al., *Structural Requirements for Yersinia YopJ inhibition of MAP kinase pathways.* Plos One, 2008(1): p. 1-9.

48. Broberg, C.A. and K. Orth, *Tipping the balance by manipulating post-translational modifications.* Current Opinion in Microbiology, 2010. **13**(34-40).

49. Viswanathan, V.K., R. Sharma, and G. Hecht, *Microbes and their products - physiologial effects upon mammalian mucosa.* Advanced Drug Delivery Reviews, 2004. **56**: p. 727-762.

50. Mittal, R., et al., *The acetyltransferase activity of the bacterial toxin YopJ of Yersinia is activated by eukaryotic host cell inositol hexakisphophate.* J Biol Chem, 2010. **285**(26): p. 19927-19934.

51. Wei, P., et al., *Bacterial virulence proteins as tools to rewire kinase pathways in yeast and immune cells.* Nature, 2012. **488**(7411): p. 384-388.

52. Mittal, R., S.Y. Peak-Chew, and H.T. McMahon, *Acetylation of MEK2 and IκB kinase (IKK) ctivation loop residues by YopJ inhibits signaling.* Proc Natl Acad Sci, 2006. **103**(49): p. 18574-18579.

53. Mukherjee, S., et al., *Yersinia YopJ acetylates and inhibits kinase activation by blocking phosphorylation.* Science, 2006. **312**: p. 1211-1214.

54. Orth, K., et al., *Disruption of Signaling by Yersinia effector YopJ, a ubiquitin-like protease.* Science, 2000. **290**: p. 1594-1597.

55. Schesser, K., et al., *The YopJ locus is required for Yersinia-mediated inhibition of NF-κB activation and cytokine expression: YopJ contains a eukaryotic SH2-like domain that is essential for its repressive activity.* Molecular Microbiology, 1998. **28**(6): p. 1067-1079.

56. Orth, K., et al., *Inhibition of the Mitogen-Activated Protein Kinase Kinase Superfamily by a Yersinia Effector.* Science, 1999. **285**(5435): p. 1920-1923.

57. Palmer, L.E., et al., *YopJ of Yersinia pseudotuberculosis is required for the inhibition of macrophage TNF-alpha production and downregulation of the MAP kinases p38 and JNK.* Molecular Microbiology, 1998. **27**(5): p. 953-965.

58. Spinner, J.L., et al., *Neutrophils are resistant to Yersinia YopJ/P-induced apoptosis and are protected from ROS-mediated cell death by the type III secretion system.* Plos One, 2010. **5**(2): p. 1-9.

59. Trosky, J.E., et al., *VopA inhibits ATP binding by acetylating the catalytic loop of MAPK Kinases.* J. Biol. Chem., 2007. **282**(47): p. 34299-34305.

60. Jones, R.M., L. Luo, and K.H. Moberg, *Aeromonas salmonicida secreted protein AopP is a potent inducer of apoptosis in a mammalian and a Drosophila model.* Cell Microbiol., 2012. **14**(2): p. 274-285.

61. Hao, Y.H., et al., *Structural requirements for Yersinia YopJ inhibition of MAP kinase pathways.* PLoS One, 2008. **3**(1): p. e1375.

62. Collier-Hyams, L.S., et al., *Cutting edge: Salmonella AvrA effector inhibits the key proinflammatory, anti-apoptotic NF-kappa B pathway.* J Immunol, 2002. **169**(6): p. 2846-50.

63. Jones, R.M., et al., *Salmonella AvrA Coordinates Suppression of Host Immune and Apoptotic Defenses via JNK Pathway Blockade.* Cell Host Microbe, 2008. **3**(4): p. 233-44.

64. Du, F. and J.E. Galan, *Selective inhibition of type III secretion activated signaling by the Salmonella effector AvrA.* PLoS Pathog, 2009. **5**(9): p. e1000595.

65. Collier-Hyams, L.S., et al., *Cutting Edge: Salmonella AvrA effector inhibits the key proinflammatory, anti-apoptotic NF-κB pathway.* The Journal of Immunology, 2002. **169**: p. 2846-2850.

66. Wu, H., R.M. Jones, and A.S. Neish, *The Salmonella effector AvrA mediates bacterial intracellular survival during infection in vivo.* Cell Microbiol., 2012. **14**(1): p. 28-39.

67. Zhou, Y., et al., *The Shigella type three secretion system effector OspG directly and specifically binds to hot ubiquitin for activation.* Plos One, 2013. **8**(2): p. e57558.

68. Szlachcic, A., M. Zakrzewska, and J. Otleski, *Longer action mand better drug: Tuning up protein therapeutics.* . Biotechnology Advances, 2011. **29**: p. 436-441.

69. Randolph, T.W. and J.F. Carpenter, *Enginering challenges of protein formulation.* AIChE Journal, 2007. **53**(8): p. 1902-1907.

70. De Groot, A.S. and D.W. Scott, *Immunogenicity of protein therapeutics.* TRENDS in Immunology, 2007. **28**(11): p. 482-490.

71. Marshall, S.A., et al., *Rational design and engineering of therapeutic proteins.* Drug Discovery Today, 2003. **8**(5): p. 212-221.

72. Tan, M.L., P.F.M. Choong, and C.R. Dass, *Recent developments in liposomes, microparticles and nanoparticles for protein and pptide drug delivery.* Peptides, 2010. **31**(184-193).

73. Peppas, N.A. and D.A. Carr, *Impact of absorption and transport on intelligent therapeutics and nanoscaly delivery of protein therapeutic agents.* Chemical Engineering Science, 2009. **64**: p. 4553-4565.

74. Lee, S.H., Z. Zhang, and S.S. Feng, *Nanoparticles of poly(lactide)-tocopheryl polyethylene glycol succinate (PLA-TPGS) copolymers for protein drug delivery.* Biomaterials, 2007. **28**: p. 2041-2050.

75. Pan, H., et al., *Post-formulation peptide drug loading of nanostructures for metered control of NF-κB signaling.* Biomaterials, 2011. **32**: p. 231-238.

76. Han, Y., et al., *Biocompatible protein nanocontainers for controlled drug release.* ACS Nano, 2010. **4**(5): p. 2838-2844.

77. Liguori, L., et al., *Liposomes-mediated delivery of pro-apoptotic therapeutic membrane proteins.* Journal of Controlled Release, 2008. **126**: p. 21-27.

78. Schluep, T., et al., *Polymeric tubulysin-peptide nanoparticles wit potent antitumor activity.* Clinical Cancer Research, 2009. **15**: p. 181-189.

79. Weber, C., et al., *Desolvation process and surface characterization of protein nanoparticles.* Int. J. Pharm., 2000. **194**: p. 91-102.

80. Mehravar, R., M. Jahanshahi, and N. Saghatoleslami, *Production of biological nanoparticles from lactalbumin for drug delivery and food science application.* Afr. J. Biotech., 2009. **8**(24): p. 6822-6827.

81. Ren, D., F. Kratz, and S.W. Wang, *Protein nanocapsules containing doxorubicin as a pH-responsive delivery system.* Small, 2011. **7**(8): p. 1051-1060.

82. Koria, P., et al., *Self-assembling elastin-like peptides growth factor chimeric nanoparticles for the treatment of chronic wounds.* Proc. Natl. Acad. Sci., 2011. **108**(3): p. 1034-1039.

83. Bessa, P.C., et al., *Thermoresponsive self-assembled elastin-based nanoparticles for delivery of BMPs.* J. Control. Rel., 2010. **142**(3): p. 312-318.

84. Langer, K., et al., *Human serum albumin (HSA) nanoparticles: Reproducibility of preparation process and kinetics of enzymatic degradation.* Int. J. Pharm., 2008. **347**: p. 109-117.

85. Langer, K., et al., *Optimization of the preparation process for human serum albumin (HSA) nanoparticles.* Int. J. Pharm, 2003. **257**: p. 169-180.

86. Hawkins, M.J., P. Soon-Shiong, and N. Desai, *Protein nanoparticles as drug carriers in clinical medicine.* Adv. Drug Deliv. Rev., 2008. **60**: p. 876-885.

87. Jahanshahi, M., et al., *Controlled fabrication of gelatin nanoparticles as drug carriers.* Conference Proceedings: Nanotechnology and Its Applications. First Sharjah International Conference, 2007: p. 228-232.

88. Gunasekaran, S., K. Sanghoon, and L. Xiao, *Use of whey proteins for encapsulation and controlled delivery applications.* J. Food Eng. , 2007. **83**: p. 31-40.

89. Biman, B.M. and S.C. Kundu, *Self assembled silk sericin/poloxamer nanoparticles as nanocarriers of hydrophobic and hydrophilic drugs for targeted delivery.* Nanotech., 2009. **20**(35): p. 355101.

90. Kratz, F., *Albumin as a drug carrier: Design of prodrugs, drug conjugates and nanoparticles* J. Control. Rel., 2008. **132**: p. 171-183.

91. Elzohghby, A.O., W.M. Samy, and N.A. Elgindy, *Albumin-based nanoparticles as potential controlled release drug delivery systems.* J. Control. Rel., 2012. **157**: p. 168-172.

92. Wang, G., et al., *Preparation of BMP-2 containing bovine serum albumin (BSA) nanoparticles stabilized by polymer coating.* Pharm. Res., 2008. **25**(12): p. 2896-2909.

93. Won, Y.W. and Y.H. Kim, *Recombinant human gelatin nanoparticles as a protein drug carrier.* J. Control. Rel., 2008. **127**: p. 154-161.

94. Ovadia, H., A.M. Carbone, and P.Y. Paterson, *Albumin magnetic micrsopheres: a novel carrier for Myelin basic protein.* J. Immunol. Methods, 1982. **53**(1): p. 109-122.

95. Sinha, V.R. and A. Trehan, *Biodegradable microspheres for protein delivery.* J. Control. Rel., 2003. **90**(3): p. 261-280.

96. Pechenov, S., et al., *Injectable controlled release formulations incorporating protein crystals.* J. Control. Rel., 2004. **96**: p. 149-158.

97. Roy, J.J. and T.E. Abraham, *Strategies in making cross-linked enzyme crystals.* Chem. Rev., 2004. **104**(9): p. 3705-3721.

98. Wang, G.L., et al., *Preparation of BMP-2 Containing Bovine Serum (BSA) Nanoparticles Stabilized by Polymer Coating.* Pharma. Res. , 2008. **25**: p. 2896-2909.

99. Sharma, S., et al., *Amperometric Biosensor: Increased Sensitivity Using Enzyme Nanoparticles* in *Int. Conf. Nanotech. Biosens.* 2011, IACSIT Press: Singapore p. 24-27.

CHAPTER 3: PRODUCTION OF PROTEIN EFFECTORS

During the course of their interaction with host cells, bacterial pathogens inject a wide variety of bacterial protein effectors that modulate eukaryotic signaling cascades [1]. These effectors regulate or mimic host proteins involved in signaling transduction [2]. Some effectors, like YopJ and AvrA, attenuate signaling mediated by post-translation modifications. YopJ and AvrA, are known to acetylate the serine/threonine residues that need to be phosphorylated for the MAPK and NF-κB pathways to be activated [3]. Interestingly, while inside the pathogen these effectors remain quiescent due to a lack of substrate or coactivator, or through binding to a bacterial chaperone [1]. YopJ and AvrA have been found to bind to IP_6 a cofactor present in eukaryotic cells that is necessary for full acetyltransferase activity [4].

Though the effect, secretion and mechanism of action of these effectors in the native pathogen and eukaryotic cells have been extensively studied, bacterial delivery of effectors for therapeutic purposes is not an option. In this Chapter recombinant techniques are used to produce the candidate effectors and create protein nanoparticles for their delivery. Recombinant production of YopJ and AvrA is not trivial and requires fusion to GST. Protein expression and purification are optimized and finally, recombinant effector proteins are characterized.

3-1 Experimental Methods

3-1-1 Cloning

YopJ, mYopJ, AvrA and mAvrA genes were a kind gift of Dr. Andrew Neish. These genes were amplified by PCR using the following primers:

YopJ and mYopJ:

5’-TCATGAATTCCCATGATCGGACCAATATCACAAATAA ATATCTCCG-3’ and 5’-GCTGAATATAAAACACTTCTCAAAGTACATCACCATC ACCATCACTAAGGGTCGACTCAGGA-3’

AvrA and mAvrA:

5’-TCATGAATTCCCATGATATTTTCGGTGCAGGAGCTATCA TG-3’ and 5’-ATGA GTCGACTTAATGATGATGATGATGATGCGGTTTAAGTAAAGACTTA TATTCAGCTATCCT-3’

Amplified genes were inserted into the bacterial expression plasmid pGEX-4T-2 (GE Lifesciences) between HindIII and SacI sites for YopJ and between SalI and EcoRI sites for AvrA. Since pGEX-4T-2 does not encode a 6xHis tag, the reverse primer was designed to introduce it. All constructs were confirmed by DNA sequencing and final sequences are presented below. eGFP and mRFP genes did not require cloning, as they were already in a bacterial expression plasmid. Both genes were in a pPROTet plasmid (Clontech Labs) and were a kind gift of Dr. Andreas Bommarius.

3-1-2 Protein expression and purification

Expression of YopJ-GST, mYopJ-GST, AvrA-GST, mAvrA-GST and eGFP was performed in BL21 *Escherichia Coli*. Bacterial cultures were grown to O.D. 0.7 at 37°C and GST fusions were induced with 0.4 mM isopropyl β-D-thiogalactoside (IPTG) at 25°C for 4 hours, while eGFP was not induced and grown at 37°C. AvrA-GST, mAvrA-GST and eGFP proteins were purified on Ni-NTA agarose (Qiagen) following manufacturer’s native purification protocols in imidazole-containing buffers. YopJ-GST

and mYopJ-GST protein were also purified on Ni-NTA agarose following the manufacturer's denaturing purification protocol. Purified proteins were buffer exchanged using 10K MWCO centrifugal ultrafiltration devices (Millipore) into PBS buffer (10 mM NaH_2PO_4, 137 mM NaCl, 2.7 mM KCl, 2 mM KH_2PO_4; pH 7.4) or 2X PBS + 5% dextrose (20 mM NaH_2PO_4, 274 mM NaCl, 5.4 mM KCl, 4 mM KH_2PO_4; pH 7.4) when necessary.

3-2 Recombinant production on YopJ and AvrA

Recombinant production of YopJ and AvrA in *E. coli* required fusion to GST. The AvrA and YopJ genes were initially cloned into pET101/D-TOPO® and pQE80 plasmids, but recombination occurred and the effectors were not expressed. The observed gene instability, bacterial cell death during expression and difficulties during the cloning procedures are indicative of protein toxicity. This was somewhat surprising because YopJ and AvrA have been shown to acetylate the Ser/Thr loop of eukaryotic kinases and *E. coli* does not have eukaryotic-like protein kinase genes [5, 6]. However, phosphoproteomic studies revealed that *E. coli* has substrates for Ser/Thr phosphorylation[7]. Thus, it is likely that interference of YopJ and AvrA with phosphorylation processes could have caused the observed toxicity.

To overcome this challenge YopJ and AvrA were cloned as fusions to GST, a common tag used to decrease protein toxicity and increase protein solubility, in a PGEX-4T-2 plasmid (GE Lifesciences). The resulting YopJ and AvrA fusion proteins were expressed as described in section 1-1-2. To determine whether YopJ-GST and AvrA-GST fusions were expressed, total cell extract and nickel purified protein were analyzed using SDS-PAGE and western blot (Figure 3.1). The expected ~60-kDa bands were present and detected by both anti-GST and anti-6xHis tag antibodies.

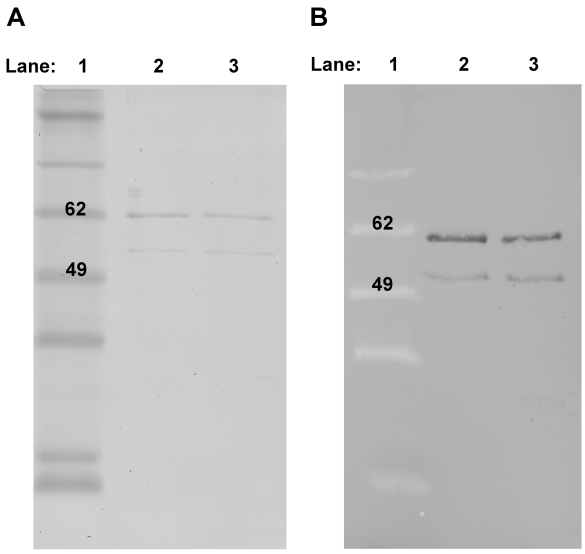

Figure 3.1. Purity of Ni-NTA purified recombinant fusion proteins. *(A)* Representative SDS-PAGE gel for YopJ-GST and mYopJ-GST. Lane 1 is protein standard, lane 2 YopJ-GST and lane 3 mYopJ-GST. *(B)* Representative western blot showing anti-5xHis antibody recognition of the bands observed in the gel, indicating they are (m)YopJ-GST. Two bands are observed, one at the expected molecular weight (60 KDa) and the second one at lower molecular weight. The second band is the result of protein degradation from the GST terminus, leaving a protein containing the entire (m)YopJ sequence and part of the GST sequence.

3-3 Solubility and stability of AvrA-GST and YopJ-GST proteins

Produced and purified YopJ-GST and AvrA-GST proteins formed large protein aggregates when dialyzed or diafiltrated into saline buffers. Since particle production via the desolvation method requires the use of soluble protein, multiple studies were performed on protein solubility and stabilization methods.

3-3-1 AvrA-GST

AvrA-GST proteins were initially purified using denaturing methods and severe protein aggregation was observed when proteins were transferred to non-denaturing saline buffers or water. In order to prevent aggregation of the protein, several purification and dialysis techniques were tested. Purification of AvrA-GST under native conditions,

in Ni-NTA or glutathione sepharose resins, yielded soluble protein and no visible aggregation when buffers were exchanged in diafiltration devices or dialysis. However, AvrA-GST was found to have a maximum solubility of ~1 mg/ml. Concentrations above 1 mg/ml led to protein aggregation and precipitation, as measured by DLS. Increases in salt concentrations and addition of detergents and dextrose did not appear to significantly affect the solubility of the protein, measured by optical density.

3-3-2 YopJ-GST

Native purification of YopJ-GST yielded < 1 mg pure protein per liter of bacterial expression, but this protein aggregated irreversibly during storage, dialysis or diafiltration. Denaturing purifications yielded ~4 mg of pure protein per liter of bacterial expression. Nonetheless, YopJ-GST proteins were not soluble in urea buffers. Analysis of elutions in native electrophoresis gels and western blots revealed the presence aggregates, visible as long smears of protein (Figure 3.2).

With the purpose of solubilizing YopJ-GST, the purified protein was dialyzed into water and lyophilized. Several buffers, acids, bases and organic solvents, listed in Table 1, were tested for protein resolubilization.YopJ-GST lyophilized proteins were found to form stable 100 nm diameter protein-aggregate nanoparticle suspensions in 2X PBS +5% dextrose and DMSO. Small 100 nm protein-aggregate nanoparticles and large micron-sized aggregates were the result of re-suspension in acetonitrile, 1% Tween-80, chloroform and saline solutions at pH values between 3 and 10. YopJ-GST lyophilized proteins did not dissolve or re-suspend in toluene, ethyl acetate, acetone, ethanol or glycerol.

Since protein folding and conformation can be affected by the environment, YopJ bioactivity in 100 nm protein-aggregate nanoparticles in DMSO and 2X PBS + 5 % dextrose was tested by studying the effect of these nanoparticles on cancer cell viability. Particles suspended in DMSO were not cytotoxic to SKBR-3 cells, while particles in 2X

PBS + 5% dextrose were highly cytotoxic (Chapter 6) to the same cells. Thus, all further studies were performed with YopJ-GST nanoparticles in 2X PBS + 5% dextrose buffers.

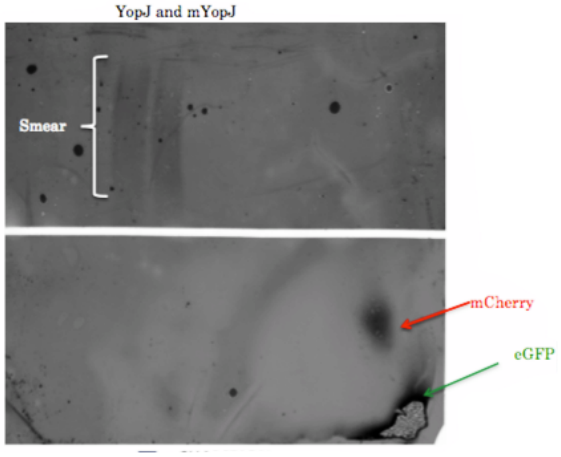

Figure 3.2. Western Blot of a native protein electrophoresis gel. YopJ and mYopJ are observed in the upper section in which smears of these proteins are visible. Smears indicate the presence of proteins of different sizes or aggregates of proteins. We used as controls mCherry and eGFP which are proteins with high solubilities, these can be observed in the lower section in which spots of protein are visible.

Next, direct dialysis and diafiltration into 2X PBS + 5% dextrose buffer was studied. Dialysis of denatured YopJ-GST nanoparticles into the buffer led to particle aggregation but diafiltration yielded a uniform suspension of the particles. Since these observations suggest that particle aggregation occurs during slow buffer exchange the rate of exchange via diafiltration was optimized. For this purpose, equal amounts of YopJ-GST in 8M urea were diafiltrated at two different rates. A slow rate, in which the buffer was changed in eight steps and a rapid one in which the buffer was exchanged in three steps. This difference was accomplished by varying the volume of added 2X PBS + 5% dextrose at each step relative to the initial volume of protein solution; rapid diafiltration was performed at a ratio of 5:1 and slow diafiltration at a ratio of 2:1. Interestingly, slower diafiltrations yielded higher final average concentrations of total

protein (0.360 mg/ml) and less particle aggregation than fast diafiltrations. More importantly, faster diafiltration processes lead particles that exhibit 60-75% higher cytotoxicity in SKBR-3 cancer cells.

3-4 GST removal

In order to evaluate the effect of GST on YopJ-GST nanoparticle stability and its effect on the biochemical function of YopJ, GST was cleaved from the fusion using thrombin. pGEX-4T-2 vectors encode the recognition sequence for site-specific cleavage by thrombin between the GST domain and the multiple cloning site, thus allowing cleavage of YopJ from GST. For this purpose, bacterial lysates for YopJ-GST and mYopJ-GST expressions were purified in Ni-NTA resins under denaturing conditions but purified proteins were not eluted. Instead the purified proteins were washed several times with PBS and then incubated for 16 hours with thrombin, as indicated by the manufacturer's instructions. GST and thrombin were removed by washing the resin several times with PBS and then YopJ proteins were eluted either in native or denaturing buffers.

Western blot analysis of these elutions demonstrated that GST was cleaved from the majority of the YopJ proteins (Figure 3.3). Nonetheless, YopJ proteins did not remain soluble in either native or denaturing buffers and large aggregates were visible in the elutions after 12 hours of storage. Analysis of the supernatants indicated that YopJ had precipitated into large fiber-like aggregates that were attached to the tube wall. These results highlight the importance of GST for YopJ-GST nanoparticle stability and particle size.

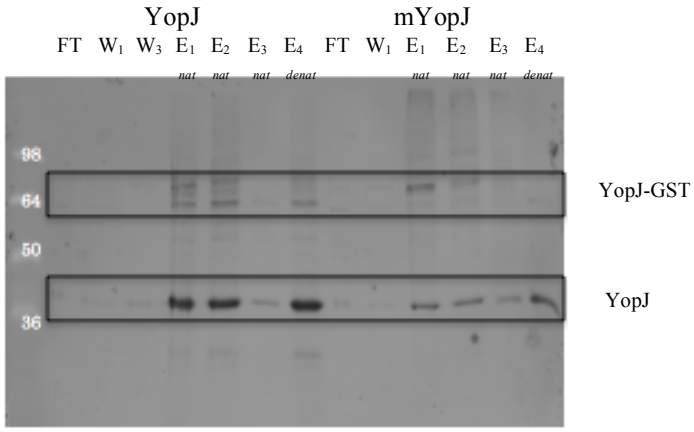

Figure 3.3. Results of digest reaction for YopJ and mYopJ with thrombin. Western Blot image of purified and cleaved YopJ using penta-HIS antibody. Notice in the western blot image that most of the protein has been cleaved but small amounts remain as full length fusion protein. Native (*nat*) and denaturing (*denat)* elutions were performed.

3-5 Summary

The results presented in this chapter illustrate the feasibility of recombinant production of bacterial effector protein, and highlights the need for GST fusion in protein production and YopJ-GST nanoparticle stability. Chapters 4 and 5 will describe the application of bacterial effector proteins and particle production methods for delivery of YopJ and AvrA in two different disease models.

3-6 References

1. Broberg, C.A. and K. Orth, *Tipping the balance by manipulating post-translational modifications.* Current Opinion in Microbiology, 2010. **13**(34-40).

2. Shames, S.R., S.D. Auweter, and B.B. Finlay, *Co-evolution and exploitation of host cell signaling pathways by bacterial pathogens.* Int J Biochem Cell Biol, 2009. **41**: p. 380-389.

3. Palmer, L.E., et al., *YopJ of Yersinia pseudotuberculosis is required for the inhibition of macrophage TNF-alpha production and downregulation of the MAP kinases p38 and JNK.* Molecular Microbiology, 1998. **27**(5): p. 953-965.

4. Mittal, R., et al., *The acetyltransferase activity of the bacterial toxin YopJ of Yersinia is activated by eukaryotic host cell inositol hexakisphophate.* J Biol Chem, 2010. **285**(26): p. 19927-19934.

5. Zorina, A., et al., *Eukaryotic-like Ser/Thr protein kinases SpkC/F/K are involved in phosphorylation of GroES in the Cyanobacterium Synechocystis.* DNA Res, 2011. **18**: p. 137-151.

6. Mukherjee, S., et al., *Yersinia YopJ acetylates and inhibits kinase activation by blocking phosphorylation.* Science, 2006. **312**: p. 1211-1214.

7. Macek, B., et al., *Phosphoproteome analysis of E. coli reveals evolutionary conservation of bacterial Ser/Thr/tyr phosphorylation.* Mol. Cell. Proteom., 2008. **7**(2): p. 299-307.

CHAPTER 4: PRODUCTION OF PROTEIN NANOPARTICLES AS ENZYME CARRIERS[a]

Enzyme therapeutics offer multiple advantages over small molecule drugs, but require modification, encapsulation or immobilization on biocompatible matrices to improve their stability and limited distribution, promote activity retention and decrease immunogenicity [1-3]. The desolvation method, which has been extensively characterized for particle production with serum albumin and gelatin [4-8], is modified and studied for the production of enzyme nanoparticles. β-galactosidase (β-gal), a hydrolase homo-tetramer, is used as a model enzyme. Hydrolysis of ortho-nitrophenyl-D-galactopyranoside (ONPG) is used to quantify β-gal enzymatic activity and pure enzyme nanoparticles are shown to retain only 25% of enzymatic activity. Therefore, bovine serum albumin (BSA) and enhanced green fluorescent protein (eGFP) are studied as enzyme carriers.

Effective internalization of nanoparticles depends on particle size, shape and surface charge. Nanoparticle size control is studied with the pure carrier proteins by varying the cross-linker type, cross-linking time, NaCl concentration, imidazole concentration and desolvation agent. Particle size is shown to be sensitive only to the type of cross-linker, cross-linking time, and the presence of imidazole. Using these results, a series of β-gal+eGFP nanoparticles are prepared under different conditions and enzymatic activity, particle size and enzyme delivery are characterized. Evidence indicates that the type of cross-linker affects size but not enzymatic activity and cross-linking time affects both factors. Flow cytometry, microscopy, ONPG hydrolysis and western blot are used to evaluate the performance of the different cross-linkers and formulations. In multiple cell types, enzyme delivery via nanoparticles is shown to be

[a] Material from this section has been published.[91]

greater than for soluble protein. Finally, successful intracellular delivery of active enzyme is achieved *in vitro* and the potential of protein nanoparticles as therapeutic enzyme drug carriers is demonstrated.

4-1 Experimental details

4-1-1 Particle preparation

Protein particles were prepared by the desolvation technique as described by Weber et al. [4]. The desolvation method was modified to decrease the initial protein concentration from 50-200 mg/ml to <10 mg/ml while keeping particle diameter below 300 nm. This was done because the solubility of effector proteins and other enzymes is not as high as that of BSA and gelatin, which are the most common proteins used for desolvation. Particles presented in this chapter were prepared using BSA (fraction V, purity 99%, Sigma), β-gal (from *E. Coli*, lyophilized powder > 500 U/g, Sigma) and eGFP produced in *E. coli* and purified under native conditions using Ni-NTA (Qiagen), as explained in Chapter 3.

In general, 2-10 mg of protein or enzyme was dissolved per ml of water, 150 mM NaCl solution (pH 8) or imidazole solution (250 mM imidazole, 300 mM NaCl, 50 mM NaH_2PO_4; pH 8). Particles that combine eGFP and β-gal were prepared with a molar ratio of 1:24 β-galactosidase to eGFP. 100 µl of protein solution are placed in a small glass vial with a magnetic microspin bar (flea) and placed on a hot plate magnetic stirrer at 25°C and 650 rpm. The protein solution was desolvated by continuous, drop-by-drop addition of 400 µl of ethanol or acetone at a rate of 1 ml/min, using a syringe pump. Immediately after desolvation, the cross-linker was added at a ratio of cross-linker to lysines of 1:2.2. Three different cross-linkers were used: glutaraldehyde (GTA)(8% solution, Sigma-Aldrich), 3,3´-Dithiobis(sulfosuccinimidylpropionate) (DTSSP) (Pierce) and bis(sulfosuc-cinimidyl)suberate (BS^3)(Pierce). All cross-linkers were dissolved or diluted in water and 60 µl of solution were added to the desolvated protein suspension.

After 10 min to 2 h of stirring, the cross-linking reaction was stopped by transferring the particle suspension to a 2 ml centrifuge tube, centrifuging at 1000 g for 1 min and removing the supernatant. Particles were re-suspended in phosphate buffered saline (PBS, 10 mM NaH_2PO_4, 137 mM NaCl, 2.7 mM KCl, 2 mM KH_2PO_4; pH 7.4) and sonicated on ice for 1s every 15 s at 30% amplitude, for a total of 5 minutes.

Particle supernatant was stored for analysis and particles were characterized within the next few hours. To determine the yield, the amount of protein that was not precipitated during the desolvation process was measured using a BCA protein assay (Pierce).

4-1-2 Determination of particle size and zeta potential

Particle size distribution was measured by dynamic light scattering using a Zetasizer Nano ZS90 (Malvern Instruments Ltd). The samples were measured at 25°C and a scattering angle of 90°. Average particle size was calculated as the arithmetic mean of the distribution of at least 3 batches of particles and the standard deviation was calculated as the variance between average diameters of the batches. Number distributions were used to describe particle size in order to remove artifacts and additional peaks caused by the presence of aggregates, that due to their size obscure the main population. Nonetheless, in all cases the main population peak in number distribution was observed to match the peak for the main population in intensity distribution.

The zeta potential of the particles was determined by measuring the electrophoretic mobility of the nanoparticles using the same instrument. Zeta potentials were measured in PBS and 10 mM HEPES buffer, which provided information about the intrinsic surface charge and the surface charge once biologically relevant ions have adsorbed to the particles. Average particle zeta potential was calculated as the arithmetic mean of the distribution of at least 3 batches of particles and the standard deviation was calculated as the variance between average zeta potential of the batches

4-1-3 Determination of β-gal activity

The activity of β-gal was measured by quantification of the hydrolysis of ortho-nitrophenyl-D-galactopyranoside (ONPG) using a colorimetric β-Gal Assay Kit (Invitrogen). Activity in particles was measured by diluting the particles to a final concentration of 0.5 ng/ml of β-gal and analyzing according to the instructions for the kit. β-gal activity in nanoparticles was compared to measured activity of the equivalent concentration of β-gal in solution.

For quantification of the activity of β-gal in cells, HeLa and 3T3 cells were seeded at a density of $1x10^4$ per well in a 96-well plate in their growth medium. After 16 h the cells were incubated with particles (87.5 ng/ml) in growth medium for 6 h. The cells were washed five times with PBS, then lysed and assayed following the kit instructions.

4-1-4 Determination of eGFP nanoparticle fluorescence

The effect of particle fabrication and the different cross-linkers on eGFP fluorescence was quantified by measuring the fluorescence intensity of eGFP before (soluble) and after (nanoparticles) desolvation and cross-linking. Equal amounts of nanoparticles and soluble eGFP, at the same concentration, were placed in a 96-well plate. Fluorescence intensity was measured in a synergy H4 multi-mode microplate reader (Bio-Tek), using filter set 1 with an excitation wavelength of 485 nm and emission wavelength of 528 nm, with optics set at the bottom, 50% gain and read height of 4 mm.

4-1-5 Cell Culture

HeLa, SK-BR-3 and NIH/3T3 cells were purchased from the American Type Culture Collection (ATCC). All cells were cultured following ATCC protocols and in the recommended growth medium. HeLa cells were cultured in Dulbecco's Modified Eagle's Medium (DMEM) and supplemented with 10% (v/v) fetal bovine serum (FBS). SK-BR-3 cells were grown in McCoy 5A Media and supplemented with 10% FBS. 3T3 cells were cultured in DMEM and supplemented with 10% calf serum. All media and serum was purchased from Cellgro, Mediatech and supplemented with 1% (v/v)

penicillin/streptomycin. Cells were incubated at 37°C in a 5% CO_2 humidified atmosphere.

Cells used in this work were passaged at 80-90% confluency and following ATCC protocols. Cells used for experiments were passaged at least two times before use and did not exceed passage number 20. Cell morphology and normal behavior were verified before use.

4-1-6 Cellular internalization of nanoparticles

Uptake of particles was assessed by flow cytometry and confocal microscopy. For flowcytometry, HeLa, SK-BR-3 and 3T3 cells were seeded at a density of $2.5x10^5$ per well in a 24-well plate in complete growth medium. After 16 h the media was changed and cells were incubated with particles (71 ng/ml eGFP or 87.5 ng/ml eGFP+β-gal) in complete growth medium for 6 h. After this period the cells were washed twice with PBS, trypsinized, and collected in 1.7 ml tubes. Cells were washed twice more by centrifugation (500 rpm for 5 min) in PBS, re-suspended in PBS, filtered with a 35 μm cell strainer and placed on ice. The cells were immediately analyzed in an Accuri C6 (Becton Dickinson and Company) flow cytometer and relative particle uptake was quantified as the ratio of mean fluorescence of the sample population to mean fluorescence of the control population (no particles given).

To ensure the observed fluorescence increase corresponded to internalized particles and not surface binding, 4°C controls were performed. For this purpose cells were seeded and incubated as previously described. But after cell attachment the media was changed and cells were incubated at 4°C for 1h to ensure cell and media temperature was low before exposure to the particles. Following this, 71 ng/ml eGFP or 87.5 ng/ml eGFP+β-gal particles were added and incubated for 6 h at 4°C. The cells were prepared and analyzed as previously described.

For confocal microscopy, HeLa cells were seeded at a density of $1.5x10^4$ cells per well in an 8-well chamber slide system (Nunc LabTek II, Thermo Scientific) with

complete growth medium. After 16-24 hours, cells were incubated with 87.5 ng/ml eGFP+β-gal nanoparticles or soluble protein in complete growth medium for 6 hours. Following incubation, cells were washed three times with PBS and fixed in 3.7% paraformaldehyde for 15 min at room temperature. Cells were rinsed three times in PBS and incubated with Hoechst (Anaspec Inc.) and 0.165 μM rhodamine phalloidin (Biotium) in blocking buffer for 20 min at room temperature. Cells were washed three times with PBS and mounted for imaging in a Zeiss LSM 700 confocal microscope. All images were captured using the same settings.

4-1-7 Particle break-up in cell lysate and *in vitro*

The effect of the cross-linking agent on particle break-up was studied by incubating eGFP nanoparticles in HeLa cell lysate for different periods of time, from 0 to 30 minutes. Particle degradation was analyzed by Western blot. For this purpose, 3 x 106 HeLa cells were lysed in 0.5 ml of NP-40 buffer (150 mM NaCl, 1% NP-40 and 50 mM Tris-HCl at pH=8). Particles were incubated in equal volume of cell lysate for the specified period of time and immediately loaded on a 10% SDS-PAGE gel, using native loading buffer (25% glycerol, 62.5 mM Tris-HCl). A SeeBlue Plus2 (Thermo Scientific) pre-stained standard was loaded for reference and gels were run at 135 V for 2.5 h. After this, the proteins were transferred to nitrocellulose membranes at 400 mA for 35 min. Next, the membranes were imaged using the blue laser and Alexa 488 filter in a Typhoon (GE Healthcare Life Sciences).

Similarly, the effect of cross-linker on β-gal release in cells was studied by incubating confluent monolayers of HeLa cells in 24-well plates with 650 μg/ml eGFP+β-gal nanoparticles (particles used for this assay contained 1:5 molar ratio β-gal:eGFP) for 6 h. Particle degradation was analyzed by Western blot, using 80μl of NP-40 buffer per well to lyse the cells and followed the protocol described above. This time, after transfer, the membranes were blocked with 5% milk in PBS-T for 1 h and washed 3 times for five minutes each time with PBS-T. Next, membranes were incubated with anti

β-gal and anti β-actin antibodies (Abcam) overnight at 4°C. After 16h, the membranes were washed as previously described with PBS-T, incubated for 1h with HRP-chemiluminescent secondary antibodies at room temperature, washed and imaged according to the manufacturer's instructions.

4-1-8 Statistical analysis

All quantitative experiments were triplicated (N=3) and presented as arithmetic mean ± standard deviation. One-way analysis of variance (ANOVA) was used to determine significance among groups, using StatPlus. P values <0.05 among groups were considered statistically significant.

4-2 Pure enzyme nanoparticles

With the aim of understanding and optimizing the production of enzyme nanoparticles, β-gal and lysozyme were used as model enzymes and particles were produced from pure enzyme. β-gal was desolvated with ethanol and cross-linked with DTSSP for 2h. The produced particles were relatively large (402 ± 138 nm in diameter) and retained only 25% of the enzymatic activity, compared to soluble β-gal. These results indicate, not unexpectedly, that β-gal is highly sensitive to the particle formation process. During the particle production the enzymes are desolvated in ethanol and then cross-linked, which can induce changes in the folded structure of the molecules. β-gal is only active as a tetramer and loss of either quaternary or tertiary structure will lead to activity loss.

Lysozyme particles were produced following the same protocol used for the fabrication of β-gal nanoparticles. Resulting particles were 1-1.6 μm in diameter, ~3-4 times larger than pure β-gal particles. Particle diameter was observed to decrease up to 25% when NaCl concentration in the initial protein solution was increased and when acetone was used a desolvation agent, instead of ethanol. Greater than 95% enzymatic

activity was lost during particle fabrication. Due to the large particle size and loss of activity, lysozyme was no longer studied as a model enzyme.

In literature, there are examples of pure enzyme microparticles produced by protein crystallization and posterior cross-linking of these [9, 10]. Proper crystallization methods prevent structural damage and thus, prevent activity loss. However, the large size of protein crystals (>1 μm) leads to large micron-size particles, which hinders efficient delivery and intracellular uptake. Considering that a protein environment may also help alleviate activity loss, albumin protein particles have been used to encapsulate a few active proteins and enzymes [11-13]. However, most of these particles are micron-sized and hence, are not suitable for intracellular delivery. Thus, the incorporation of a carrier protein was henceforth used to reduce activity loss.

4-3 Optimization of carrier protein nanoparticle

The production of protein particles with BSA is well established, making it a good carrier candidate for enzyme-protein particle production [5, 14]. Reproducible BSA nanoparticles have been fabricated with high protein concentrations (> 50 mg/ml), which are ideal for encapsulation of small molecules. However, many proteins and enzymes often have a lower solubility than BSA and therefore, it was desirable to work at low carrier protein concentrations that could yield higher therapeutic enzyme to carrier ratios. For this purpose, it was necessary to optimize the desolvation method for the production of small nanoparticles with low protein concentrations (< 10mg/ml).

Different concentrations of BSA in PBS, ranging from 2-10 mg/ml, were tested for particle fabrication using ethanol as a desolvation agent and DTSSP as a cross-linker. Particle size was observed to depend on protein concentration and varied between 100-500 nm; low concentrations produced larger particles (400-500 nm) and wider size distributions, whereas concentrations higher than 6 mg/ml produced reproducible small nanoparticles (< 200 nm). Nonetheless, desolvation of BSA always produced a

population of aggregates (> 5 μm). Varying the desolvation agent, ratio of protein volume to desolvation agent volume, type of cross-linker, cross-linking time and sonication method were not enough to prevent the formation of such aggregates.

Due to the challenge of BSA particle aggregates and with the purpose of facilitating cellular uptake measurements and tracking of particle internalization, fluorescent proteins were chosen as protein carrier candidates. Green fluorescent protein (GFP), enhanced green fluorescent protein (eGFP) and mCherry were tested and eGFP was identified as the best candidate. eGFP consistently produced small (< 300 nm diameter) and highly fluorescent nanoparticles, at concentrations as low as 6 mg/ml, whereas GFP produced nanoparticles with low fluorescence. mCherry did not produce stable nanoparticles when cross-linked with GTA or DTTSP.

The following sections will present the effect of various desolvation fabrication parameters on carrier particle properties.

4-3-1 Effect of desolvation agent

Particle production via the desolvation method depends on the ability of the desolvation agent to induce protein precipitation. Two common desolvation agents, ethanol and acetone, were studied. Carrier proteins were desolvated at a ratio of 1:4 protein solution to desolvation agent volume and cross-linked with DTSSP for 2 hours. No significant difference in average particle diameter or size distribution was observed between ethanol and acetone, for eGFP or BSA carrier proteins (Figure 4.1). Therefore, all further studies were performed using ethanol as the desolvation agent.

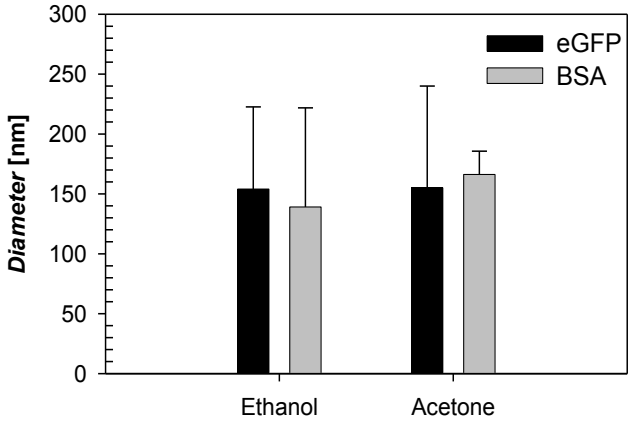

Figure 4.1. Effect of desolvation agent on the size of protein nanoparticles made with eGFP and BSA, at 1:4 protein solution to desolvation agent ratio and cross-linked with DTSSP for 2 h. There is no significant difference in measured particle diameters.

4-3-2 Effect of NaCl on nanoparticle fabrication

The desolvation process was hypothesized to be the result of a balance between protein solubility, salt type and concentration, and the amount of desolvant that is added. In order to establish the effect of salt content, the concentration of sodium chloride in the starting protein solution was varied. In all cases the protein concentration was kept at 6 mg/ml and the amount of ethanol added was 4 times the volume of the initial protein solution. The presence of NaCl, as an additive, at low protein concentrations (<10mg/ml) was observed to be a critical factor for the production of particles. In the absence of NaCl the protein did not precipitate, which indicates that at such protein concentrations the contribution of salting-in and salting-out effects is important for particle formation. Wang et al.[13] showed that increasing the concentration of protein leads to formation of smaller nanoparticles. This is presumed to be the result of increased nucleation of the protein upon exposure to the desolvation agent. The low concentrations of proteins used in this work may delay or prevent the nucleation process and thus lead to the absence of coacervation. However, for therapeutic enzymes with low solubilities, an increase in

initial protein solution concentration would lead to decreased enzyme to carrier ratios, which is undesirable.

With the addition of NaCl we observed particle formation. Increase in salt concentration changed the distribution from a single population into multiple populations, but no clear trend in particle diameter was observed (Figure 4.2).

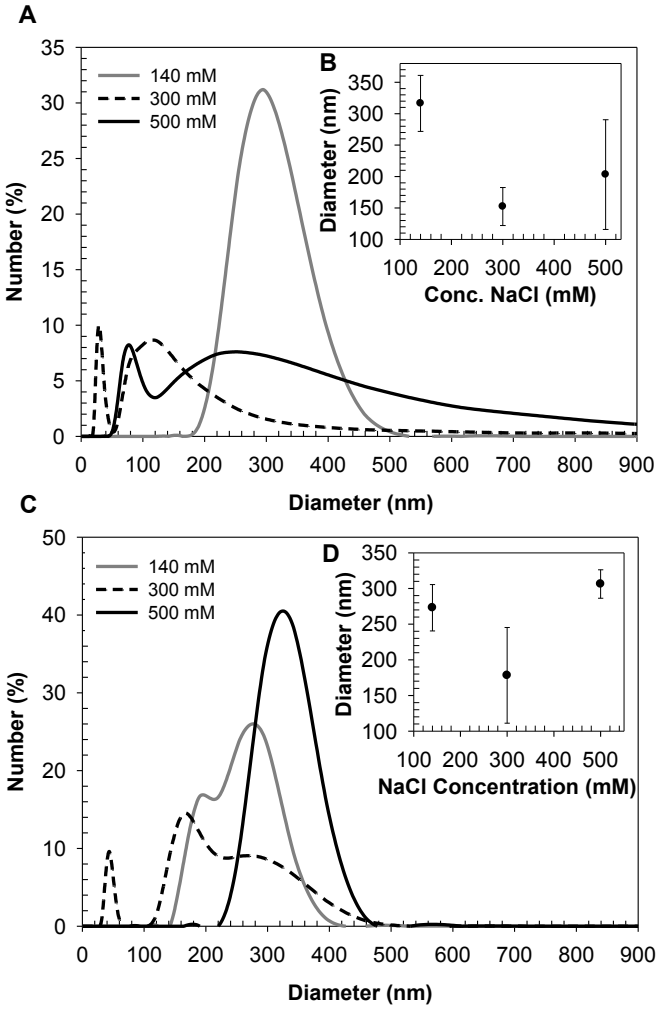

Figure 4.2. Effect of NaCl concentration on the diameter of protein nanoparticles: (a) size distribution curves for representative samples of BSA nanoparticles, (b) average diameter of BSA nanoparticles, (c) size distribution curves for representative samples of eGFP nanoparticles, and (d) average diameter of eGFP nanoparticles.

Formation of particles appears to be the result of combined effects of the salting out process, the excluded volume effect produced by ethanol, and hydrogen bonds that form between water and ethanol. Salt influences protein precipitation according to the salting-out principle, in which the solubility of a protein decreases as the ionic strength of the solution increases [15]. When there is a low concentration of salt molecules in the protein solution, more water molecules are available for solvating the protein. As the salt concentration increases, the water molecules interact with the salt ions and fewer are available for solvating the protein. This brings the protein molecules closer to each other, leading to precipitation. Ethanol also interacts with water molecules and forms hydrogen bonds, leading to decreased protein solvation. Additionally, ethanol has a higher excluded volume than water and therefore, can lead to protein precipitation [16].

4-3-3 Effect of imidazole on carrier particle size

In addition to salt, protein precipitation is also affected by the presence of other additives in the initial protein solution [16]. Since many recombinant proteins are purified with histidine tags (His-tag), the effect of imidazole on particle production was explored. The effect of imidazole on both carriers, eGFP with a His-tag and BSA without, was analyzed. The results indicated that imidazole affects the size of particles made with both carriers (Figure 4.3). The diameter of eGFP nanoparticles decreased as the concentration of imidazole increased (Figure 4.3A-B). Furthermore, the size distribution changed significantly. Increasing the concentration of imidazole from 0 mM to 90 mM yielded the formation of two separate populations of particles, one at approximately 60 nm and another at 120 nm. Each of these peaks is narrower than the peak observed when no imidazole is present. A further increase in imidazole concentration to 250 mM yields a single peak with a narrow distribution, which indicates that imidazole not only controls eGFP particle size but also particle size distribution, which is critical for drug delivery applications.

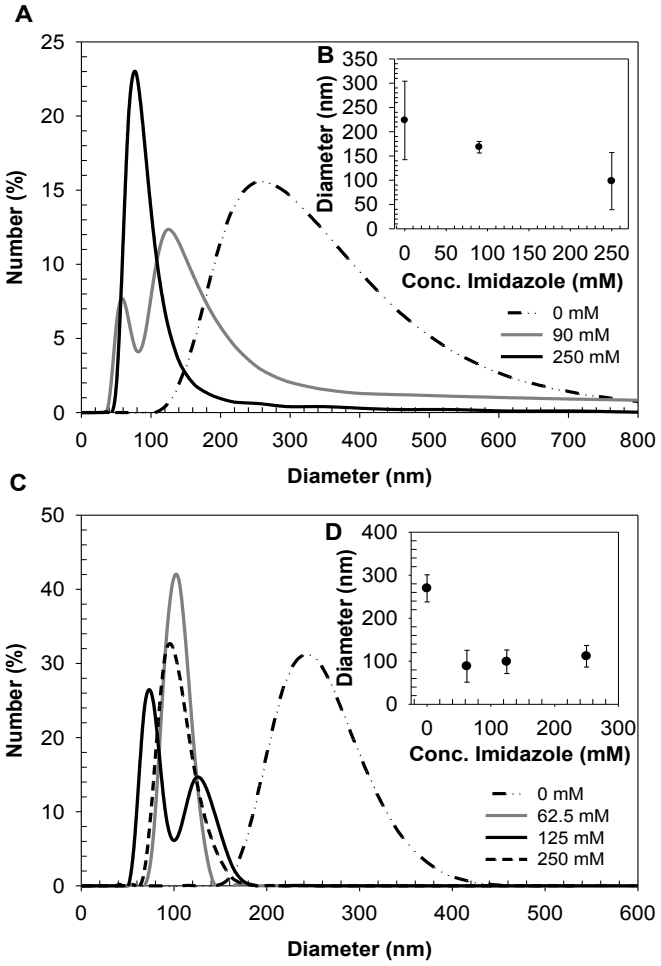

Figure 4.3. Effect of imidazole concentration on particle size: (A) size distribution curves for eGFP nanoparticles, (B) average diameter of eGFP nanoparticles, (C) size distribution for BSA nanoparticles, and (D) average BSA particle diameter.

Interestingly, in the case of BSA, particle size is not affected by the amount of imidazole only by its presence (Figure 4.3C-D). The diameter of BSA particles decreased approximately 60% when imidazole was present. Varying the concentration of imidazole in between 62.5-250 mM did not significantly affect the size but it did change the size distribution from one population to two populations. The difference in response between BSA and eGFP suggests that each protein interacts differently with imidazole and therefore, the effect of imidazole on size will vary from protein to protein and that the effect depends on how imidazole interacts with each protein.

Imidazole has been reported to increase the solubility of histidine tagged proteins, although the mechanism is still unknown [17]. It is possible that by increasing the solubility of eGFP, imidazole is decreasing the size of eGFP particles. Higher protein solubility was hypothesized to delay protein nucleation and thus, lead to the formation of smaller particles. Although the effect of imidazole on the solubility of BSA has not been characterized, imidazole has been observed to bind to BSA, which contains 17 histidine residues [18]. This binding could affect the solubility of the protein and/or interaction with ethanol, and explain the decrease in particle size. In addition, imidazole affected the polydispersity of the particles; the width of the size distribution decreased in the presence of imidazole. This could be the result of a more uniform nucleation process possibly due to increased solubility. Thus, imidazole can be used to tune particle size according to the requirements of the application.

It is important to note that the particle fabrication process is reproducible, resulting in similar size distributions and average diameter of particle made from the same batch of protein (Figure 4.4). However, particle size and size distribution were observed to depend on protein purity. The presence of protein impurities resulted in larger average particle diameters and wider size distribution peaks. Possibly as a result of the different solubilities, that may cause one protein to precipitate before others and begin the nucleation process earlier, giving more time for particle growth.

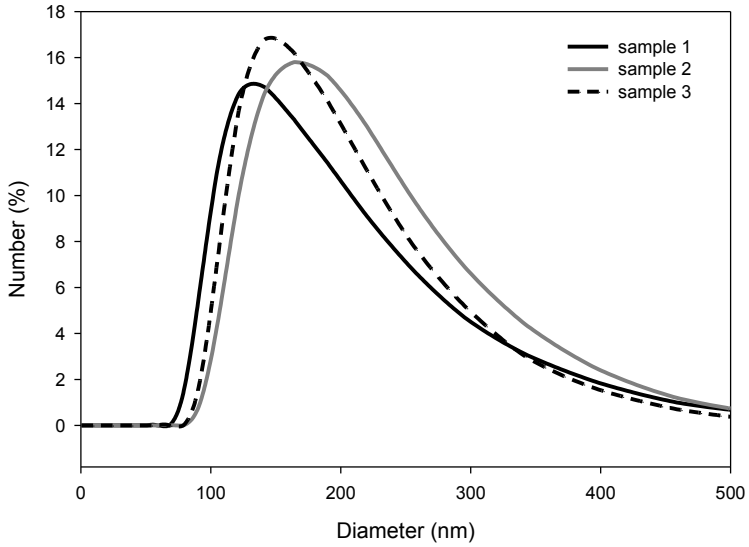

Figure 4.4. Variation in particle size distribution across three different particle productions made from the same batch of eGFP and same fabrication conditions (125mM imidazole buffer and DTSSP). No significant variation in particle size and size distribution is observed within the same batch of protein.

4-3-4 Effect of cross-linker on carrier particle size

Once the particles have been formed via desolvation it is necessary to cross-link them in order to stabilize them. Otherwise, removal of ethanol can lead to re-solubilization of the protein. The effect of three different cross-linkers was evaluated. The first, glutaraldehyde (GTA), has historically been the most commonly used cross-linking agent for production of protein nanoparticles. GTA is a highly reactive and irreversible cross-linker that interacts with multiple functional groups, such as amine, thiol, phenol and imidazole groups [19]. The second cross-linker is a degradable primary amine cross-linking agent 3,3′-Dithiobis(sulfosuccinimidylpropionate) (DTSSP). DTSSP contains a disulfide bond, which is cleaved in reducing environments. The intracellular environment is known to have reducing conditions [20], and therefore could trigger release of soluble

enzyme. The final cross-linking agent, bis[sulfosuccinimidyl] suberate (BS^3), is identical to DTSSP but does not contain the disulfide bond, making it irreversible.

In order to establish the effect of these cross-linkers on size, particles were produced with the carrier proteins, eGFP and BSA, dissolved in PBS. Particles were cross-linked for 2 hours keeping the cross-linker to lysine ratio constant. The resultant particles showed significantly higher particle size when GTA was used as the cross-linker (Figure 4.5A,C). There was no significant difference in particle diameter between DTSSP and BS^3 (Figure 4.5B,D). These results indicate that highly reactive cross-linkers, like GTA, lead to the formation of larger particles than those formed with less reactive cross-linkers, such as DTSSP, and BS^3 [19]. Given the similarity of the chemical structure and identical sulfo-NHS ester reactive ends of DTSSP and BS^3, similar reactivity levels are expected. Furthermore, the sulfo-NHS ester ends react only with primary amines. However, GTA is a smaller molecule with carbonyl reactive ends and is known to be highly reactive to multiple functional groups [19]. Thus, there are more reactive sites that can be linked to bind smaller particles together into large particles or aggregates.

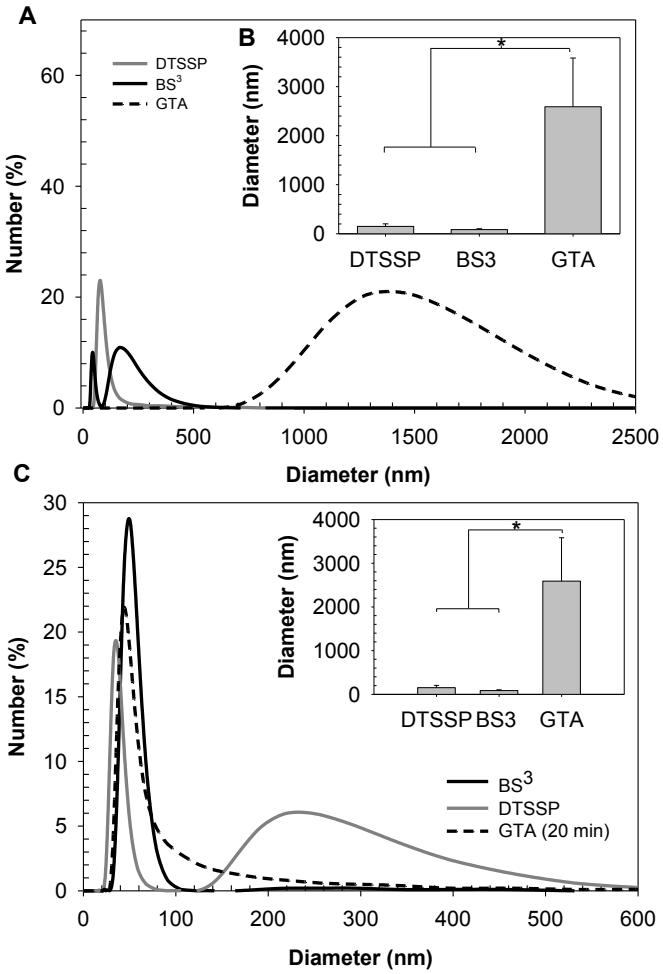

Figure 4.5. Effect of cross-linkers on particle size: (a) size distribution curves for eGFP nanoparticles, (b) average hydrodynamic diameter of eGFP nanoparticles, (c) size distribution curves for BSA nanoparticles (note GTA cross-linking time was 20 min) and (d) average hydrodynamic diameter of BSA nanoparticles.

4-3-5 Effect of cross-linker on fluorescence and particle break-up

Precipitation and cross-linking affects the structure of proteins and enzymes, as was observed during pure β-gal particle fabrication. In order to establish the effect of the particle production process on carrier proteins we used eGFP. The fluorescence of eGFP depends on its structure, a β-barrel fold with a chromophore-containing helix running through the core of it[21]. Though eGFP is highly stable, changes in conformation greatly affect its fluorescence intensity[22]. Thus, the effect of particle production and cross-

linking was evaluated. Analysis of the fluorescence of eGFP in particles compared to the fluorescence of soluble eGFP, demonstrated that there is a 9-18% loss in fluorescence after desolvation and stabilization with the three cross-linkers. However, there was no significant difference between the cross-linkers (Figure 4.6). The small loss in fluorescence, compared to high enzymatic activity loss of β-gal in pure enzyme particles, indicated that eGFP retained its structure better than β-gal. This suggests that eGFP could be used to help protect enzyme structure during protein fabrication.

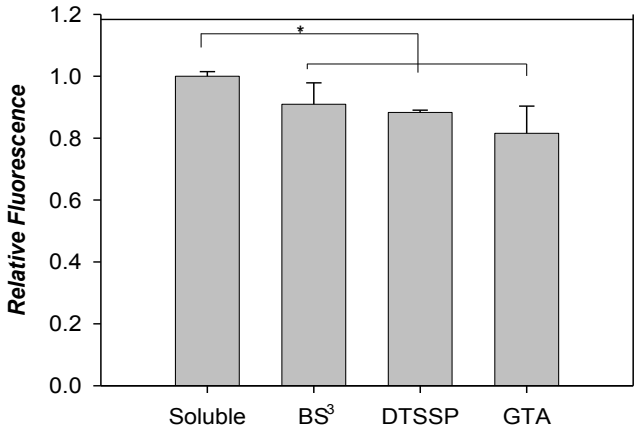

Figure 4.6. Effect of cross-linker on eGFP fluorescence. Relative fluorescence of nanoparticles suspended in PBS, after protein desolvation and cross-linking with BS^3, DTSSP and GTA for 2 h. Data are the measured fluorescence of eGFP nanoparticles relative to soluble eGFP (* $p<0.05$).

Next, the capacity of particles fabricated with the three different cross-linkers to break-up and release fluorescent eGFP was assessed. For this purpose, eGFP particles were incubated in HeLa cell lysate, which simulates intracellular conditions, for 0 to 30 minutes. Particle break-up and protein release were analyzed by western blot, using the fluorescence of eGFP. DTSSP and BS^3 cross-linked particles were observed to disassemble and release soluble fluorescent eGFP in HeLa lysates (Figure 4.7A). However, GTA cross-linked particles did not release soluble eGFP (Figure 4.7B). These

observations indicate that DTSSP and BS^3 should be used when intracellular protein or enzyme release is necessary, and GTA when particle should remain intact.

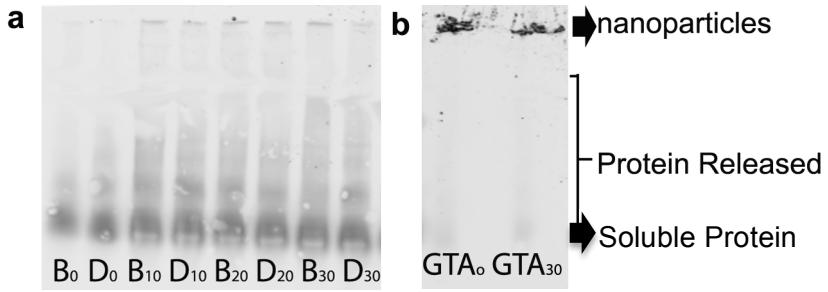

Figure 4.7. eGFP particle break-up in HeLa cell lysates. (a) Western blot showing break-up of particles cross-linked with BS^3 (B_t) or DTSSP (D_t) over time in minutes (indicated by subscript). (b) Western blot for eGFP particles cross-linked with GTA at 0 and 30 minutes. All particles were produced with ethanol and cross-linked for 2 h.

4-4 Optimization of carrier and enzyme nanoparticles

Just as eGFP and BSA desolvate differently when formulated as particles under different conditions, addition of an enzyme has the potential to alter particle size and distribution, which are highly relevant to cellular particle internalization. Studies with eGFP demonstrated that the presence of protein impurities lead to the production of larger particles and wide size distributions. These observations indicated that the addition of an enzyme would also change particle size and size distribution.

Differences between the carrier protein and enzyme size, charge and solubility affect the desolvation process. Therefore, it was necessary to optimize the desolvation process for particle size tuning and enzymatic activity retention. Incorporation of β-gal into eGFP and BSA yielded larger particles than pure carrier desolvation. BSA continued to produce large aggregates and thus, further studies with β-gal were performed using only eGFP as a carrier.

The following sections present the effect on particle properties and enzymatic activity of various desolvation fabrication parameters for carrier-enzyme particles.

4-4-1 Effect of enzyme addition on particle size and fabrication yield

The properties of different added proteins may vary considerably from those of eGFP and hence, affect the nucleation and precipitation process. Introducing β-gal in the eGFP formulation (eGFP+β-gal) yielded slight variations in the particle size and size distribution (Figure 4.8a). Increasing imidazole concentration to 250 mM significantly increased particle size (Figure 4.8b). This behavior is contrary to the observed effect of imidazole on eGFP particle size.

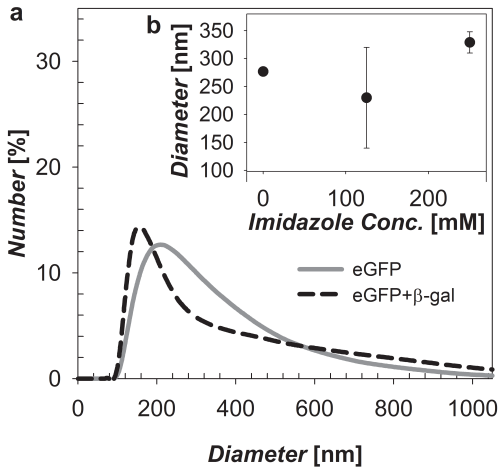

Figure 4.8. Effect of enzyme on particle size: (a) size distribution curves of eGFP nanoparticles, eGFP+βgal and eGFP+AvrA nanoparticles produced with 250 mM imidazole buffer and (b) average particle diameter of eGFP+βgal nanoparticles with varying imidazole concentrations.

The pH for particle fabrication in this work (7.4) was above the pI of eGFP (6.2) and β-gal (4.6) and thus, both proteins were negatively charged. However, their level of ionization was different and so was their solubility. The closer a protein is to its pI the lower its solubility and the more prone it is to aggregation; therefore, desolvation will

yield larger aggregates or particles [13]. In this case, eGFP is closer to its pI than β-gal, which could explain the slight decrease in particle size when the enzyme was added.

Some additional differences between eGFP and β-gal that may also affect the size distribution behavior are their size (26.9 kDa and 465.2 kDa, respectively), solubility in aqueous buffers (eGFP > β-gal) and presence of His-tag (eGFP contains His-tag, β-gal does not). The absence of the histidine tag in β-gal could imply that imidazole has no effect on protein solubility. Imidazole is also known to form strong hydrogen bonds with water [23]. This last characteristic of imidazole is shared with salts and thus, can lead to a salting-out effect. Proteins with lower solubility precipitate sooner in the desolvation process, which leads to longer particle growth periods after nucleation and hence, larger particles.

The addition of β-gal also affected the yield of the particle production process, which was measured by quantifying the amount of protein that remains soluble after desolvation and cross-linking and comparing to the initial amount of protein used. The average amount of protein that formed eGFP particles was 94%. But when β-gal is introduced in the formulation the yield is 85%. These yields are high compared to many polymeric or lipid nanoparticle formulations containing protein [1].

4-4-2 Effect of cross-linker on enzymatic activity

Cross-linking can alter the structure and activity of enzymes; hence, the effect of GTA, DTSSP and BS^3 on enzymatic activity was evaluated. The substrate of β-gal (ONPG) is small enough to diffuse into cross-linked particles. Therefore, bioactivity and therapeutic potential could be measured for both reversible and irreversible cross-linkers. eGFP+β-gal particles were prepared with each cross-linker. β-gal was observed to lose approximately 25% of activity after desolvation and cross-linking (Figure 4.9A). This loss is 3 times lower than the observed activity loss of pure β-gal nanoparticles. The level of activity of β-gal in particles produced with these cross-linkers did not vary

significantly between cross-linkers for a cross-linking time of 2 h (Figure 4.9B). This indicates that the loss of enzyme structure caused by cross-linking is similar between cross-linkers.

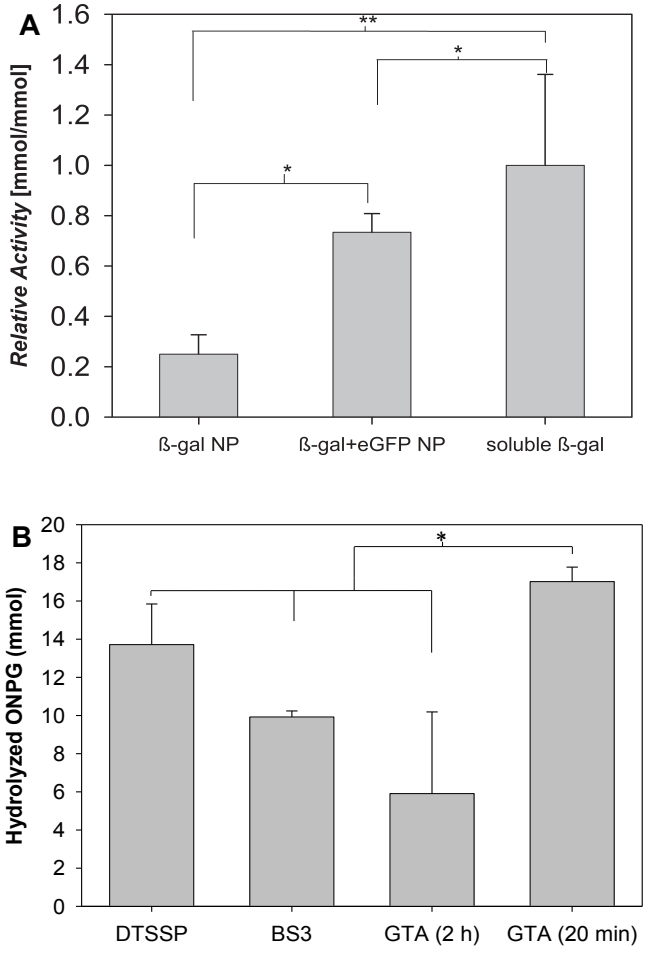

Figure 4.9. (A) Relative β-gal activity retention for different particle formulations. Particles were produced from pure β-gal (β-gal NP) or a mixture of eGFP and β-gal (eGFP+β-gal) and cross-linked for 2 h with DTSSP. Data are the measured β-gal activity in the nanoparticles relative to soluble β-gal. (B) Effect of cross-linker on β-gal activity (* $p<0.05$, ** $p<0.01$).

In order to reduce particle size when using GTA, for intracellular delivery, it was necessary to shorten the cross-linking time, this limits the extent of the reaction and

prevents the possible binding of smaller particles into large aggregates. By decreasing the cross-linking time of eGFP+β-gal particles with GTA from 2 hours to 20 minutes we observed a significant decrease in particle size. The resulting particles were approximately 270 nm in diameter, compared to 700 nm after 2 hours of reaction. Thus, reduction of cross-linking time yielded GTA cross-linked nanoparticles of comparable size to those produced with DTSSP and BS^3. Not surprisingly, enzymatic activity and activity retention increased significantly when the cross-linking time was reduced (Figure 9b). This indicates that the process of cross-linking inactivates the enzyme, or that higher cross-linking levels inhibit substrate access to the enzyme for the irreversible cross-linkers GTA and BS^3.

4-4-3 Protective effect of particle on enzyme activity

There are many challenges associated with the stability of enzymes given their large size and complex tertiary or quaternary structure that can be highly sensitive to the environment [1]. With the purpose of establishing the capacity of protein nanoparticles for protecting their enzyme cargo, eGFP+β-gal particles were incubated in simulated intestinal fluid (SIF) or human serum for 0.5-2 hours. Preliminary assays with DTSSP cross-linked eGFP nanoparticles indicated that incubation in human serum yields 15-20% protein fluorescence loss. Whereas, soluble eGFP incubated in human serum lost only 10%. Further studies using eGFP+β-gal particles showed that there was no significant difference in enzymatic activity loss for nanoparticles and soluble enzyme incubated in SIF; both soluble and nanoparticle formulations lost 25-30% enzymatic activity.

Similar studies performed with human serum, indicated there was no enzymatic activity loss for soluble enzymes incubated in it, instead a 10% increase in activity is onserved, relative to incubation in PBS. eGFP+β-gal particles exhibit 40% higher activity levels in human serum than those observed for particles in PBS. These results were unexpected and could be the result of higher enzymatic activity in the new environment

or an artifact of the assay. Further studies with eGFP+β-gal nanoparticles confirmed the increase in enzymatic activity. Assessment with another enzyme, lysozyme, confirmed increased enzymatic activity in human serum for soluble and particle formulations, compared to PBS.

SIF and human serum were chosen for *in vitro* bioactivity assessment of enzyme-carrier nanoparticles. However these two fluids are very different from each other and hence, assess different conditions. SIF is a harsh complex mix of bile salts and lecithin at pH=6.5, thus is meant to simulate the environment in the small intestine and correlates to oral delivery; whereas human serum can be used to assess conditions in the blood stream. Protein nanoparticles did not exhibit enzymatic activity protection in SIF, suggesting that further protection may be necessary for gastrointestinal stability. Unfortunately, the effect of protein nanoparticles on enzyme stability protection for blood delivery is not clear.

4-5 Intracellular delivery of enzymes

To assess the potential of protein particles for intracellular delivery of enzymatic drugs, cellular uptake studies with different types of cells were performed. Three well established cell lines, NIH/3T3 (murine fibroblasts), HeLa (human cervix adenocarcinoma cells) and SK-BR-3 (human breast adenocarcinoma cells), were used as representative cell types. eGFP+β-gal and eGFP only particles were prepared in 0 mM imidazole solution and cross-linked with DTSSP for 2 h, as previously described, to obtain similar particle size distributions. eGFP+β-gal particles had an average diameter of 283.1 nm and eGFP particles were 287.3 nm (Figure 4.10).

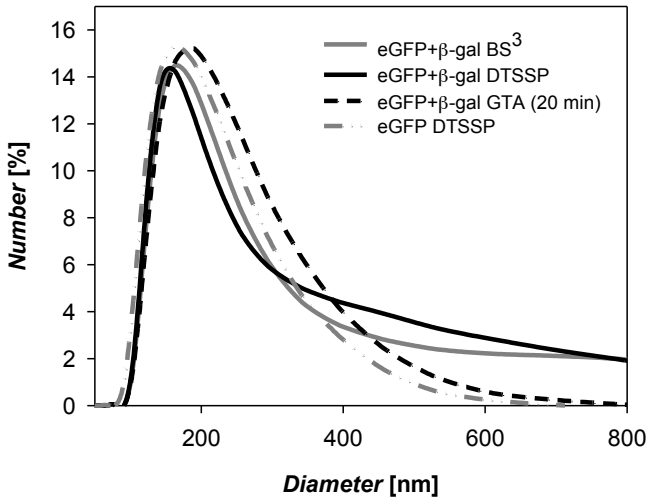

Figure 4.10. Size distribution curves of particles used for cell experiments. eGFP or eGFP+β-gal particles were produced with ethanol and cross-linked with DTSSP and BS^3 for 2 h, or with GTA for 20 min to obtain similar nanoparticle average sizes and size distributions.

In addition to size, particle surface charge is also important for effective particle delivery and internalization. It is well established that neutral particles decrease immune recognition and increase circulation times, but charged particles exhibit higher cellular internalization [13]. For protein particles, the surface charge is dictated by the identity of the protein and specifically, which residues are exposed. eGFP and eGFP+β-gal nanoparticles exhibit very similar zeta-potentials as a result of the high content of eGFP in all formulations. eGFP+β-gal particles had an average zeta-potential of -12.9 mV in PBS or -26.4 mV in HEPES and eGFP particles of -11.5 mV in PBS or -27.5mV in HEPES. The results shown here prove that the produced protein particles are inherently charged, as indicated by the strongly negative zeta-potentials measured in HEPES buffer. However, in the presence of ions, such as those observed in physiological conditions (PBS), the measured zeta-potential value decreases drastically. This indicates that ions adsorb to the surface of the particles and shield its charge, which causes the particles to

seem only slightly charged [24]. Particle charge is important for three main reasons: first, cell membranes are negatively charged and positively charged particles bind to the cell surface which can lead to particle internalization; second, neutral particles have longer blood circulation times; and third, neutral particles are prone to aggregation.

In order to establish if the produced protein-enzyme nanoparticles are capable of effectively delivering their cargo to cells, particle uptake was quantified using flow cytometry. The increase in green fluorescence of cells incubated with nanoparticles or soluble protein was measured and compared to cells incubated with PBS only. First, soluble eGFP and eGFP nanoparticles were used to establish particle internalization in the different cell lines. Despite the low particle charge, there was significant eGFP particle uptake in all cell lines. HeLa cells exhibited the highest particle uptake; the mean fluorescence of cells incubated with nanoparticles was 4.7 times higher than the fluorescence of cells incubated with soluble protein (Figure 4.11a). Mean fluorescence increased 1.62 and 1.22-fold for SKBR-3 and 3T3 cells, respectively. While particle uptake varied among cell types, in all cases higher intracellular protein levels were achieved with particles than soluble protein. Further confirmation of particle internalization was obtained by confocal imaging of HeLa cells incubated with eGFP+β-gal nanoparticles or soluble eGFP and β-gal. Figure 4.11b shows that there is higher eGFP fluorescence in cells incubated with the nanoparticle formulation in comparison to the soluble.

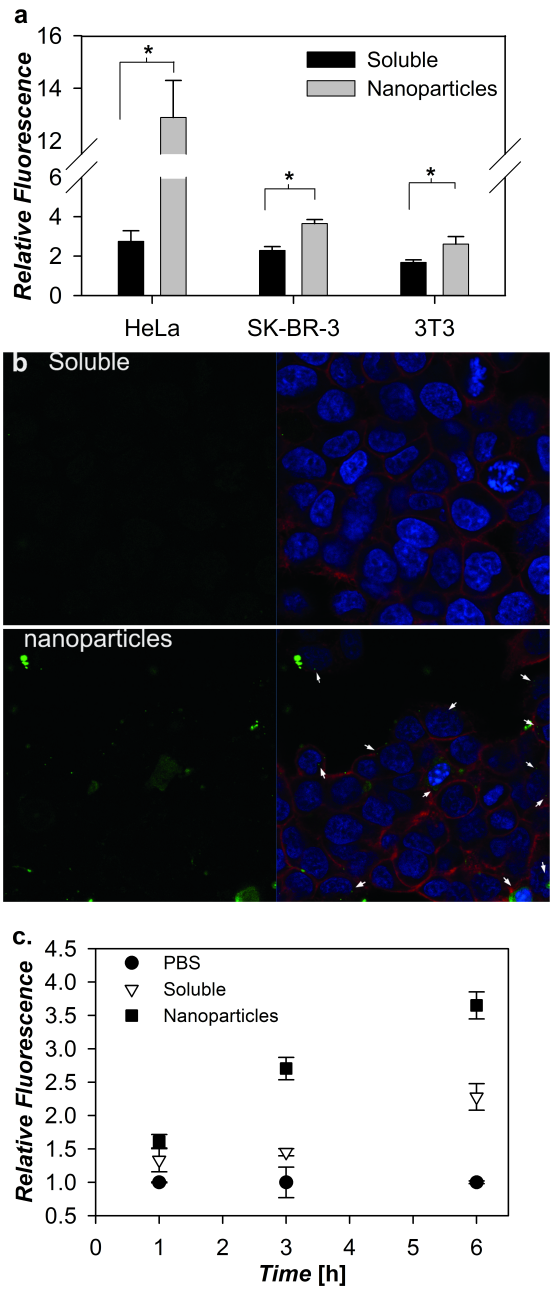

Figure 4.11. Uptake of protein nanoparticles compared to soluble protein: (a) Relative fluorescence of different cell lines after 6 hours of incubation with eGFP nanoparticles and (b) SK-BR-3 cell uptake of eGFP nanoparticles over time. Data reported here shows the measured fluorescence of cells treated with soluble or nanoparticle protein relative to the fluorescence of cells treated with PBS. Error bars represent standard deviation, N=3 (* indicates $p<0.05$)

A time-lapse study revealed the strong dependence of particle uptake on incubation time (Figure 11c). Cells incubated with DTSSP cross-linked eGFP particles for 3 h show a 1.67 fold increase in fluorescence above those incubated for only 1 h. After an additional 3 h of incubation (6 h time point) a fluorescence increase of 2.3 fold, with respect to those incubated for 1 h, was observed. Cells incubated with soluble eGFP for 3h show negligible increase in fluorescence, but after 6h show a 1.7 fold increase in fluorescence, with respect to those incubated for 1h. Experiments at 4°C showed no increase in fluorescence over time (Figure 4.12). The low particle uptake reported at 4°C, compared to 37°C, indicates that particles are internalized by active uptake mechanisms, such as endocytic processes [25, 26].

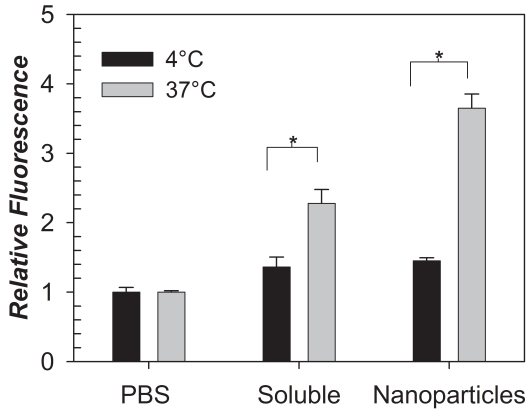

Figure 4.12. Energy dependent particle uptake. SK-BR-3 cells were incubated with eGFP nanoparticles for 6 h at 4°C and 37°C. Particles used for this experiment were produced with ethanol, 250 mM imidazole buffer and cross-linked with DTSSP for 2 h. Average particle diameter was 117 nm and zeta potential was –11.5 mV in PBS. Data are the measured fluorescence of cells incubated with soluble or nanoparticle eGFP relative to the fluorescence of cells incubated with PBS. Error bars represent standard deviation, N=3 (* $p<0.05$).

To establish the presence of active β-gal inside cells, we measured hydrolysis of ONPG in HeLa cells following particle uptake and cell lysis. β-gal activity in cells incubated with eGFP+βgal nanoparticles was substantially higher than in cells incubated with a solution of β-gal and eGFP (Figure 4.13). The 5-fold increase in activity of particles over soluble is comparable to the 4.7-fold increase in fluorescence corresponding to higher particle uptake. These results confirm that enzymatic activity is retained not only during the particle fabrication process but also following cellular uptake and a significant amount of active enzyme can be delivered intracellularly.

To test the effect of the different cross-linkers on particle internalization and activity of delivered β-gal, we incubated 3T3 cells for 6 hours with eGFP+β-gal nanoparticles cross-linked with DTSSP, BS^3 and glutaraldehyde. Since the size of glutaraldehyde cross-linked nanoparticles depends strongly on reaction time, we used particles cross-linked for 20 min to match the particle diameter to BS^3 and DTSSP particles. Particles with similar distributions and zeta potentials were used (Figure 4.10). The relative fluorescence of the cells was not significantly different, suggesting particle uptake is not affected by cross-linker (Figure 4.14A). This was expected due to the similarity in particle size and zeta potential.

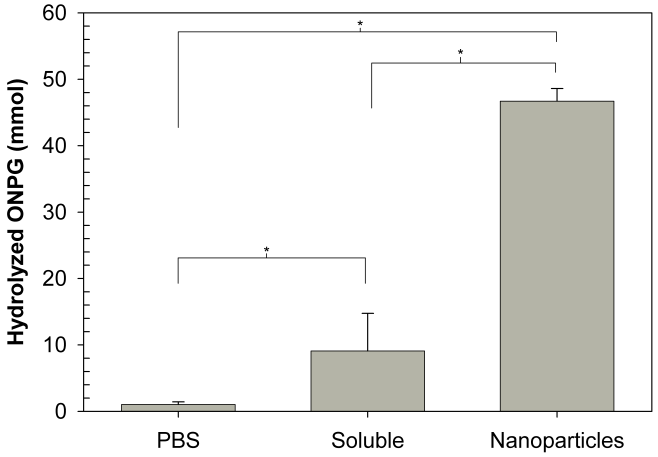

Figure 4.13. β-gal activity levels in HeLa cells after 6h of incubation. Cells were incubated with PBS, soluble of eGFP and β-gal, or eGFP+β-gal nanoparticles. The latter

two samples contain the same amount of total protein and a 1:24 molar ratio of β-gal to eGFP. Error bars represent standard deviation, N=3 (* indicates $p<0.05$)

Measured β-gal activity after intracellular delivery was also similar for DTSSP, BS^3 and GTA particles (Figure 4.14B). Previous experiments in which the activity of the enzyme was measured after particle production (Figure 4.9B) indicated that there is no significant difference in activity between BS^3 and DTSSP. This supports the observed similarity in activity levels of the enzyme inside the cells. However, the activity of the internalized GTA cross-linked particles was expected to be higher than that of internalized particles cross-linked with BS^3 and DTSSP. The activity of β-gal in 20min GTA cross-linked particles, measured after particle production, was significantly higher than the activity of the enzyme in particles cross-linked with BS^3 and DTSSP (Figure 4.5). This difference could be the result of GTA-linked particles allowing less substrate access to the enzyme due to decreased cross-linker length.

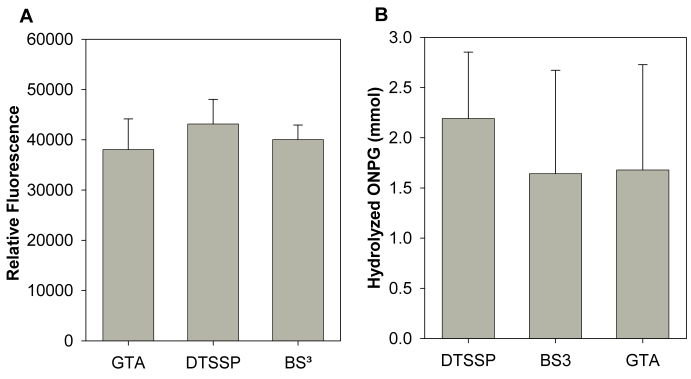

Figure 4.14. Effect of cross-linkers on: (a) eGFP+β-gal particle uptake in 3T3 cells, and (b) β-gal activity levels in 3T3 cells incubated with eGFP+β-gal nanoparticles relative to cells incubated without particles. Error bars represent standard deviation, N=3.

Studies performed with the three types of particles in HeLa cell lysates indicated that DTSSP and BS^3 particles are broken apart at similar rates, possibly by the reducing agents and proteases found in cells; whereas, particles cross-linked for 2h with GTA are

not degraded (Figure 7). Additional studies with eGFP+ β-gal indicate that that BS^3 and DTSSP particles break apart while inside of the cells, releasing the enzyme and achieving the same activity levels of their higher activity counterpart, 20 min GTA cross-linked particles, which do not break apart (Figure 4.15). Intact GTA particles may have increased mass transfer limitations for substrate access compared to the DTSSP and BS^3 cross-linked particles. DTSSP and BS^3 cross-linked nanoparticles break up inside the cells, which cancels the increased activity seen for the GTA particles when all are evaluated intact in solution. Thus the use of reducible or degradable cross-linkers may prove advantageous for enzyme or protein intracellular delivery. The relative importance of each particle property must now be evaluated in specific disease models both *in vitro* and *in vivo.*

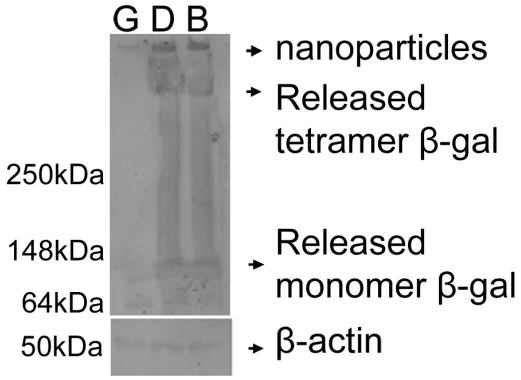

Figure 4.15. eGFP+β-gal particle break-up in cells. Western blot showing break-up of particles cross-linked with GTA (G), DTSSP (D) or BS3 (B). Confluent monolayers of HeLa cells were incubated with particles for 6h. eGFP+β-gal (1:5 enzyme:eGFP) particles were produced with ethanol and cross-linked with DTSSP and BS3 for 2 h, or with GTA for 20 min. Particles sizes were 263, 241 and 233 nm, respectively.

4-6 Particle stability during storage

We observed that particles stored in PBS at 4°C formed large aggregates after 6 months; however, these aggregates will dissociate into the original nanoparticles after

brief sonication (Figure 4.16). However, the enzymatic activity of the enzyme decreased 40-80% after dissociation of the aggregates. Pharmaceutical proteins and enzymes are often stored in solid form to achieve an acceptable shelf life. eGFP+β-gal nanoparticles lyophilized in PBS, retain 84% ± 10% of β-gal enzymatic activity after re-suspension, while their size decreases by 5 to 35% depending on the type of cross-linker and cross-linker time (Figure 18). The observed decrease in size is most likely the result of particle drying. As the water trapped inside the particles is removed, they collapse into smaller more dense particles, which can be advantageous for drug delivery.

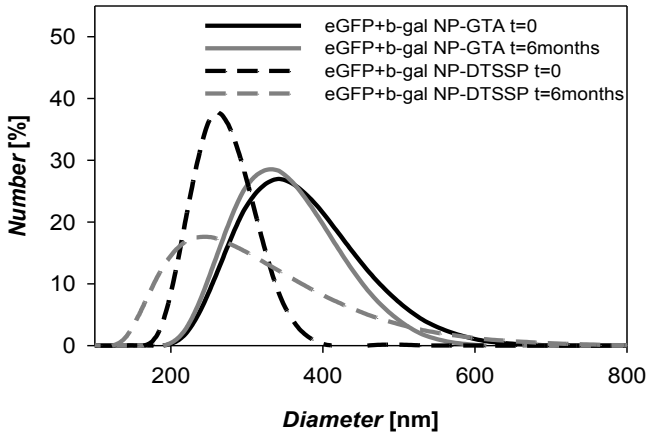

Figure 4.16. Effect of storage at 4°C on eGFP+β-gal (representative) particle size distribution. GTA cross-linked nanoparticles and DTSSP cross-linked particles are shown immediately after fabrication and after 6 months of storage and sonication.

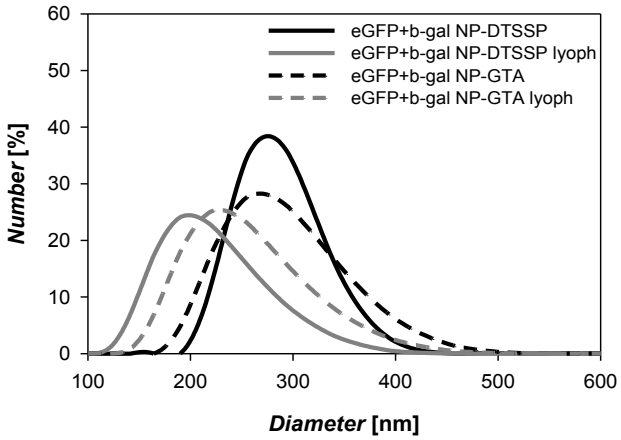

Figure 4.17. Effect of lyophilization on eGFP+β-gal (representative) particle size. GTA cross-linked nanoparticles and DTSSP cross-linked particles are shown after fabrication and after lyophilization, re-suspension, and sonication.

4-7 Summary

The results presented in this chapter illustrate the feasibility of producing protein nanoparticles for delivery of therapeutic enzymes. It was demonstrated that particle size can be tuned by adjusting fabrication parameters and the effect of each parameter is dependent on the carrier protein and enzyme. Salt and imidazole concentration and cross-linking time were identified as crucial parameters for size control. In addition, high enzymatic activity retention was observed after desolvation and cross-linking of enzymes with carrier proteins. Multiple cell lines exhibited greater internalization of enzyme-protein nanoparticles than soluble protein. Most significantly, it was established that this protein particle delivery system effectively delivers active enzymes inside cells. These results are very promising for therapeutic enzyme delivery and provide a new application for protein nanoparticles drug carriers. The next two chapters will describe the application of protein particles for delivery of enzymes in two different disease models

4-8 References

1. Holcenberg, J.S., *Enzyme therapy: problems and solutions.* Ann. Rev. Biochem., 1982. **51**: p. 795-812.

2. Holcenberg, J.S. and J. Roberts, *Enzymes as drugs.* Ann. Rev. Pharm., 1977. **17**: p. 97-116.

3. Gu, Z., et al., *Tailoring nanocarriers for intracellular protein delivery.* Chem. Soc. Rev., 2011. **40**: p. 3638-3655.

4. Weber, C., et al., *Desolvation process and surface characterization of protein nanoparticles.* Int. J. Pharm., 2000. **194**: p. 91-102.

5. Langer, K., et al., *Optimization of the preparation process for human serum albumin (HSA) nanoparticles.* Int. J. Pharm, 2003. **257**: p. 169-180.

6. Langer, K., et al., *Human serum albumin (HSA) nanoparticles: Reproducibility of preparation process and kinetics of enzymatic degradation.* Int. J. Pharm., 2008. **347**: p. 109-117.

7. Mehravar, R., M. Jahanshahi, and N. Saghatoleslami, *Production of biological nanoparticles from lactalbumin for drug delivery and food science application.* Afr. J. Biotech., 2009. **8**(24): p. 6822-6827.

8. Gunasekaran, S., K. Sanghoon, and L. Xiao, *Use of whey proteins for encapsulation and controlled delivery applications.* J. Food Eng. , 2007. **83**: p. 31-40.

9. Pechenov, S., et al., *Injectable controlled release formulations incorporating protein crystals.* J. Control. Rel., 2004. **96**: p. 149-158.

10. Roy, J.J. and T.E. Abraham, *Strategies in making cross-linked enzyme crystals.* Chem. Rev., 2004. **104**(9): p. 3705-3721.

11. Ovadia, H., A.M. Carbone, and P.Y. Paterson, *Albumin magnetic micrsopheres: a novel carrier for Myelin basic protein.* J. Immunol. Methods, 1982. **53**(1): p. 109-122.

12. Sinha, V.R. and A. Trehan, *Biodegradable microspheres for protein delivery.* J. Control. Rel., 2003. **90**(3): p. 261-280.

13. Wang, G., et al., *Preparation of BMP-2 containing bovine serum albumin (BSA) nanoparticles stabilized by polymer coating.* Pharm. Res., 2008. **25**(12): p. 2896-2909.

14. Elzohghby, A.O., W.M. Samy, and N.A. Elgindy, *Albumin-based nanoparticles as potential controlled release drug delivery systems.* J. Control. Rel., 2012. **157**: p. 168-172.

15. Arakawa, T. and S.N. Timasheff, *Mechanism of protein salting in and salting out by divalent cation salts: balance between hydration and salt binding.* Biochem., 1984. **23**: p. 5912-5923.

16. Munishkina, L.A., et al., *Guiding protein aggregation with macromolecular crowding.* Biochem., 2008. **47**(34): p. 8993-9006.

17. Hamilton, S., et al., *Effect of imidazole on the solubility of a his-tagged antibody fragment.* Hybrid Hybridomics., 2003. **22**(6): p. 347-355.

18. Jayabharathi, J., et al., *Binding interaction of bioactive imidazole with bovine serum albumin - A mechanistic investigation.* Spectrochim Acta A, 2011. **83**(1): p. 587-591.

19. Migneault, I., et al., *Glutaraldehyde: behavior in aqueous solution, reaction with proteins, and application to enzyme crosslinking* BioTech. , 2004. **37**: p. 790-802.

20. Dooley, C., et al., *Imaging dynamic redox changes in mammalian cells with green fluorescent protein indicators.* J. Biol. Chem., 2004. **279**(22284-22293).

21. Arpino, J.A., P.J. Rizkallah, and D.D. Jones, *Crystal strcuture of enhanced green fluorescent protein to 1.35 Å resolution reveals alternative conformation for Glu222.* Plos One, 2012. **7**(10): p. e47132.

22. Royant, A. and M. Noirclerc-Savoye, *Stabilizing role of glutamic acid 222 in the structure of Enhanced Green Fluorescent Protein.* J. Struct. Biol., 2011. **174**(2): p. 385-390.

23. Clark, J.H., et al., *Imidazole-Trimethyl phosphate system: characterization of the hydrogen bonding by fast=atom-bombardment mass spectrometry and X-ray crystallography.* JACS, 1984. **106**: p. 4056.

24. Lieleg, O., R.M. Baumgartel, and A.R. Bausch, *Selective filtering of particles by the extracellular matrix: an electrostatic bandpass.* Biophys J., 2009. **97**: p. 1569-1577.

25. Weigel, P.H. and J.A. Oka, *Temperature dependence of endocytosis mediated by the asialoglycoprotein receptor in isolated rat hepatocytes.* J. Biol. Chem., 1981. **256**: p. 2615-2617.

26. Silverstein, S.C., R.M. Steinman, and Z.A. Cohn, *Endocytosis.* Ann. Rev. Biochem., 1977. **46**: p. 669-722.

CHAPTER 5: USE OF BACTERIAL EFFECTOR NANOPARTICLES FOR THE TREATMENT OF INFLAMMATORY BOWEL DISEASE

Bacterial pathogens have evolved mechanisms to suppress inflammatory and immunoregulatory pathways through active modulation of intracellular signalling pathways [1, 2]. *Salmonella,* is one such pathogen. It uses AvrA, an acetyltransferase protein effector, to covalently modify and inactivate members of the MAPK and NF-κB pathways [3]. AvrA specifically blocks activation of NF-κB and MAPK JNK signaling [4, 5] and thus, can act as a potent inflammatory suppressor.

For this reason, AvrA has potential as a therapeutic agent for inflammatory bowel disease (IBD), a group of chronic relapsing disorders of the intestinal tract. IBD manifests with acute and chronic inflammation orchestrated by inflammatory cytokines[6] that could be decreased by the activity of AvrA. However, delivery through the harsh environment of the gastrointestinal tract to the resident epithelial and immune cells remains a challenge. As shown in Chapter 4, nanoparticles deliver protein and enzymes to a variety of cells more efficiently than soluble formulations. Multiple types of nanoparticles have been investigated for delivery of IBD therapeutics [7-11]. Nanoparticles enable drug accumulation in inflamed tissue with higher efficiency than when given in solution [11], reduce side effects and lower dose requirements[12]. In addition, these delivery vehicles have the ability to pass through physiological barriers, evade phagocytosis and more importantly, induce longer lasting results than soluble formulations [10].

In this chapter, the desolvation process that was previously presented is adapted to create environment-responsive eGFP+AvrA nanoparticles using DTSSP as the cross-linking agent. Particle size is controlled by varying the concentration of imidazole.

Resulting particles are 100-300 nm in diameter for different concentrations of imidazole and size distribution width is observed to decrease with increasing imidazole concentration. eGFP+AvrA nanoparticles are characterized in various buffers that simulate reducing conditions in the cytoplasm and harsh conditions in the gastrointestinal tract. Evidence suggests that DTSSP cross-linked nanoparticles aggregate in reducing buffers but disassemble into single molecules inside of cells. Intestinal fluid simulations demonstrate that particle formulations do not offer additional protection to proteins in harsh conditions, in comparison to soluble formulations. Finally, particle internalization and delivery of active AvrA to model epithelial and immune cells is demonstrated.

5-1 Experimental details

5-1-1 Particle preparation

Protein particles were prepared as described in Chapter 4. In brief, 600 μg of eGFP and ~25 μg of AvrA or mutant AvrA (mAvrA) in 100 μl imidazole solution (250 mM imidazole, 300 mM NaCl, 50 mM NaH_2PO_4; pH 8) were placed in a glass vial. The protein solution was desolvated by continuous, drop-by-drop addition of 400 μl ethanol at a rate of 1 ml/min. After desolvation, particles were cross-linked with DTSSP (Pierce) at a ratio of cross-linker to lysines of 1:2.2. After 2 h stirring at 650 rpm, the cross-linking reaction was stopped by centrifugation at 1000 g for 1 min and removal of supernatant. Particles were re-suspended in 2 ml of phosphate buffered saline (PBS, 10 mM NaH_2PO_4, 137 mM NaCl, 2.7 mM KCl, 2 mM KH_2PO_4; pH 7.4) and sonicated on ice for 1s every 15 s at 30% amplitude, for a total of 5 minutes.

5-1-2 Calculation of AvrA molecules in particles

In order to calculate the approximate number of AvrA molecules in a given particle the maximal density theorem or Kepler conjecture was used. Kepler stated that the maximal density of sphere packing in three dimensions occurs for face-centered cubic

or hexagonal close packing, in which $\pi/\sqrt{18}$ of the volume is occupied by spheres [13, 14]. This theorem assumes that all spheres are the same size and that they are uniformly packed. For this reason, all proteins were assumed to be spheres of the same diameter. Since, eGFP and GST are ~4 nm in diameter when measured with DLS and AvrA-GST fusion proteins are ~6-8 nm, the fusion proteins were assumed to be two independent spheres (each d= 4 nm) bound together by a flexible bridge. Thus, the number of AvrA molecules was calculated as follows:

The number of protein spheres per particle

$$N_s = \frac{\frac{4}{3}\pi(r_n)^3 \cdot \frac{\pi}{\sqrt{18}}}{\frac{4}{3}\pi(r_p)^3}$$

And the number of AvrA molecules per particle

$$N_{AvrA} = N_s \cdot X_{AvrA}$$

Where r_n is the radius of the particles, r_p is the radius of the protein spheres (2 nm) and X_{AvrA} is the molar fraction of AvrA in the particle.

5-1-3 Determination of particle size and zeta potential

Particle size distribution and zeta potential were measured and reported as explained in Chapter 4.

5-1-4 Particle preparation for scanning electron microscopy and atomic force microscopy

Scanning electron microscopy (SEM) and atomic force microscopy (AFM) were used to visualize the size and shape of produced eGFP+AvrA and eGFP+mAvrA particles. Particles were prepared for imaging by further crosslinking with glutaraldehyde after fabrication. 5 µl droplets of nanoparticles suspended in water were placed on an SEM specimen stub or on a glass slide. The droplet was then frozen in liquid nitrogen vapor and immediately lyophilized for 24 hours. Samples were coated with gold/palladium and imaged at 3 kV using a Zeiss Ultra60 FE-SEM or an Agilent picoplus AFM system.

5-1-5 Cell Culture

J774 macrophage cells were purchased from the American Type Culture Collection (ATCC) and SK-CO15 epithelial cells were a generous gift from Dr. Andrew Neish. J774 cells were cultured in Dulbecco's Modified Eagle's Medium (DMEM), supplemented with 10% (v/v) fetal bovine serum (FBS). SK-CO15 epithelial cells were cultured in DMEM with 10% FBS and 1% non-essential amino acids. All media and serum was purchased from Cellgro, Mediatech and supplemented with 1% (v/v) penicillin/streptomycin. Cells were incubated at 37°C in a 5% CO_2 humidified atmosphere.

Cells used for experiments were passaged at least two times before use and did not exceed passage number 20. Cell morphology and normal behavior were verified before use.

5-1-6 Cellular internalization of nanoparticles

Uptake of particles was assessed by flow cytometry. Cells were seeded at a density of $1x10^5$ per well in a 48-well plate in complete growth medium. After 16 h cell culture media was changed and cells were incubated with eGFP+AvrA particles (150 μg/ml) in complete growth medium for 6 h. Cells were washed twice with PBS, trypsinized, and collected in 1.7 ml tubes. Cells were washed twice more by centrifugation (500 rpm for 5 min) in PBS, re-suspended in PBS, filtered with a 35 μm cell strainer and placed on ice. The cells were immediately analyzed in an Accuri C6 (Becton Dickinson and Company) flow cytometer and relative particle uptake was quantified as the ratio of mean fluorescence of the sample population to mean fluorescence of the control population (no particles given).

5-1-7 Intracellular detection of AvrA particles

J774 macrophages or SK-CO15 epithelial cells were plated at a density of $2x10^5$ cells per well in a 24-well dish. After 14-16 hours of incubation, cell media was replaced with fresh media containing 300 μg/ml AvrA nanoparticles or soluble AvrA and incubated for 6 hours. Control cells were incubated with AvrA nanoparticles or soluble AvrA at 4^oC. Next, cells were washed twice with ice cold PBS and scrapped or trypsinized and fixed with 3.7% paraformaldehyde for 15 minutes at room temperature. Fixed cells were washed 3 times by centrifugation with ice cold PBS and then permeabilized with 0.25% Triton X-100 in PBS for 15 minutes at room temperature. Cells were rinsed three times in PBS and incubated with anti-AvrA serum in 6% BSA and 10% FBS in PBS for 1h. After this, cells were washed 3 times with PBS and then incubated with 20nM Qdot 655 VIVID secondary antibody conjugate (Invitrogen) in 6% BSA in PBS, for 1h. Finally, cell were washes 3 more times with PBS. Labeled cells and controls were analyzed in an LSR II flowcytometer (Becton Dickinson and Company) flow cytometer. Positive events were identified as cells with simultaneous increase in green fluorescence and quantum dot fluorescence.

5-1-8 Particle break-up in cell lysate and *in vitro*

To detect the break-up of eGFP+AvrA nanoparticles 200 μg/ml of particles were incubated 1-10 mM GSH in PBS, to simulate reducing conditions observed in the intracellular cell environment. After 0-60 minutes of incubation particles were loaded onto 12% SDS-PAGE gels using a non-reducing loading buffer (62.5 mM Tris-HCl, 10% glycerol, 1% SDS and 0.005% Bromophenol blue). Gels were run at 135 V for 120 minutes and proteins were transferred to nitrocellulose membranes at 400mV for 40 minutes. Proteins were detected using anti-penta HIS antibodies conjugated to Alexa 488 (Qiagen). Membranes were imaged in a Typhoon Imager (GE Healthcare) at 550 PMT.

5-1-9 Statistical analysis

All quantitative experiments were triplicated and presented as arithmetic mean ± standard deviation. One-way analysis of variance (ANOVA) was used to determine

significance among groups, using StatPlus. P values <0.05 among groups were considered statistically significant.

5-2 AvrA nanoparticle design considerations

IBD presents a challenging target for drug delivery. Contrary to most oral therapeutic regimes, maximal intestinal wall drug absorption is required while minimal systemic levels are desired [15]. Several delivery strategies are currently being employed to accomplish this goal. Local enemas, drug molecule modification for X benefit/goal, controlled and delayed-release particle formulations are some examples of these strategies [16, 17] .

Nanoparticles have been found to accumulate in inflamed tissue in the gut and thus, can increase drug levels in the affected intestinal wall while reducing systemic absorption [11]. For this reason, encapsulation of AvrA in nanoparticles was hypothesized to be advantageous for effective delivery to intestinal epithelial and immune cells affected by IBD. In order for these particles to serve as a successful delivery system, three conditions must be met. First, particles must be able to cross the mucosal layer that lines the intestine and reach the target cells. Second, AvrA must be released from the nanoparticles in the cell cytoplasm for it to bind and acetylate its molecular targets in the MAPK/JNK and NF-κB pathways. Third, drug doses must be carefully balanced to reduce inflammation while preventing systemic alterations such as immunosuppression.

5-2-1 Effector delivery to cells

Though nanoparticles provide a major advantage for IBD drug delivery in their ability to accumulate in inflamed tissues, penetration of the surface mucus layer and entry into cells are important barriers that must be overcome, as per the first condition. Particle size and surface chemistry have been identified as key factors that greatly affect both mucus penetration and cellular internalization [18].

The initial barrier the particles will encounter is the surface mucus layer that lines the intestine (Figure 5.1). Mucus is a complex viscoelastic gel, which serves as a physical barrier that protects tissue that would otherwise be exposed to the external environment. At the microscopic level, mucus is a hydrated network of cross-linked and entangled mucin fibers [19]. In order for particles to traverse the mucus layer low particle adhesive interaction with mucin fibers and particle diameter must be smaller or of similar size as the average interfiber spacing [18-20]. Mucin is negatively charged and highly hydrophobic. To prevent adhesion to mucin fibers, the AvrA nanoparticle surface should be hydrophilic and anionic or neutral. In addition, particle diameter should be smaller than ~500nm to be able to fit through the average interfiber spaces and diffuse through the mucus [20].

The next barrier the particles will encounter is entry into cells. In IBD, immune cells and epithelial cells are at the core of alterations in mucosal immunity and gastrointestinal physiology [21, 22]. Epithelial cells are the major constituents of the intestine, and these undergo rapid and remarkable changes in response to elevated levels of inflammatory cytokines produced by immune cells. For this reason, AvrA particles must be able to deliver their cargo to both types of cells.

Epithelial cells internalize particles through a variety of mechanisms that include clathrin-mediated, caveolae-mediated and receptor-mediated endocytosis, or macropinocytosis [23]. Immune cells, such as macrophages, continuously sample their environment and thus, uptake significant amounts of particles [24, 25]. Though macrophages are usually associated with phagocytosis, macropinocytosis and endocytosis are also common particle internalization mechanisms, especially nanoparticles. All of these particle internalization routes are energy dependent and are affected by particle size, shape and surface chemistry. Small particles (50-200 nm in diameter) are internalized at higher rates than larger particles [26]. Increased particle internalization has been observed for charged particles versus neutral particles [27]. Internalization of

nanoparticles with higher-aspect-ratio occurs more rapidly and efficiently than more symmetric particles [28].

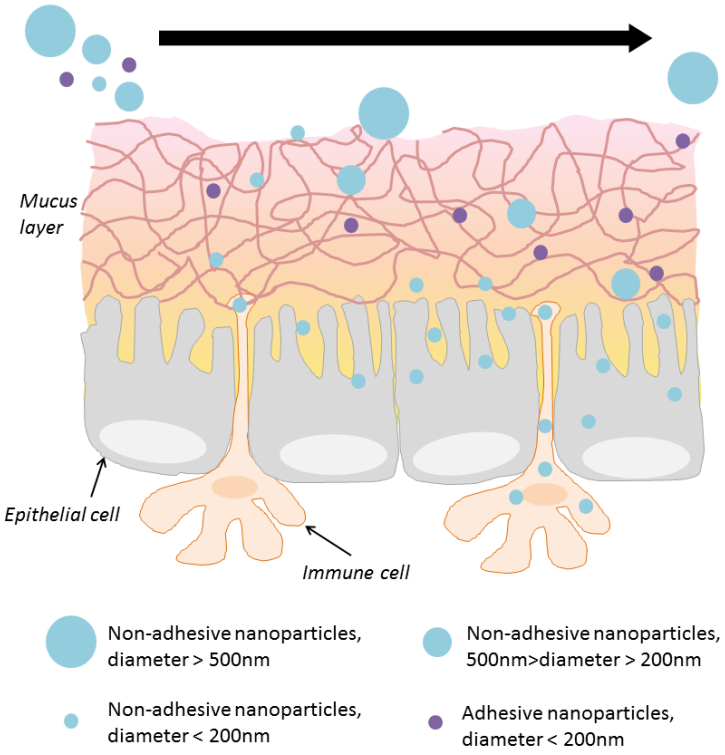

Figure 5.1. Schematic representation of the effect of particle size and surface properties on effective AvrA delivery to cells. Large particles (>500 nm) are unable to penetrate the mucus layer and thus, are unable to deliver the effector to the cells. Medium sized particles (200-500 nm) are able to penetrate the mucus layer but are not readily internalized by cells. Small particles that adhere to mucin are able to penetrate the mucosa but do not effectively reach the cells. Small particles (<200nm) traverse the mucosal layer and are readily internalized by cells. Adhesive nanoparticles (hydrophobic and/or cationic) bind to mucin fibers and are unable to deliver the effector to the cells. Schematic representation not drawn to scale.

In order to effectively deliver AvrA to cells, particles must simultaneously meet the necessary conditions for traversing mucus and particle internalization. In general,

small particles (50-200 nm in diameter) would be able to diffuse through the mucus pores formed by mucin mesh spacing and be easily internalized by cells (Figure 5.1). In addition, particles must not adhere to mucin fibers so should be hydrophilic and near neutral. Since AvrA contains several hydrophobic patches within its sequence, it is possible that it may adhere to the fibers if unfolded by the desolvation process. This possibility and the enzymatic activity loss observed in chapter 4, indicate that AvrA particles should include a carrier protein. BSA and eGFP are good candidates for carrier proteins, but as previously shown eGFP yields reproducible particles that are easy to visualize inside cells. Additionally, eGFP is highly hydrophilic and negatively charged at physiological pH and hence, would not adhere to mucin.

5-2-2 AvrA release inside cells

Next, as per the second condition, AvrA particles must be able to release their cargo inside cells so that the effector protein reaches its target molecules in the cytoplasm. As shown in the previous chapter, DTSSP and BS^3 cross-linking of enzyme+carrier particles yields particle break-up inside cells and active enzyme release. Consequently, AvrA particles were cross-linked with DTSSP to enable AvrA release from nanoparticles inside cells.

5-2-3 AvrA dosage

The dose of AvrA must be balanced to reduce inflammation while preventing systemic immunosuppression and other side effects. Real time imaging of a *Salmonella* model infection has shown that a different TTSS-secreted effector, SipA, mediates biochemical functions within minutes of infection at a concentration of 1000 molecules/cell [29]. Thus, pathogens efficiently modulate cellular activity with low effector doses. For this reason, mimicking these low doses was hypothesized to provide a balance between function and prevention of side effects. By applying the maximal density theorem [13, 14] and assuming that each protein is a sphere, the number of molecules of AvrA in a particle can be estimated. Each 150 nm-diameter particle made

entirely of AvrA contains ~19,500 AvrA-GST molecules. eGFP+AvrA particle, containing 3.5wt% AvrA, has ~550 AvrA-GST molecules. In summary, particles were designed to efficiently deliver AvrA to affected cells by selecting eGFP as a carrier, DTSSP as cross-linker and particle size restrictions of 50-200 nm in diameter (Figure 5.2).

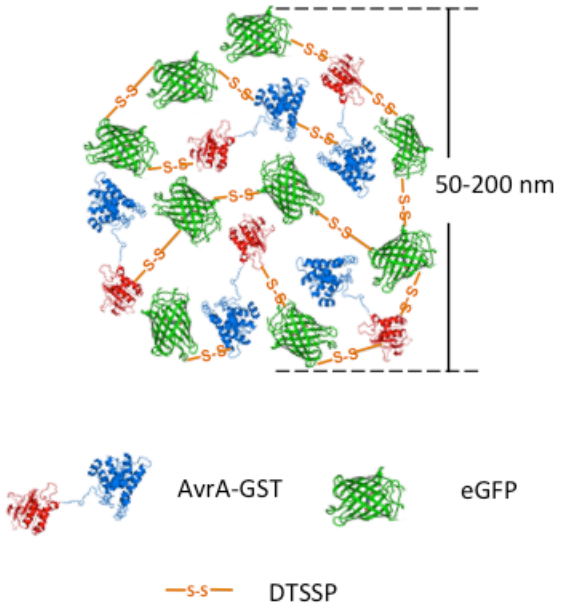

Figure 5.2. eGFP+AvrA nanoparticle design. Small particles (50-200nm) made of DTSSP cross-linked AvrA and eGFP are expected to penetrate the mucus barrier, enter target cells and break-up in reducing conditions observed inside cells to release AvrA.

To account for side effects induced simply by the presence of bacterial proteins and establish that therapeutic activity results solely from enzymatic action of AvrA, a mutant version of AvrA (mAvrA) was used. The mutant form contains a single cysteine substitution (C186A) that renders the acetyltransferase inactive and eliminates JNK inhibition and attenuates NF-κB suppressive activity [4]. Since mAvrA differs from AvrA by a single amino acid mutation in the catalytic site, particle production,

optimization and characteristic were expected to be similar. The next sections show particle size optimization, characterization and delivery of AvrA/mAvrA to cells.

5-3 Optimization of AvrA+eGFP nanoparticles

In the previous chapter, production of β-gal+eGFP nanoparticles was studied, characterized and optimized. However, the properties of eGFP, β-gal and AvrA-GST vary significantly and so will the exact fabrication conditions for optimal particles. The main differences between eGFP, β-gal and AvrA-GST/mAvrA are size (26.9 kDa, 465.2 kDa and 61 kDa, respectively), solubility (eGFP > β-gal>> AvrA-GST) and presence of His-tag (eGFP and AvrA-GST contain His-tag, β-gal does not). These differences affect the desolvation process and yield different particle sizes and process efficiencies. This section focuses on optimization of eGFP+AvrA/mAvrA particle size to fit the requirements for traversing mucus and cellular internalization.

5-3-1 Pure AvrA nanoparticles

Production of particles directly from AvrA/mAvrA yielded large particles. Average particle diameter was >400 nm and larger aggregates were observed. Due to the large particle size of pure enzyme particles, possible enzyme activity loss during fabrication, AvrA dosage requirements and imaging capabilities when eGFP is used as a carrier protein, pure AvrA/mAvrA nanoparticles were not pursued any further.

5-3-2 Effect of imidazole on particle size

Introducing β-gal in the eGFP formulation (eGFP+β-gal) was previously shown to yield two distinct particle populations. However, incorporation of AvrA to eGFP formulations (eGFP+AvrA) yielded a single population of particles with average diameters of 303 ± 45nm (Figure 5.3); similar results were observed with mAvrA. Since

the maximum desirable particle diameter was 200 nm, the process was optimized for smaller particle production.

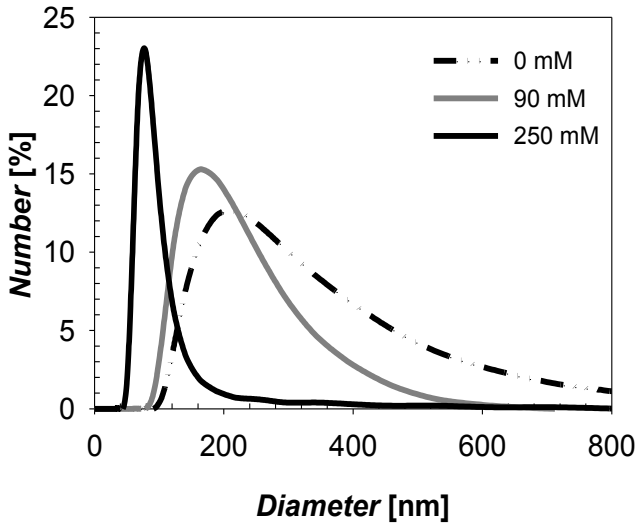

Figure 5.3. Effect of imidazole on eGFP+AvrA particle size and distribution. Different concentrations of imidazole were used in the initial protein solution to control particle size.

Earlier studies showed imidazole decreases eGFP particle size as a result of increased protein solubility. Similarly, imidazole was observed to control eGFP+AvrA/mAvrA particle size; increasing imidazole concentration significantly decreased average particle diameter (Figure 5.3). As mentioned in the previous chapter, high protein solubility delays protein nucleation and thus, leads to the formation of smaller particles. Both AvrA/mAvrA and eGFP contain a C-terminal 6-His tag. Thus, their solubility is increased in the presence of imidazole, which in turn explains the observed decrease in particle size. In addition to controlling particle size, imidazole affected the polydispersity of the particles. The width of the size distribution peak

decreased as the amount of imidazole increased (Figure 5.4). This could be the result of a more uniform nucleation process due to increased solubility.

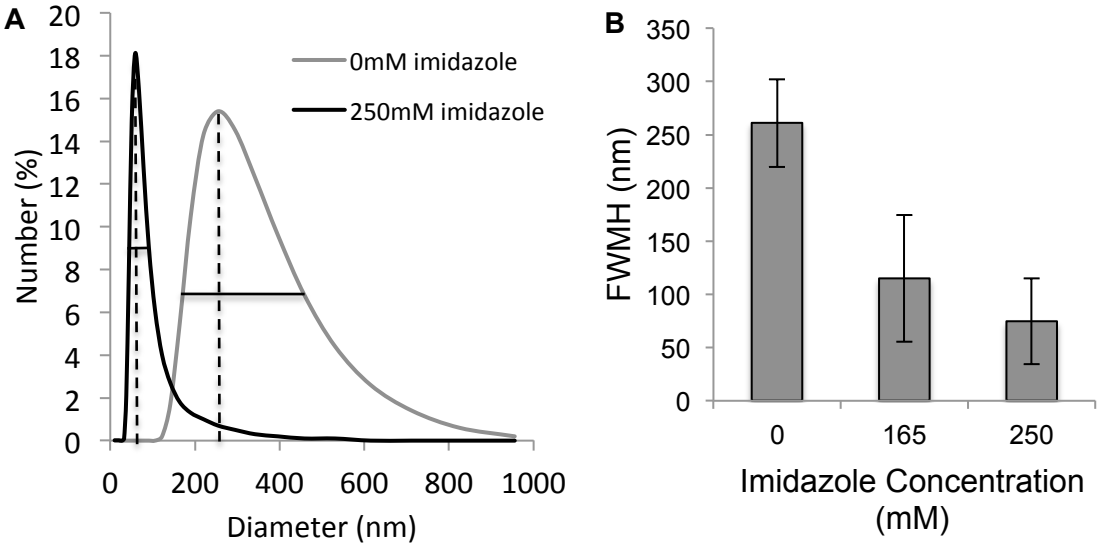

Figure 5.4. Effect of imidazole on eGFP+AvrA particle size polydispersity. ***(A)*** comparison of size distribution peak width for particles fabricated in 0 mM and 250 mM ***(B)*** average full-width at maximum height (FWMH) for particles fabricated in different imidazole concentrations. Error bars represent standard deviation, N=3.

Particles produced in the presence of imidazole exhibit average diameters within the desirable size range (50-200 nm). eGFP+AvrA particles produced in 125 and 250 mM imidazole were 131±47 nm and 95±18 nm in average diameter, respectively. Since smaller delivery vehicles could lead to higher accessibility to target cells, *in vitro* and *in vivo* studies were performed only with eGFP+AvrA/mAvrA particles produced in 250 mM imidazole. Production yield of these particles was measured by quantifying the amount of protein that remains soluble after desolvation and cross-linking, and comparing it to the initial amount of protein used. The average amount of protein that formed eGFP+AvrA/mAvrA particles was 91% of the initial amount.

After particle size was optimized, the surface charge of particles was established. Zeta-potential was -11.6 ± 0.7 mV in PBS and -24.3 ± 1.1 mV in 10 mM HEPES buffer.

No significant difference in surface charge was observed between eGFP+AvrA and eGFP+mAvrA particles. All particles exhibited negative zeta-potential in 10 mM HEPES, a low ionic strength buffer, indicating inherent negative surface charge. In the presence of biologically relevant concentrations of ions (PBS), only slightly negative zeta-potentials were observed. This indicates that in physiological milieu ions adsorb to the particle surface and partially shield the surface charge. Nonetheless, near neutral or negatively charged particles can prevent attractive electrostatic interactions with negatively charged mucin fibers and decrease the potential for adhesion to mucus. These observations demonstrate that optimized eGFP+AvrA/mAvrA particles meet the size and surface charge criteria specified in the nanoparticle design.

5-3-3 SEM and AFM characterization of nanoparticles

The morphology of eGFP+AvrA/mAvrA particles was studied by SEM and AFM. Initial SEM imaging attempts demonstrated that DTSSP cross-linked nanoparticles are soft, which leads to shape loss during dehydration and preparation for imaging. Particles were also observed to fuse together, possibly during preparation or exposure to the electron beam, even at low acceleration voltage. Since particle features were not visible, new sample preparation techniques were implemented.

In order to increase particle stiffness and shape retention, particles were cross-linked a second time with GTA after fabrication and DTSSP crosslinking. Particles were then frozen, lyophilized and imaged, but shape loss and particle fusion persisted. Hence, the sample preparation process was modified and particles were frozen in liquid nitrogen vapor prior to lyophilization. This technique partially decreased particle fusion and shape loss, enough to allow visualization of some individual nanoparticles (Figure 5.5).

Individual nanoparticles were in the expected size range and exhibited sphere-like morphology. Interestingly, some small particulates were also visible on the surface of the protein nanoparticles and on the stub. SDS-PAGE analysis of eGFP+AvrA/mAvrA particles under non-reducing conditions revealed the presence of a band that corresponds

to eGFP, indicating there are soluble or "free" protein molecules in the particle suspension. It remains unclear if these proteins are on the surface of the particles, inside the particles or in solution. The small particulates observed in these images could be small clusters of the "free" eGFP protein, which are probably held together by the GTA used to stabilize the particles before imaging since they were not observed in samples without GTA crosslinking.

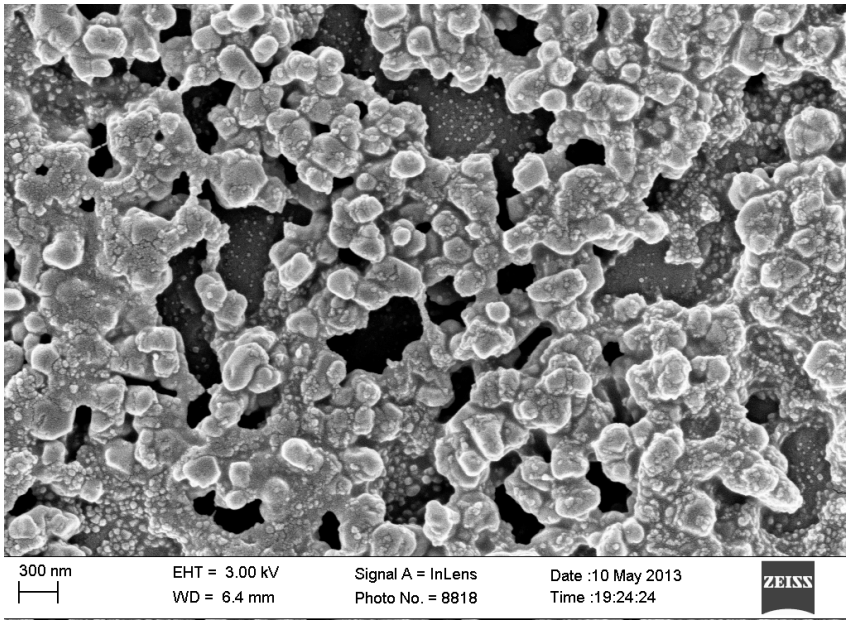

Figure 5.5. SEM image of eGFP+AvrA nanoparticles. Particles were further cross-linked with GTA after fabrication, frozen in liquid nitrogen and then lyophilized.

eGFP+AvrA/mAvrA particles were also imaged using atomic force microscopy. Images revealed the presence of small particles (<200 nm) and a few large aggregates (Figure 5.6). These large aggregates could be the result of additional cross-linking with GTA, similar to those observed in SEM images.

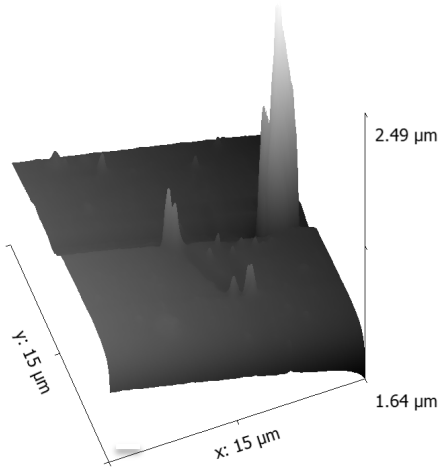

Figure 5.6. AFM image of eGFP+AvrA nanoparticles. 3D simulation of surface topography, note the existence of the small particles and large aggregates. Particles were prepared by further cross-linking with GTA, frozen in liquid nitrogen and lyophilized.

5-4 Characterization of nanoparticles in biologically relevant fluids

5-4-1 Effect of intestinal simulation fluids

Enzymes are highly sensitive to harsh environments and therefore, effective delivery to intestinal cells presents a challenge. Gastrointestinal fluids contain bile salts, lecithin and proteases, that could greatly affect enzymatic activity. In order to predict *in vivo* performance of eGFP+AvrA/mAvrA nanoparticles the effect of simulated intestinal fluids on eGFP fluorescence was measured.

Particles were incubated in fasted-state simulated intestinal fluid (FaSSIF) with or without 10 mg/ml pancreatin [30], for up to 5 hours. The fluorescence of soluble eGFP, eGFP nanoparticles and eGFP+AvrA nanoparticles was measured over time. No significant differences in fluorescence loss were observed between soluble and nanoparticle formulations incubated in FaSSIF with or without pancreatin. These results suggest that the nanoparticle formulation does not offer shielding or additional protection to the enzyme cargo, in comparison to soluble delivery.

5-4-2 Effect of intracellular reducing conditions

eGFP+AvrA/mAvrA nanoparticles were designed to release effector proteins only inside cells. DTSSP, the cross-linking agent, contains a disulfide bond that breaks in reducing conditions, as is observed inside cells. To establish the capacity of DTSSP cross-linked nanoparticles to break-up and release AvrA or mAvrA inside cells, intracellular conditions were simulated. For this purpose, particles were incubated in simulated intracellular reducing conditions using 1-10 mM glutathione (GSH) in PBS for 0-60 minutes. Particle breakup was studied using SDS-PAGE and western blot.

Particles incubated in GSH solutions were observed to release individual proteins before and after reducing treatments. However, longer incubation times yielded signal loss and hence, protein/enzyme release results were inconclusive. Figure 5.7 shows a preliminary study using eGFP+AvrA particles incubated in 5 mM GSH, separated in native PAGE and analyzed by western blot. Results were compared to particles cross-linked with GTA after standard fabrication (DTSSP, 250 mM imidazole), and to soluble eGFP+AvrA. GTA cross-linked particles served as non-reducible particle controls and soluble proteins indicated the location of soluble protein bands. As expected, no soluble protein bands were observed for GTA cross-linked particles. DTSSP cross-linked particles released single proteins with and without incubation in GSH. Intact particles did not penetrate the gel and were not visible in the western blot.

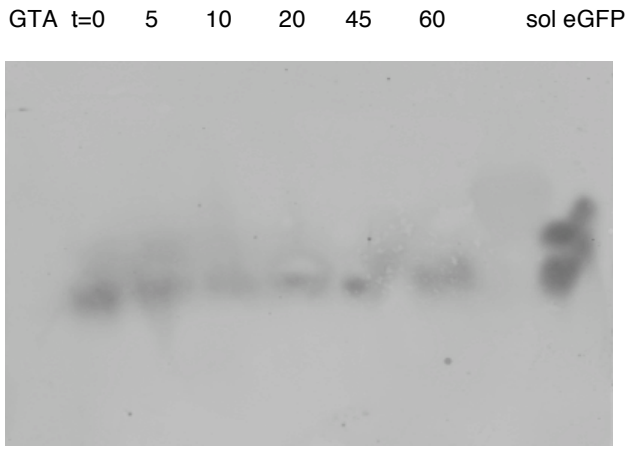

Figure 5.7. eGFP+AvrA particle degradation in 5mM GSH. Western blot probed with anti penta-His antibody showing release of soluble protein separated using a native protein electrophoresis gel. GTA cross-linked particles and soluble eGFP were used as controls

Further studies on eGFP+AvrA/mAvrA particle break-up were performed in non-reducing SDS-PAGE gels, in order to visualize intact particles. Several GSH concentrations were tested and no significant difference in particle break-up was observed for a range of 1-10 mM GSH. Similarly, no differences were observed in particle disassembly between eGFP+AvrA or eGFP+mAvrA. Figure 5.8 shows a time analysis of protein release in 10 mM GSH. SDS-PAGE and western blot results show the presence of "free" or soluble protein before and after exposure to reducing conditions. These findings suggest that particles are only partially cross-linked when DTSSP is used and SDS or the electric field helps to extract soluble protein.

By using SDS-PAGE gels instead of native gels intact particles or large pieces of the particles were able to partially penetrate the gel and thus, were visible in both the gel and western blot. Interestingly, the intensity of the nanoparticle bands was observed to decrease with time in the western blot but gel band intensity did not follow the same trend. Additional assays revealed that soluble or "free" protein band intensity also decreases with incubation time, in both gel and western blot studies.

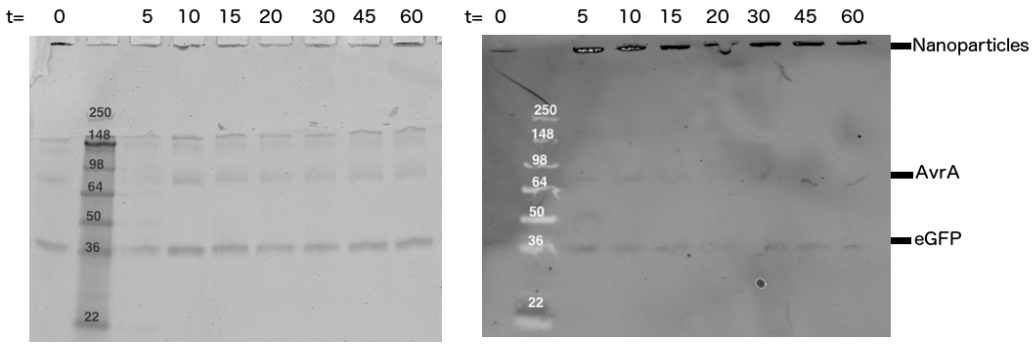

Figure 5.8. Time analysis of AvrA-eGFP nanoparticle break-up in 10mM GSH solution. *(left)* SDS-PAGE gel stained with coomasie blue *(right)* western blot probed with anti penta-His antibodies.

To understand these observations, particle size was monitored over time. Particles were incubated in 5 mM GSH and particle size distributions were measured every 15 minutes. DLS measurements indicated that particles aggregate in reducing buffers (Figure 5.9). Similar behavior has been reported in literature. Cheng et al. found that polymeric micelles cross-linked with DTSSP aggregate in reducing buffers, but interestingly not in cells [31]. Studies presented in chapter 4 show that DTSSP cross-linked eGFP particles break-up in HeLa cell lysates and release soluble protein.

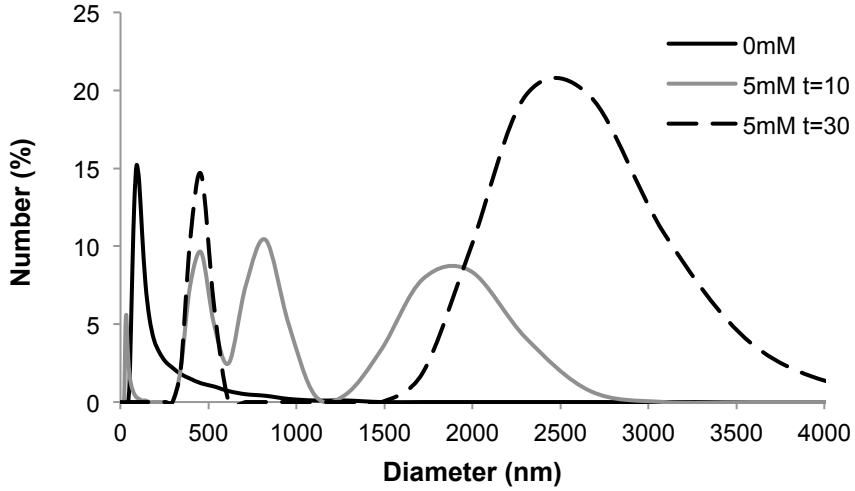

Figure 5.9. Effect of reducing conditions on size distribution of AvrA-eGFP nanoparticles. Particles were incubated with 5 mM GSH for 10-30 minutes. Size distribution of particles before incubation is shown for comparison (0 mM).

Since large aggregates or particles can mask signal from free proteins in DLS measurements, protein aggregates were removed by centrifugation (10,000g for 5 minutes) and samples were re-analyzed. Individual and smaller protein aggregates were observed (Figure 5.10). With the purpose of measuring the amount of free protein over time, 100 kDa ultrafiltration devices were used to separate particles and aggregates from free protein. However, the separation was not successful because intact particles went through the filters and consequently, changes in free protein concentration could not be accurately measured.

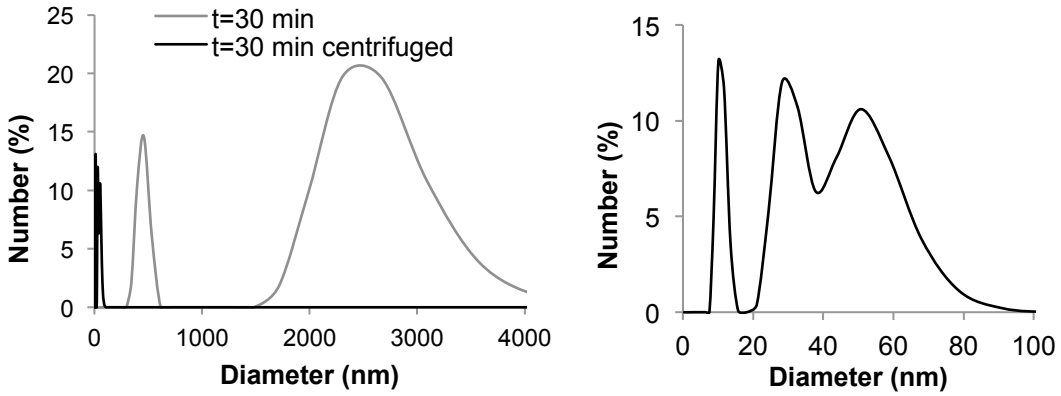

Figure 5.10. DLS measurements of eGFP+AvrA nanoparticles in 5 mM GSH *(left*) comparison of size distribution before and after centrifugation, and *(right)* size distribution detail of centrifuged eGFP+AvrA nanoparticles in 5mM GSH.

5-5 Delivery of AvrA effector to cells

Efficient delivery of AvrA to intestinal cells is crucial for effective treatment of IBD. Therefore, eGFP+AvrA/mAvrA nanoparticle uptake was measured in model epithelial and immune cells. Particle uptake was evaluated by quantifying the increase in cell fluorescence due to the presence of eGFP and using anti-AvrA antibodies to establish the presence of AvrA specifically within cells.

5-5-1 Particle internalization

As shown in chapter 4, internalization of particles varies from one cell type to another. For this reason, the particle uptake behavior of model intestinal epithelial cells and immune cells was performed. SK-CO15, a human intestinal epithelial cell line and J774.A1, a murine macrophage cell line, were used to measure uptake of soluble and nanoparticle formulations of AvrA. Particle internalization quantification by flow cytometry, measured by the increase in green fluorescence of cells, revealed that J774.A1 cells internalize much larger quantities of particles than SK-CO15 cells. The fluorescence of macrophages incubated with soluble and nanoparticle formulations of AvrA increased 35 and 114-fold, respectively (Figure 5.11). Whereas the fluorescence of epithelial cells

increased 2.2 and 2.4-fold when incubated with soluble AvrA with eGFP and eGFP+AvrA particles, respectively (Figure 5.12). These results were not surprising, since macrophages constantly sample their environment and are known to uptake higher amounts of particles than many other types of cells [25].

Cells were also incubated with AvrA at 4°C and uptake of particles and soluble protein was evaluated. Macrophages showed a 40-fold fluorescence increase when incubated with eGFP+AvrA particles and 2-fold increase when incubated with soluble formulations. Meanwhile, SK-CO15 did not show significant fluorescence increase when incubated with particle or soluble formulations of AvrA and eGFP. These results suggested that epithelial cells use only energy dependent mechanisms to internalize AvrA+eGFP nanoparticles and macrophages use a combination of energy dependent and independent uptake mechanisms.

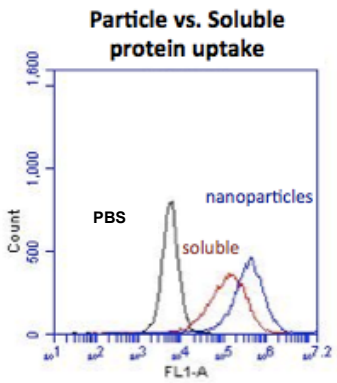

Figure 5.11. Particle internalization of J774.A1 cells. Representative flowcytometry fluorescence intensity histogram for cells incubated for 6 hours with PBS, soluble AvrA with eGFP and eGFP+AvrA nanoparticles.

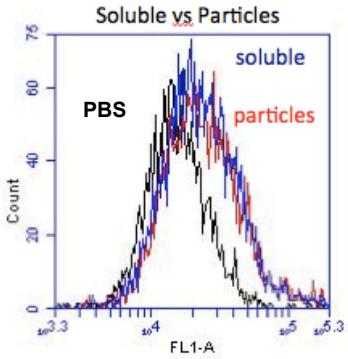

Figure 5.12. Particle internalization of SK-CO15 cells. Representative flowcytometry fluorescence intensity histogram for cells incubated for 6 hours with PBS, soluble AvrA with eGFP and eGFP+AvrA nanoparticles.

5-5-2 Intracellular detection of AvrA particles

Particle internalization assays presented above did not directly establish the presence of AvrA inside the cells. The evidence of internalized eGFP only suggested that AvrA was also co-delivered and internalized. To specifically quantify the uptake of AvrA, flow cytometry and anti-AvrA antibodies were used. Since the dose of AvrA delivered to the cell is very low (each 100nm particle contains approximately 117 molecules of AvrA), signal from the antibody was amplified using secondary antibodies bound to quantum dots.

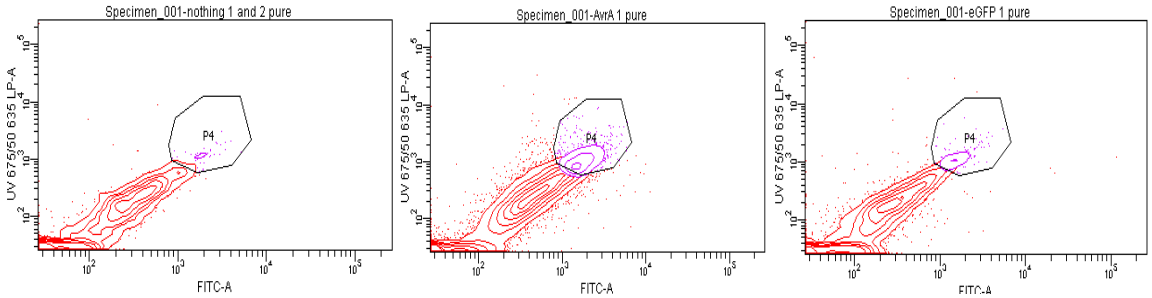

Figure 5.13. AvrA internalization studies on SK-CO15 cells. Topographical map shows distribution of cell populations for cell incubated for 6 hours with cell media, eGFP+AvrA nanoparticles or eGFP nanoparticles (from left to right). Cells were studied for anti-AvrA antibody fluorescence (y-axis) and eGFP fluorescence (x-axis).

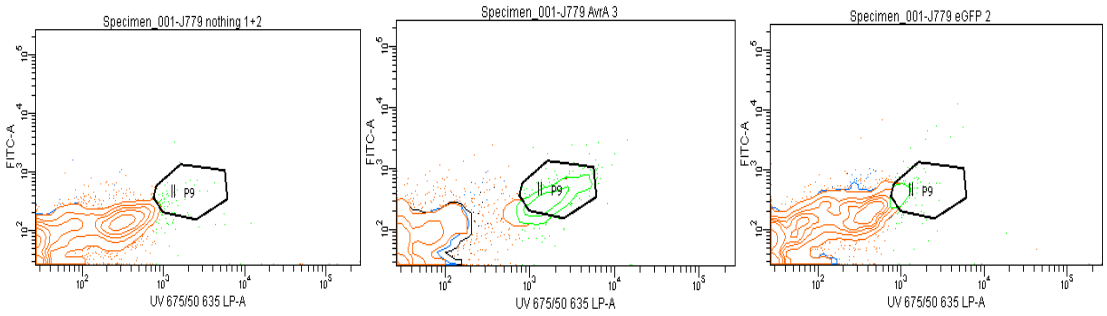

Figure 5.14. AvrA internalization studies on J774 cells. Heat map shows distribution of cell populations for cell incubated for 6 hours with cell media, eGFP+AvrA nanoparticles or eGFP nanoparticles (from left to right). Cells were studied for anti-AvrA antibody fluorescence (y-axis) and eGFP fluorescence (x-axis).

Uptake of eGFP+AvrA nanoparticles was established by counting the population of cells that showed a simultaneous increase in eGFP and anti-AvrA (quantum dot) fluorescence. SK-CO15 cells incubated with eGFP+AvrA antibodies exhibit a shift in population fluorescence of both fluorescent signals, greater than when incubated with eGFP only particles (Figure 5.13). This simultaneous increase is indicative of the presence of both eGFP and AvrA within the cells. Similarly, J774.A1 macrophages incubated with eGFP+AvrA nanoparticles form a new population that is positive for eGFP fluorescence and AvrA antibody binding (Figure 5.14). These results suggest that, in general, nanoparticle formulations delivered more AvrA effectors to cells (Figure 5.15).

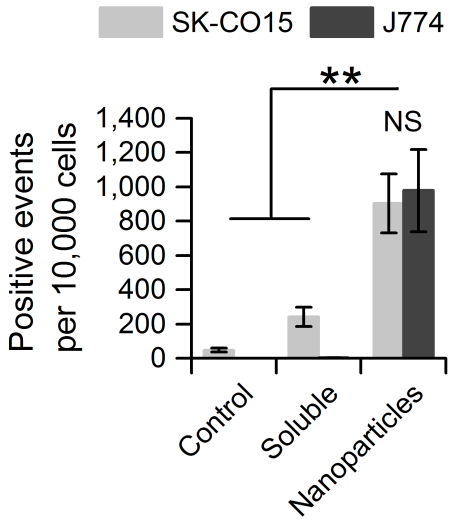

Figure 5.15. Summary of flow cytometry internalization data measuring AvrA in SK-CO15 and J774.A1 cells incubated with protein for 6 hours. Positive events were established by counting the population of cells that showed a simultaneous increase in eGFP and anti-AvrA.

5-6 Cytotoxicity of AvrA nanoparticles

Treatment of IBD requires reduction of inflammation in affected tissues without damage or cytotoxicity to the intestinal tissue. *Salmonella* injected AvrA has been previously shown to subvert the MAPK JNK and NF-κB pathways without inducing cell death [5]. Therefore, nanoparticle formulations were not expected to be cytotoxic to cells. Particle and soluble formulations of recombinant eGFP and AvrA/mAvrA were incubated with cells and no significant difference in cytotoxicity is observed between them and a control cells incubated with PBS (Figure 5.16).

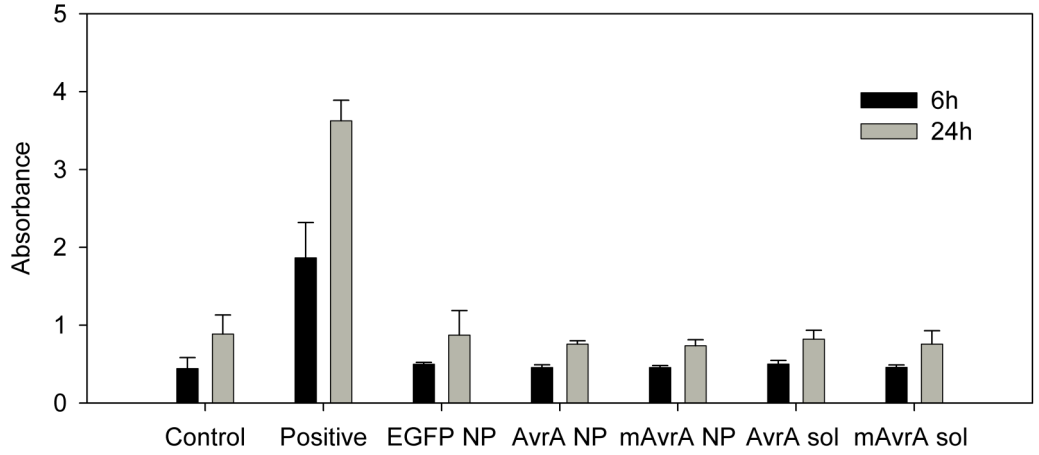

Figure 5.16. LDH cytotoxicity assay for J774.A1 cells incubated with soluble and nanoparticle formulations of eGFP+AvrA/mAvrA for 6 or 24 hours. Control cells were incubated with media and PBS, whereas positive cells were incubated with a cell lysis agent.

5-7 Evaluation of eGFP+AvrA particles *in vitro* and *in vivo*

Once particles were optimized, the Neish lab at Emory University evaluated the performance of eGFP+AvrA nanoparticles in *in vitro* and *in vivo* models of the disease. AvrA nanoparticles were shown to disassemble and release soluble AvrA in model polarized intestinal epithelial monolayers (T84 cells) and macrophages. Delivered AvrA was successful in partly suppressing both TNF-α induced JNK activation and IκB degradation in T84 cells. Additionally, AvrA nanoparticles markedly reduced secretion of the pro-inflammatory cytokine IL-8. eGFP+AvrA nanoparticles strongly inhibited primary murine polymorphonuclear leukocyte translocation across T84 monolayers, a critical inflammatory behavior.

To detect particle uptake into immune and endothelial cells *in vivo,* eGFP+AvrA nanoparticles were administered to mice via transrectal instillation into healthy and inflamed colons. Immediately after instillation, eGFP fluorescence was observed in the extracellular mucosal layer of normal and inflamed colon. After 3 hours, in healthy colon,

eGFP fluorescence was detected in epithelial cells and occasionally in immune cells. In inflamed colon, fluorescence markedly increased immune cells. This data proved that optimized eGFP+AvrA nanoparticles were capable of traversing the mucosal layer and were effectively internalized by epithelial and immune cells.

Furthermore, the anti-inflammatory potential of AvrA nanoparticles was demonstrated in multiple murine models. In a traditional murine peritonitis model of acute inflammation, pretreatment with AvrA particles resulted in significant reduction of neutrophil influx into the peritoneal cavity, an indicator of reduced inflammation. TNBS and DSS murine colitis models also showed eGFP+AvrA particles suppressed histologic inflammation and clinical symptoms for both pretreated tissues and in simulated therapy of existing disease.

5-8 Summary

The results presented in this chapter demonstrate the versatility of the protein+enzyme particle fabrication method and show the potential of bacterial effectors for therapeutic purposes. Specifically, this chapter focused on application of the effector AvrA for treatment of IBD. AvrA particles were designed to cross the mucosal layer that lines the intestine and deliver the enzyme to epithelial and immune cells that drive and sustain the disease. AvrA was successfully incorporated into eGFP nanoparticle formulations and particle size was controlled by varying imidazole concentration during fabrication. eGFP+AvrA nanoparticles were shown to aggregate in reducing buffers but disassembled into single proteins in reducing cellular environments. Furthermore, it was established that these protein particles effectively delivered AvrA to cells without cytotoxic effects. Significantly, *in vivo* studies performed by the Neish lab at Emory demonstrated eGFP+AvrA nanoparticles cross the mucosal layer, deliver the enzyme to epithelial and immune cells, and reduce inflammation. These results show the potential of

AvrA and other effectors as therapeutic agents and provide proof of the promise of protein particles for intracellular enzyme delivery.

5-9 References

1. Donnenberg, M.S., *Pathogenic strategies of enteric bacteria.* Nature, 2000. **406**: p. 768-774.

2. Ruter, C. and P.R. Hardwidge, *"Drug from bugs': bacterial effector protein as promising biological (immune-)therapeutics.* FEMS Microb. Lett., 2014. **351**: p. 126-132.

3. Du, F. and J.E. Galan, *Selective inhibition of type III secretion activated signaling by the Salmonella effector AvrA.* PLoS Pathog, 2009. **5**(9): p. e1000595.

4. Collier-Hyams, L.S., et al., *Cutting edge: Salmonella AvrA effector inhibits the key proinflammatory, anti-apoptotic NF-kappa B pathway.* J Immunol, 2002. **169**(6): p. 2846-50.

5. Jones, R.M., et al., *Salmonella AvrA coordinates suppression of host immune and apoptotic defenses via JNK pathway blockade.* Cell Host Microbe, 2008. **3**(4): p. 233-244.

6. Cosnes, J., et al., *Epidemiology and natural history of inflammatory bowel diseases.* Gastroenterology, 2011. **140**(6): p. 1785-1794 e4.

7. Meissner, Y., Y. Pellequer, and A. Lamprecht, *Nanoparticles in inflammatory bowel disease: particle targeting versus pH-sensitive delivery.* Pharma. Nanotech., 2006. **316**(1-2): p. 138-143.

8. Meissner, Y. and A. Lamprecht, *Alternative drug delivery approaches for the therapy of inflammatory bowel disease.* Journal of Pharmaceutical Sciences, 2008. **97**(8): p. 2878-2891.

9. Laroui, H., et al., *Drug-loaded nanoparticles targeted to the colon with polysaccharide hydrogel reduce colitis in a mouse model.* Gastroenterology, 2010. **138**(3): p. 843-853.

10. Lamprecht, A., et al., *Biodegradable nanoparticles for targeted drug delivery in treatment of inflammaory bowel disease.* J. Pharmacol. Exp. Ther., 2001. **299**(2): p. 775-781.

11. Laroui, H., et al., *Targeting intestinal inflammation with CD98 siRNA/PEI-loaded nanoparticles.* Molec. Ther., 2014. **22**(169-80).

12. Wachsmann, P. and A. Lamprecht, *Polymeric nanoparticles for the selective therapy of inflammatory bowel disease.* Methods Enzymol., 2012. **508**: p. 377-397.

13. Blachman, N.M., *The closet packing of equal spheres in a larger sphere.* Am. J. Math. Monthly, 1963. **70**(5): p. 526-529.

14. Hales, T.C., *Cannonballs and honeycombs.* Notices Am. Math. Soc. , 2000. **47**(4): p. 440-449.

15. Kesisoglou, F. and E.M. Zimmermann, *Novel drug delivery strategies for the treatment of inflammatory bowel disease.* Expert Opin. Drug. Deliv., 2005. **2**(3): p. 451-463.

16. Fiorino, G., et al., *New drug delivery systems in inflammatory bowel disease: MMX and tailored delivery to the gut.* Curr. Med. Chem., 2010. **17**(17): p. 1851-1857.

17. Lautenschlager, C., et al., *Drug delivery strategies in the therapy of inflammatory bowel disease.* Adv. Drug Deliver. Rev., 2014. **71**: p. 58-76.

18. Lai, S.K., Y.Y. Wang, and J. Hanes, *Mucus-penetrating nanoparticles for drug and gene delivery to mucosal tissues.* Advanced Drug Delivery Reviews, 2009. **61**(2): p. 158-171.

19. Dawson, M., et al., *Transport of polymeric nanoparticle gene carriers in gastric mucus.* Biotechnol. Prog. , 2004. **20**: p. 851-857.

20. Lai, S.K., et al., *Micro- and macrorheology of mucus.* Adv. Drug Deliv. Rev., 2009. **61**(2): p. 86-100.

21. Cromer, W.E., et al., *Role of the endothelium in inflammatory bowel diseases.* World J. Gastroenterol., 2011. **17**(5): p. 578-593.

22. Neurath, M.F., *Cytokines in inflammatory bowel disease.* Nat. Rev. Immunol., 2014. **14**: p. 329-342.

23. Silverstein, S.C., R.M. Steinman, and Z.A. Cohn, *Endocytosis.* Ann. Rev. Biochem., 1977. **46**: p. 669-722.

24. Lawrence, T. and N. Gioacchino, *Transcriptional regulation of macrophage polarization: enabling diversity with identity.* Nat. Rev. Immunol. , 2011. **11**: p. 750-761.

25. Weissleder, R., M. Nahrendorf, and M.J. Pittet, *Imaging macrophages with nanoparticles.* Nature Materials, 2014. **13**: p. 125-138.

26. Rejman, J., et al., *Size-dependent internalization of particles via the pathways of clathrin- and caveolae-mediated endocytosis.* Biochem. J., 2004. **377**: p. 159-169.

27. Wang, G., et al., *Preparation of BMP-2 containing bovine serum albumin (BSA) nanoparticles stabilized by polymer coating.* Pharm. Res., 2008. **25**(12): p. 2896-2909.

28. Gratton, S.E.A., et al., *The effect of particle design on cellular internalization pathways.* Proc. Nat. Acad. Sci. , 2008. **105**(33): p. 11613-11618.

29. Schlumberger, M.C., et al., *Real-time imaging of type III secretion: Salmonella SipA injection into host cells.* Proc Natl Acad Sci U S A, 2005. **102**(35): p. 12548-53.

30. Marques, M.R.C., R. Loebenberg, and M. Almukainzi, *Simulated biological fluids with possible application in dissolution testing.* Dissolution Tech., 2011. **3**: p. 15-28.

31. Cheng, X., R. Liu, and Y. He, *A simple method for the preparation of monodisperse protein-loaded microspheres with high encapsulation efficiencies.* European Journal of Pharmaceutics and Biopharmaceutics, 2010. **76**(3): p. 336-341.

CHAPTER 6: SELF-ASSEMBLED YOPJ NANOPARTICLES FOR THE TREATMENT OF BREAST CANCER

Bacterial pathogen evolution has produced proteins that can trigger apoptosis of host cells during infection by inhibiting protein synthesis, forming pores on cell membranes, or by activating the death machinery of cells[1]. Some of these proteins, known as bacterial effectors, activate the death machinery by co-targeting multiple intracellular signaling pathways [2-5]. These effectors have high potential as therapeutic agents for cancer because they can trigger apoptosis through a variety of different mechanisms[6].

YopJ and its homologue, YopP, are potent pro-apoptotic effectors from *Yersinia pestis and Yersinia pseudotuberculosis*. These effectors inhibit the MAPK and NF-κB pathways by acetylating key kinases [7, 8]. Among these inhibited pathways is the extracellular signal-regulated kinase (ERK), which has been correlated to invasion and metastasis in multiple breast cancer models [9]. In addition, YopJ/P is cell selective, as it induces apoptosis in macrophages but not in endothelial cells or neutrophils [10, 11]. These traits make YopJ/P an exceptional candidate for treatment of breast cancer. Nonetheless, the intrinsic bacterial pathogenicity, lack of targeting, and possible genetic instability are difficult challenges that currently preclude the use of *Yersinia* or other bacterial pathogens in the clinic.

In this chapter, feasible YopJ cancer therapeutics are created by replacing the pathogen secretion mechanism with a delivery vehicle made of YopJ protein itself. For this purpose, YopJ is genetically fused to glutathione S-transferase (GST) to induce self-assembly, via protein-protein interactions, into stable 100 nm diameter particles. These nanoparticles are characterized under different conditions and are shown to successfully deliver YopJ to cancer cells. The effect of YopJ-GST particles on various breast cancer

cell lines is studied and compared to a common chemotherapeutic agent, doxorubicin (dox). Evidence indicates that YopJ-GST is more effective than dox in inducing cell death in all breast cancer cell lines. Unlike dox, sub-lethal doses of YopJ-GST particles are shown to decrease cell migration and down-regulate the ERK1/2 pathway. Finally, the selective cytotoxicity of the nanoparticles is demonstrated as YopJ-GST nanoparticles are not cytotoxic to NIH/3T3 or HeLa cells, unlike dox.

6-1 Experimental details

6-1-1 Determination of particle size and zeta potential

Particle size distribution was measured by dynamic light scattering using a Zetasizer Nano ZS90 (Malvern Instruments Ltd). The samples were measured at 25°C and a scattering angle of 90°. Average particle size was calculated as the arithmetic mean of the distribution of at least 3 batches of particles and the standard deviation was calculated as the variance between average diameters of the batches. Number distributions were used to describe particle size in order to remove artifacts and additional peaks caused by the presence of aggregates, that due to their size obscure the main population. Nonetheless, in all cases the main population peak in number distribution was observed to match the peak for the main population in intensity distribution.

The zeta potential of the particles was determined by measuring the electrophoretic mobility of the nanoparticles using the same instrument. Zeta potentials were measured in PBS and 10 mM HEPES buffer, which provided information about the intrinsic surface charge and the surface charge once biologically relevant ions have adsorbed to the particles. Average particle zeta potential was calculated as the arithmetic mean of the distribution of at least 3 batches of particles and the standard deviation was calculated as the variance between average zeta potential of the batches.

6-1-2 Nanoparticle disassembly

Conditions for particle disassembly were evaluated using SDS-PAGE and western blot after suspending particles in reducing Laemmli buffer (10% glycerol, 60 mM Tris-HCl, 2% SDS, 1.25% 2-mercaptoethanol), non-reducing Laemmli buffer (10% glycerol, 60 mM Tris-HCl, 2% SDS) or native buffer (25% glycerol, 62.5 mM Tris-HCl). Treated particles were run in 10% SDS-PAGE gels and stained with coomassie blue, or transferred to a nitrocellulose membrane and immunostained with anti-5xHis tag Alexa 488-conjugated antibody (Qiagen).

6-1-3 Cell culture

SKBR-3, MCF-7, MDA-MB-231, MDA-MB-468, HeLa and NIH/3T3 cells were purchased from American Type Culture Collection. SK-BR-3 cells were grown in McCoy 5A Media supplemented with 10% fetal bovine serum (FBS). MCF-7 cells were grown in Eagle's minimum essential medium supplemented with 0.01 mg/ml human recombinant insulin and 10% FBS. MDA-MB-231 and MDA-MB-468 were cultured in Leibovitz's L-15 medium supplemented with 10% FBS. HeLa cells were cultured in Dulbecco's Modified Eagle's Medium (DMEM), supplemented with 10% FBS. NIH/3T3 cells were cultured in DMEM supplemented with 10% calf serum. All media was supplemented with 1% penicillin/streptomycin and cells were incubated at 37°C in a 5% CO_2 humidified atmosphere, except for MDA-MB-231 and MDA-MB-468 which were incubated without CO_2. Dox resistant SKBR-3 cells were derived from the parental cell line by continuously exposing cells to increasing dox concentrations that began at 0.05 μM and ended at 0.4 μM. Cells were allowed to recover from treatment for 3 days in dox free media before increasing the dox dose.

Cells used in this work were passaged at 80-90% confluency and following ATCC protocols. Cells used for experiments were passaged at least two times before use and did not exceed passage number 20. Cell morphology and normal behavior were verified before use.

6-1-4 Confocal microscopy

Cells were seeded at a density of $1.5x10^4$ cells per well in an 8-well chamber slide system (Nunc LabTek II, Thermo Scientific) with growth medium. After 16-24 hours, cells were incubated with mYopJ-GST particles (0.8 μM) or equivalent volume of 2X PBS + 5% dextrose in growth medium for 72 hours. After incubation cells were washed three times with PBS and fixed in 3.7% paraformaldehyde for 15 min at room temperature. They were rinsed with PBS three times, for 5 min each and incubated in blocking buffer (PBS with 1% BSA and 0.3% Triton X-100) for 1 hour. After blocking, cells were incubated in blocking buffer containing diluted anti-GST Dylight-488 antibody (1:100) for 1 hour. Cells were rinsed three times in PBS and incubated with 2 μM TO-PRO-3 (Invitrogen) and 0.165 μM rhodamine phalloidin (Biotium) in blocking buffer for 20 min at room temperature. Cells were washed three times with PBS and mounted for imaging in a Zeiss LSM 700 confocal microscope.

6-1-5 Cellular internalization of nanoparticles

Uptake of particles was assessed by flow cytometry. Cells were seeded at a density of $3x10^5$ per well in a 24-well plate in growth medium. After 16 hours the cells were incubated with mYopJ-GST particles (0.4 μM) or equivalent volume of 2X PBS + 5% dextrose in growth medium for 72 hours, unless otherwise stated. After incubation cells were washed three times with PBS to remove surface bound particles, trypsinized, and collected. Cells were prepared following Cell Signaling Technology flow cytometry protocol. In brief, cells were washed twice by centrifugation (500 rpm for 5 min), re-suspended in 3.7% para-formaldehyde, and fixed for 10 minutes at 37°C. Immediately after fixing, cells were permeabilized by addition of ice-cold methanol to a final concentration of 90% and incubated on ice for 30 min. Next, cells were washed twice with PBS and incubated with blocking buffer (0.5% bovine serum albumin (BSA) in PBS) for 10 minutes. Cells were washed with blocking buffer by centrifugation, resuspended in blocking buffer containing 1:100 anti-GST conjugated to Dylight-488

(Rockland Inc.) and incubated for 1 hour. Finally, cells were washed three times with blocking buffer by centrifugation, resuspended in cold PBS, and filtered with a 35 μm cell strainer. Labeled cells and controls were analyzed with an Accuri C6 (Becton Dickinson and Company) flow cytometer. Relative uptake was quantified as the ratio of mean fluorescence intensity of the sample population to mean fluorescence of the control population (no particles given).

6-1-6 Cytotoxicity evaluation of YopJ nanoparticles

Cytotoxicity of YopJ was evaluated using flow cytometry. For flow cytometry studies, cells were seeded at $9x10^4$ cells per well in a 48-well plate in growth medium. After 12 hours of incubation the medium was changed and cells were incubated with 0.4 μM YopJ-GST or mYopJ-GST nanoparticles, 0.4 μM or 2 μM dox, or 2X PBS + 5% dextrose in growth medium for 72 hours. Cells were washed with PBS, trypsinized and collected. Cells were prepared for live/dead staining or cell counting. Live/dead staining of cells was performed with annexin V Alexa Fluor 488 and Sytox green dye (Invitrogen) or using annexin V Alexa Fluor 488 and propidium iodide (Invitrogen), as indicated by the manufacturer's protocol. At least 10^4 cells and controls were analyzed with an Accuri C6 flow cytometer. Since YopJ-GST nanoparticles induced cell fragmentation, whole cells were counted to measure the viable population. Cells were prepared for counting by resuspension in cold PBS and cells within the normal cell population gate were counted to excluded cell fragments. Percent live cells were calculated as number of gated cells in sample relative to average number of gated cells in control.

MTT cell metabolic activity assays were used to confirm flow cytometry results. For this purpose, $1x10^4$ cells were seeded in each well of a 96-well plate and incubated in growth medium. After 16 hours the medium was changed and cells were incubated with 0.4 μM YopJ-GST or mYopJ-GST nanoparticles, 0.4 μM or 2 μM dox, or 2X PBS + 5% dextrose in growth medium for 72 hours. Then the media was changed with fresh media and samples were prepared by the manufacturer's MTT assay protocol (Biotium).

6-1-7 Evaluation of ERK 1/2 Activity

The activity levels of the ERK 1/2 pathway were assessed by flow cytometry. 1x106 SKBR-3 cells per well were seeded in a 6-well plate and incubated in growth medium for 16 hours. Next, cells were incubated in serum-free growth medium with 0.16 μM YopJ-GST, mYopJ-GST, or 2X PBS + 5% glucose for 24 hours. Cells were stimulated with 20 ng/ml EGF for 15 minutes, fixed, permeabilized and blocked as described in section 5-1-7. Cells were incubated in 1:2000 dilution of anti-phospho ERK 1/2 (Thr202/Tyr204) (Cell Signaling Technology) in blocking buffer for 1 hour. This was followed by three washes in blocking buffer and incubation with 1:5000 dilution of anti-mouse antibody conjugated to Alexa Fluor® 635 (Invitrogen). Cells and controls were analyzed with an Accuri C6 flow cytometer.

6-1-8 Evaluation of NF-κB Activity

Activation of the NF-κB pathway was assessed using western blots, ELISA and flowcytometry. SKBR-3 cells were seeded at a density of $1.5x10^6$ cells/well in a 6-well plate for western blotting, $3x10^5$ cells/well in 24-well plate and $1x10^4$ cells/well in a 96-well ELISA plate, these were incubated overnight. Cell media was then substituted with Hank's balanced salt solution (Gibco) and nanoparticles (0.16 μM) or 2X PBS + 5% dextrose were added. After 24 hours of incubation, the NF-κB pathway was stimulated with 20 ng/ml rhTNFα (R&D systems).

Cells were harvested for western blotting after 15 minutes, washed in PBS and lysed in RIPA buffer (150 mM sodium chloride, 1.0% Triton X-100, 0.5% sodium deoxycholate, 0.1% SDS, 50 mM Tris, pH8.0). Lysates were separated by 10% SDS-PAGE at 130 V for 120 minutes. Proteins were transferred to nitrocellulose membranes and immunostained with anti-IκBα antibodies.

For flowcytometry assays cells were harvested after 15 minutes, washed twice in PBS fixed, permeabilized and blocked as described in section 5-1-7. Cells were incubated in 1:2000 dilution of anti-phospho IκBα (Cell Signaling Technology) in blocking buffer

for 1 hour. This was followed by three washes in blocking buffer and incubation with 1:5000 dilution of anti-mouse antibody conjugated to Alexa Fluor® 635 (Invitrogen). Cells and controls were analyzed with an Accuri C6 flow cytometer.

Human phospho-IκBα (S32/S36) cell-based ELISA (R&D systems) procedures were prepared, ran and analyzed as recommended by the manufacturer for adherent cells.

6-1-9 Evaluation of cell migration and invasion

Migration of SKBR-3 cells was studied in a Cultrex® migration assay (Trevigen). For this purpose, cells were starved by incubation in serum-free medium for 24 hours prior to the assay. 5 x 10^4 cells per well were suspended in 200 μL serum-free medium with 0.16 μM YopJ-GST, mYopJ-GST, dox, or 2X PBS + 5% dextrose and seeded in the upper chamber. The lower chamber was filled with growth medium containing 10% FBS as the chemoattractant. After 48 hours, cells on the upper side of the membrane were aspirated and cells in the bottom chamber were dissociated and stained with Calcein AM. Fluorescence was determined in a Biotek Synergy H4 plate reader and compared to a standard curve as described by the assay's protocol.

An *in vitro* wound-healing assay was used to assess the effect of YopJ-GST nanoparticles on cell motility. Briefly, 5 x 10^5 SKBR-3 cells per well were seeded in 6-well plates in complete growth medium. When the culture had reached 90% confluency, the cell layer was scratched with a sterile 200 μl plastic tip, washed twice with PBS, and cultured in complete growth medium with 0.16 μM YopJ-GST, mYopJ-GST, dox, or 2X PBS + 5% dextrose for 24 hours. Phase contrast images of the plates were acquired with an Axio Observer Z1 (Carl Zeiss) microscope and analyzed as described by Valster et al. [12] Wound healing was measured at 0 and 48 hours.

6-1-10 Statistical analysis

All quantitative experiments were triplicated and presented as arithmetic mean ± standard deviation. One-way analysis of variance (ANOVA) was used to determine

significance among groups, using StatPlus. P values <0.05 among groups were considered statistically significant.

6-2 YopJ nanoparticle design considerations

Breast cancer remains as the second leading cause of death for women worldwide. However, the main cause of death is not usually the primary tumor, but metastases that develop in the liver, lungs, and bones [13]. To effectively treat this disease and reduce metastasis risk, many women undergo chemotherapy. Chemotherapy, while effective at increasing the rate of patient survival, has a variety of acute and long-term adverse effects. As most chemotherapeutic agents are small molecules, their size allows them to reach almost any tissue in the body, leading to off-target activity and significant side effects [14]. For these reasons, there is a need for new therapeutics that can decrease the risk of metastases while having fewer adverse side effects.

Proteins, unlike chemotherapeutics and small molecule targeted therapies, are large macromolecules with complex structures that can confer the specificity and selectivity [15] necessary for better therapeutics. However, given their size and complexity there are many challenges associated with their biodistribution, effective intracellular delivery and activity retention [16]. For optimal therapeutic efficacy, sufficient amounts of protein must reach malignant tissues and enter the cells to induce cancer cell death while simultaneously not inducing adverse effects on normal tissues.

As discussed in Chapter 4, efficient intracellular delivery of therapeutic proteins requires the use of nanoparticles that not only increase the amount of protein delivered but that may also help reduce immunogenicity. Protein nanoparticles are ideal for this task and, as shown in the previous chapters, have high potential for therapeutic protein and enzyme delivery. Transport of these particles to cancer cells is a three-step process in which particles must first reach the tumor area and extravasate from blood vessel walls. Then they must diffuse through the interstitial space and be internalized by cancer cells.

In order for these steps to occur, the size, surface charge, shape and rigidity of the proteins or delivery vehicles must be controlled.

6-2-1 Dose considerations

For effective cancer therapy it is desirable to deliver a sufficient number of therapeutic molecules to completely inhibit the MAPK and NF-κB pathways and rapidly induce apoptosis of cancer cells. Thus, it is advantageous to produce YopJ delivery particles entirely from YopJ-GST, without adding a carrier protein. Applying the maximal density theorem, as explained in section 5-1-2, it is estimated that in a 100 nm spherical particle there are approximately 5,785 YopJ-GST molecules. This is more than 5 times the amount of SipA molecules, a *Salmonella* effector, that has been found to affect biochemical functions within minutes [17] and was hypothesized to be sufficient for rapid induction of apoptosis.

6-2-2 Surface charge

Nanoparticle surface charge plays a crucial role in extravasation to tumors, interstitial transport and cellular internalization, which are fundamental steps for effective delivery of YopJ to tumor cells. Neutral particles have been shown to have longer systemic circulation times than charged particles [18]; but among charged particles, anionic particles show lower serum protein binding and longer circulation times than cationic particles [19]. Longer systemic circulation times can enhance delivery to target tissues by allowing more passes through the body.

Once nanoparticles have reached the tumor vicinity they must cross the vascular wall to enter the tissue. Cationic nanoparticles exhibit higher vascular permeability than their neutral or anionic counterparts [20]. However, neutral nanoparticles diffuse faster and achieve more homogeneous distributions inside the tumor interstitial space, as a result of lower interactions with positively charged collagen and negatively charged hyaluronan in the extracellular matrix [21]. Finally, nanoparticles must enter target cells

in order to deliver the drug. Higher particle internalization has been observed for charged particles versus neutral particles [22].

Together, these findings indicate that in order to effectively deliver YopJ to the cells, it is preferable to produce particles with neutral or near neutral surface charge. Nevertheless, the charge of YopJ-GST will determine surface charge and thus, surface modification with polymers or peptides could be necessary to improve delivery.

6-2-3 Nanoparticle size

One of the main reasons nanomedicine for cancer therapy is advantageous over conventional soluble therapies, is its potential to enable preferential delivery of drugs to tumors. It is well established that the endothelial lining of tumor vasculature is more permeable than in normal tissue. The increased permeability is the result of blood vessels with defective architecture and larger pores (Figure 6.1), which leads to higher hydraulic conductivity [23]. As a result, particles ranging from 50-500 nm in size can leave the vascular bed and accumulate in tumor tissue [21, 24]. This is known as the enhanced permeability and retention (EPR) effect that has now become the "gold standard" for cancer drug delivery design. In addition, the EPR effect has not only been observed in advanced solid tumors, it has also been observed during the early stages of carcinogenesis, such as dysplasia and hyperplasia lesions [25]. Therefore, this effect can also facilitate treatment of cancer at early stages.

However, the defective blood vessel architecture can also make homogeneous particle delivery difficult. Unlike normal blood vessels, tumor vessels are heterogeneous in their spatial distribution, leaving avascular spaces [21]. Thus, once nanoparticles have reached the tumor the main challenge for effective treatment becomes uniform delivery throughout the tumor or lesion. In order for nanoparticles to reach the avascular spaces they must diffuse through the dense extracellular matrix in the interstitial spaces. The tumor interstitial matrix consists of a highly interconnected network of collagen fibers. Collagen content varies between tumors and is a major determinant of nanoparticle

diffusion; diffusion is hindered to a greater extent in tumors rich in collagen [26]. Spherical rigid particles larger than 60 nm in diameter are not able to effectively penetrate the tumor interstitial space, but elongated, semi-flexible and soft particles diffuse more efficiently than their rigid counterparts [27, 28].

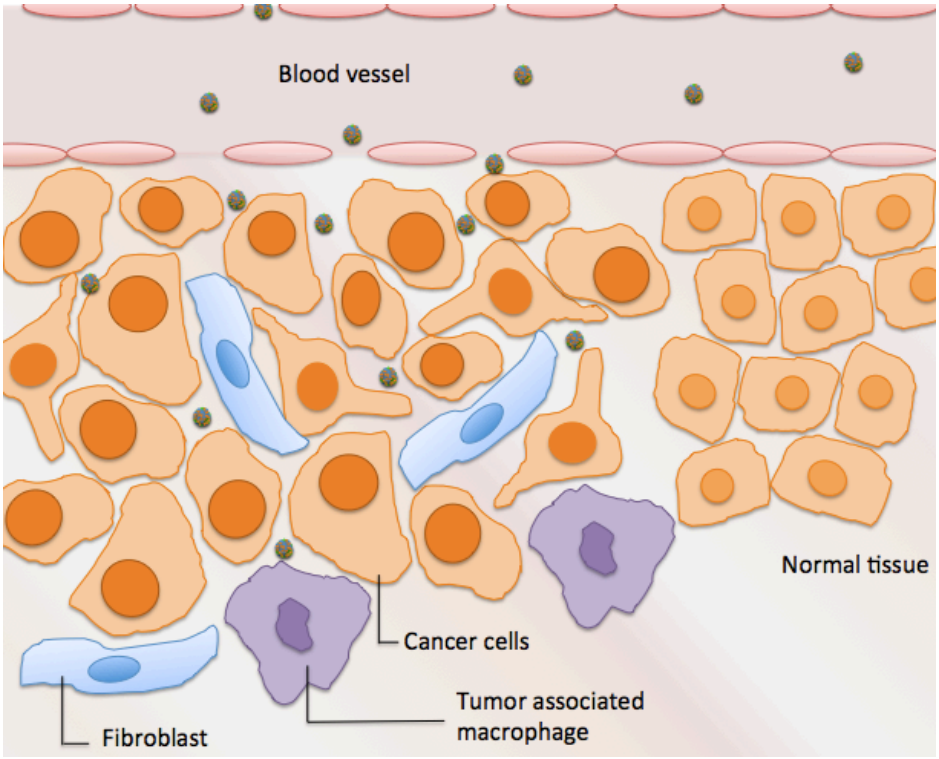

Figure 6.1. EPR effect in tumor vasculature. Passive targeting of nanoparticles between 50-550 nm to tumors occurs through the increased permeability of the tumor vasculature (schematic not drawn to scale).

Particle size also plays a crucial role in cellular internalization. Cancer cells have been found to uptake relatively large amounts of particles via energy dependent mechanisms, which are highly affected by particle size [29]. Published data has shown that small particles (50-200 nm in diameter) are internalized at higher rates than larger particles [30].

6-2-4 General design

In order to replace the T3SS mechanisms and effectively deliver YopJ to breast cancer cells to induce cell death, it is necessary to produce particles that meet the necessary conditions for extravasation into tumor tissue, diffusion through the interstitial space, internalization into mammalian cells. Since it desirable to deliver sufficient therapeutic molecules to completely inhibit the MAPK and NF-κB pathways and rapidly induce apoptosis in cancer cells, YopJ delivery vehicles particles should be made directly from YopJ-GST. These particles, like those described in Chapter 4 and 5, must be able to release their cargo inside cells (Figure 6.2). As shown in the previous chapters, particles held together by disulfide bonds are environment-responsive and disassemble inside cells, releasing soluble proteins. Thus, YopJ-GST nanoparticles held together by disulfide bonds could also release their cargo inside of cells.

In general, small soft particles (50-100 nm in diameter) would be able to leave systemic circulation and accumulate in tumor tissues, while still being able to diffuse through the intracellular matrix and be internalized by cancer cells. It was hypothesized that protein nanoparticles can be made soft by cross-linking the proteins at a low ratio of cross-linker to lysine residues (≤ 1:2.2, ratio used in Chapters 4 and 5) or by using self-assembly methods. This would allow particles to be semi-flexible and diffuse easier through the extracellular matrix. In addition, YopJ delivery vehicles should be neutral or nearly neutral to increase blood circulation times, and decrease adhesion and interaction with collagen fibers and hyaluran.

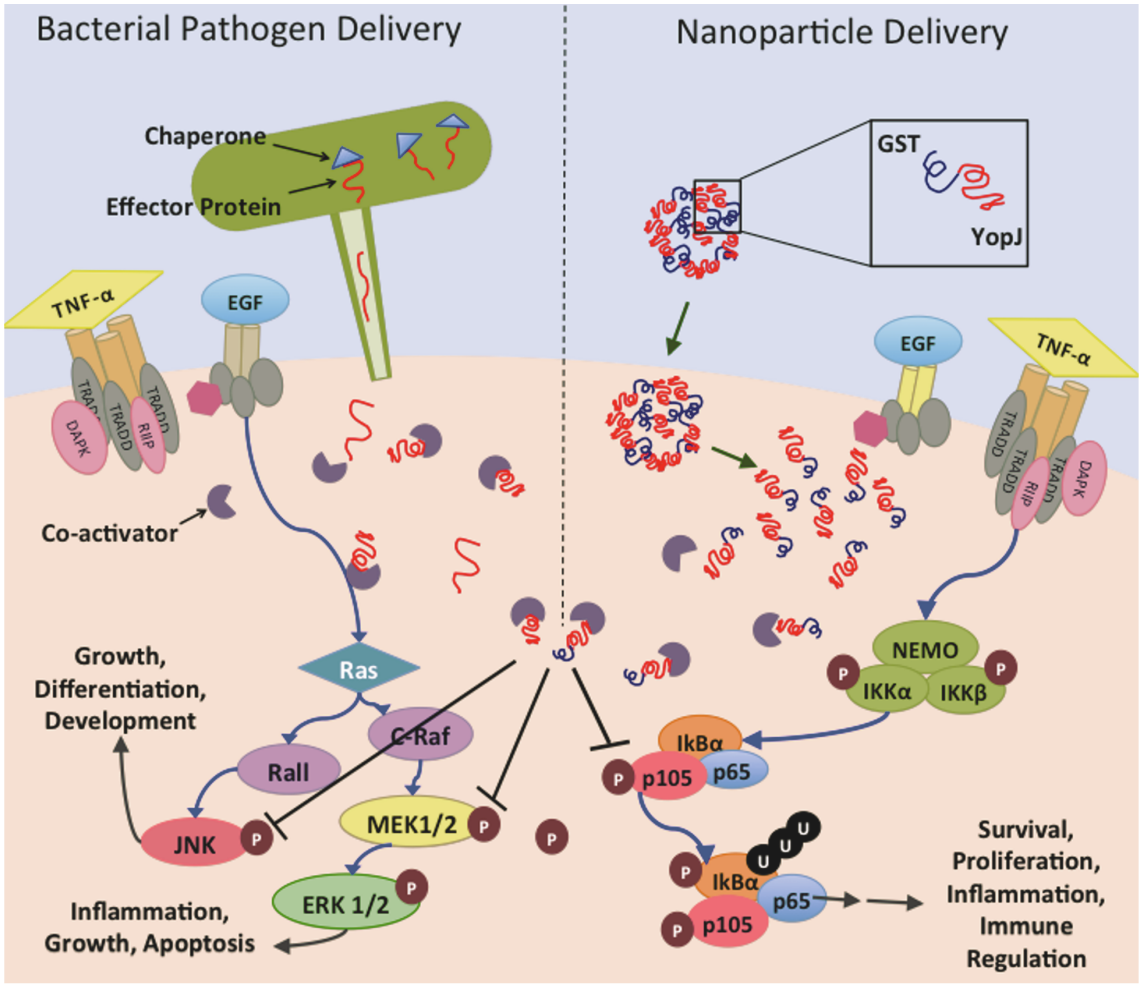

Figure 6.2. Schematic representation of bacterial T3SS effector delivery and proposed protein nanoparticle delivery. Bacterial pathogens inject effector proteins directly into the cytoplasm of host cells through needle-like structures (left). In the cytoplasm effectors bind their co-activator or chaperone that refolds them and potentiates their action [31]. Effectors are capable of subverting multiple intracellular pathways to control multiple cellular functions. The proposed strategy is to deliver the YopJ in self-assembled effector nanoparticles (right) to cancer cells to induce cell death and decrease activity in metastasis-associated pathways.

6-3 Production and characterization of YopJ-GST nanoparticles

Bacterial protein effectors have several advantages as therapeutic agents for cancer, including their ability to target pathways associated with cancer hallmarks, cell

migration and metastasis [32, 33]. However, bacterial effector proteins cannot be therapeutically delivered by the pathogenic bacteria that produce them. In order to deliver active proteins to cancer cells, it is necessary to engineer a delivery system.

Recombinant technology was used to produce YopJ in E. coli, as explained in Chapter 3. In brief, production of YopJ in E. coli required fusion to GST, a common protein tag used to decrease protein toxicity and increase solubility. An inactive C172A mutant of YopJ fused with GST (mYopJ-GST) was also cloned and produced. This mutation removes acetyltransferase activity, and serves as a control for nonspecific effects of bacterial proteins [31].

Fusion of YopJ and mYopJ to GST induced protein self-assembly into stable nanoparticles with zeta potential of –17.4 ± 3.4 mV in 20 mM Hepes buffer. This indicates that YopJ-GST nanoparticles are negatively charged in low ionic strength buffers. However, as was also observed in the previous chapters, the zeta potential increases between 40-45% in physiologically relevant salt concentrations to -10.2 ± 2.9 mV. This increase, caused by ion adsorption, leads to low apparent negative surface charge and can prevent particle interaction with extracellular matrix components.

Dynamic light scattering (DLS) indicated that both fusion proteins self-assembled into nanoparticles during expression and purification processes. As shown in Figure 6.3, the average YopJ-GST particle diameter was 150 nm in 8 M urea purification buffer. However, the average hydrodynamic diameter decreased to 100 nm when the particles were suspended in 2X phosphate buffered saline (PBS) with 5% dextrose (nanoparticle storage buffer) or in organic solvents. Particles with 100 nm diameter are ideal for cancer treatment due to the enhanced permeability and retention effect in tumors[18]. In addition, this small size and will allow diffusion through the interstitial space and internalization of particles by tumor cells [34]. The observed difference in particle size between saline buffers and denaturing agents suggests that denaturing conditions unfold or partially unfold the proteins in the particles causing them to expand or swell.

Interestingly, denaturing conditions are not sufficient to cause particle disassembly, which indicates that YopJ-GST nanoparticles are highly stable.

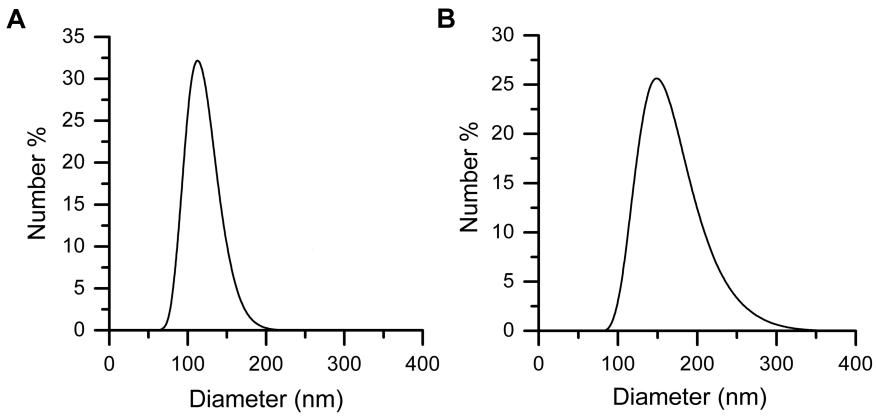

Figure 6.3. Characterization of self-assembled YopJ-GST nanoparticle size. (*A*) Representative DLS nanoparticle size distribution in 2X PBS + 5% dextrose. (*B*) Representative DLS nanoparticle size distribution in 8M urea, shows particle swelling in denaturing conditions.

To establish which forces stabilize YopJ-GST nanoparticles, particles were exposed to denaturing agents (SDS buffer, heat), reducing agent (1% β-mercaptoethanol) and native conditions (Tris-HCl buffer). Treated particles were evaluated by SDS-PAGE and western blot to identify which conditions led to particle disassembly and release of soluble YopJ-GST protein. Figure 6.4 shows that a combination of reducing and denaturing conditions are necessary for complete particle disassembly. Denaturing conditions alone release some soluble protein, evidenced by a less intense band at 60 kDa. Under native conditions a very dim band was observed, indicating little protein was released from the particles.

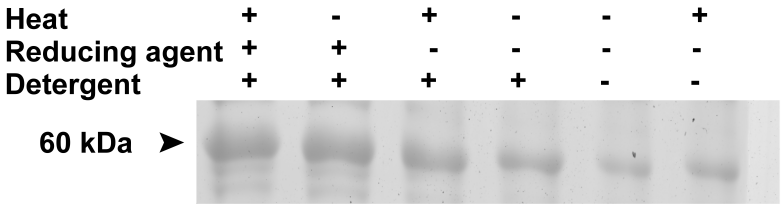

Figure 6.4. Analysis of SDS-PAGE gel shows YopJ-GST nanoparticle disassembly in the presence of denaturing agents (detergent: SDS and heat: 100°C), reducing agent (β-mercaptoethanol) or under native conditions. Band intensity is correlated to amount of protein released.

These results indicate that hydrophobic interactions and disulfide bonds stabilize the particles. Both YopJ and GST contain cysteine (Cys) residues and hydrophobic regions that can initiate and sustain particle self-assembly. GST contains 4 Cys residues that have been shown to be accessible and facilitate oxidative aggregation when GST or GST fusions are overexpressed [35]. Furthermore, there are multiple small segments within GST that can form strong intermolecular hydrophobic interactions, such as the "lock and key" formed by the phenyl ring of phenylalanine at position 52 and a pocket between α-helices 4 and 5 of a neighboring GST molecule [36]. YopJ contains 2 cysteine residues in its sequence and a large number of hydrophobic residues that are potentially exposed when the protein is unfolded or partially folded following *E. coli* expression. YopJ requires binding to a mammalian co-activator for proper protein folding[31], and prior to this, the exposed hydrophobic domains may interact with each other. Also, many effector proteins, including YopJ, are kept unfolded by a chaperone in the native bacteria [37]. This chaperone is not present in the *E. coli* expression system, which can lead to interactions that cause aggregation. The combination of these intermolecular interactions is likely responsible for the initial assembly of YopJ-GST nanoparticles and their stability in multiple buffers and solvents.

6-4 Delivery and effect on SKBR-3 cells

6-4-1 Intracellular delivery of particles to SKBR-3 cells

The bacterial pathogen *Yersinia,* uses the needle-like type III secretion system (T3SS) to directly inject effector proteins into the cytoplasm of host cells [3]. To determine whether nanoparticles could replace the T3SS mechanism and deliver effector proteins to breast cancer cells, SKBR-3 cells were used. SKBR-3 is a breast cancer cell line that over-expresses human epidermal receptor-2 (HER2) and is estrogen receptor (ER) and progesterone receptor (PR) negative [38]. In addition, these cells show upregulation of MAPK and NF-κB pathways [39].

To evaluate particle internalization, cells were incubated with 0.4 μM mYopJ-GST nanoparticles and washed to remove externally bound particles. The mutant fusion protein was used to avoid interference of cell death with the assay. The fusion protein was detected by fluorescent immunolabeling with anti-GST. As shown by flow cytometry, treated cells exhibited a time dependent increase in fluorescence intensity (Figure 6.5A). At 24 hours, mYopJ-GST is detected in cells at very low levels. After 72 hours of incubation, cells showed a 1.2-fold increase in median fluorescence intensity. Confocal microscopy images support this data (Figure 6.5B-E). A significant amount of protein was located inside cells, indicating the self-assembled YopJ-GST particles effectively deliver protein to SKBR-3 cells.

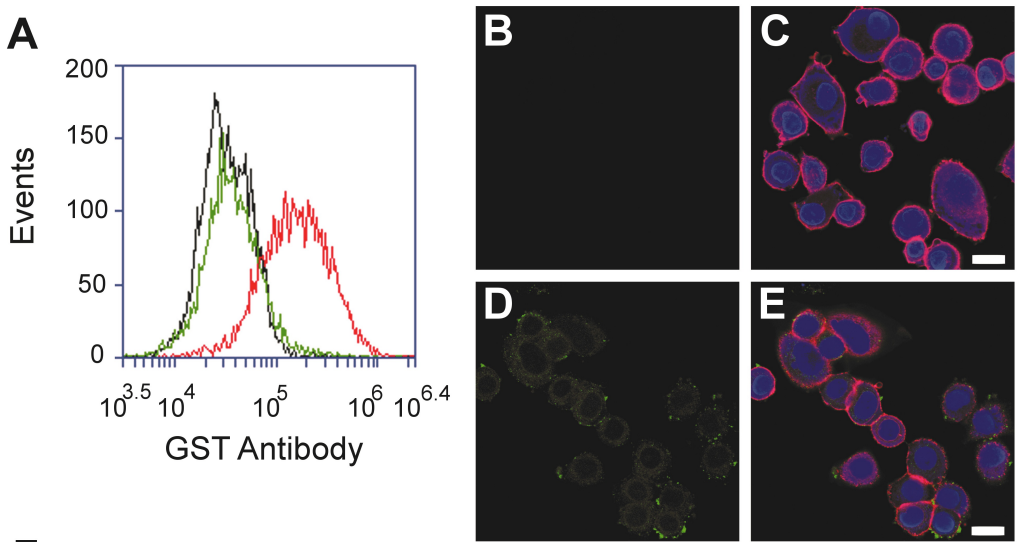

Figure 6.5. Interaction of YopJ-GST nanoparticles with SKBR-3 cells. *(A)* Flow cytometry analysis of untreated cells (black) compared to cells treated with 0.4 μM mYopJ-GST nanoparticles for 24 or 72 hours (green, red), labeled with anti-GST Dylight 488. *(B-E)* Confocal immunofluorescence analysis of (*B, C*) untreated cells or (*D, E*) cells treated with 2x dose (0.8 μM) of mYopJ-GST nanoparticles for 72 hours, using anti-GST Dylight 488 (green). Actin filaments are labeled with rhodamine phalloidin (red) and DNA (nucleus) with TO-PRO-3 (blue). Scale bar is 20 μm.

6-4-2 Cytotoxic effect of YopJ-GST nanoparticles

To establish the effect of YopJ on SKBR-3 cell viability, multiple concentrations of particles were tested. A concentration of 0.4 μM YopJ-GST nanoparticles was sufficient to induce significant cell death, but lower concentrations (0.05, 0.12, and 0.25 μM YopJ-GST) did not affect cell viability. Doxorubicin (dox), a highly cytotoxic chemotherapeutic agent often administered to breast cancer patients [40], was used as a reference. The cytotoxic effect of YopJ-GST nanoparticles was assessed by microscopy, flowcytometry, live/dead dyes, and MTT assay.

Treatment with YopJ-GST induced 84% cell death in 24 hours (Figure 6.6), even though the presence of the particles was barely detectable within this time period. This is indicative of the high potency of YopJ [17]. After 72 hours, only 3% of cells remained

viable, while 11% of cells treated with the same molar concentration of dox survived. To achieve the same level of cell death as YopJ-GST, the dox concentration had to be increased 5-fold, to 2 μM. Microscopy studies of cells incubated with YopJ-GST nanoparticles revealed that after 72 hours only a few cells had survived and remained attached (Figure 6.7). MTT assays confirmed these observations (Figure 6.8).

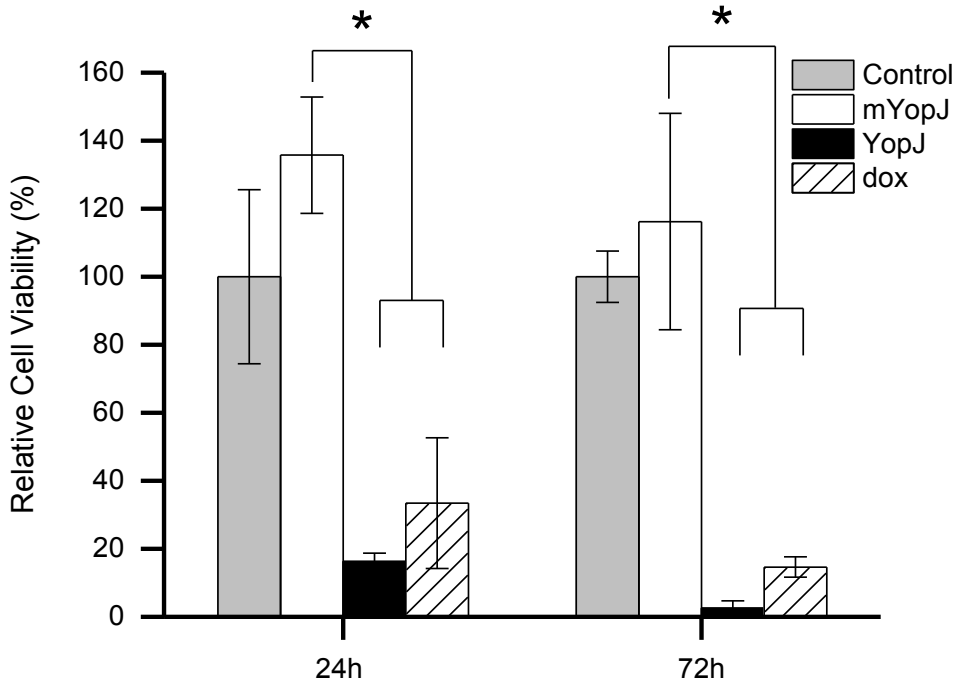

Figure 6.6. Viability of SKBR-3 cells treated with YopJ-GST nanoparticles. Cell metabolic activity, measured by flowcytometry, after 72 hours of treatment with 0.4 μM YopJ-GST or mYopJ-GST nanoparticles or 2 μM dox, compared to control cells incubated with 2X PBS + 5% dextrose. Error bars represent standard deviation, N=3 (*$p<0.01$).

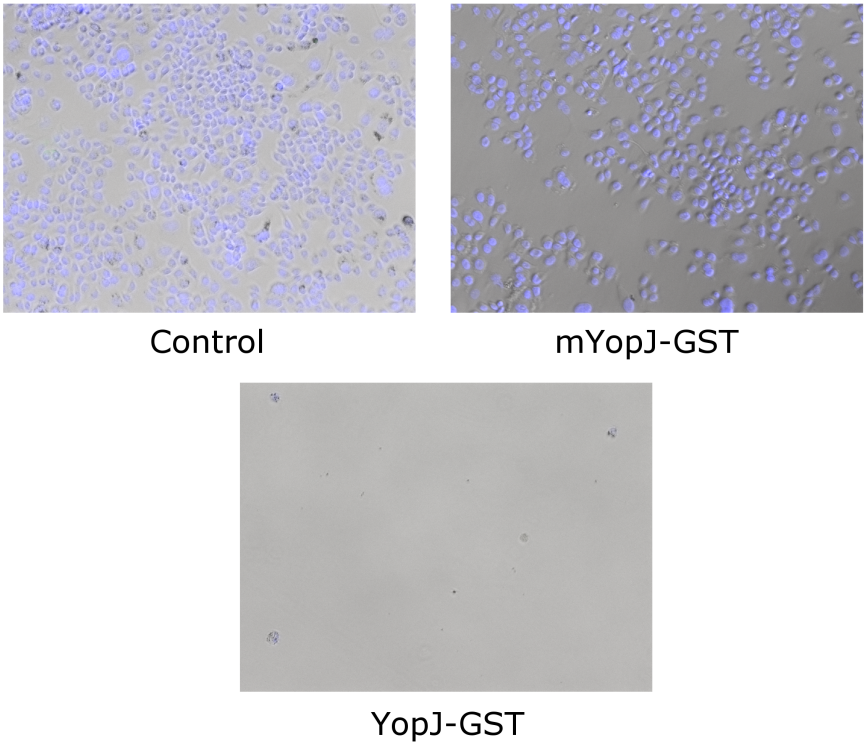

Figure 6.7. Fluorescence microscopy images of cells incubated with YopJ-GST nanoparticles and controls for 72 hours. Cell nuclei were stained with Hoechst and cells were imaged with 10X objective.

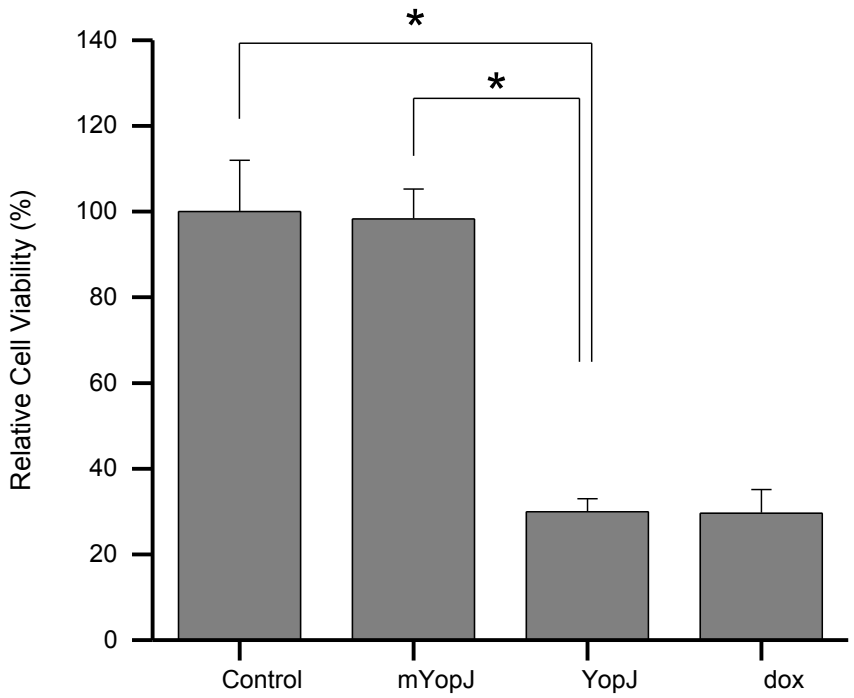

Figure 6.8. Cytoxicity of YopJ-GST nanoparticles on SKBR-3 cells. Cell metabolic activity, measured by MTT assay, after 72 hours of treatment with 0.4 μM YopJ-GST or mYopJ-GST nanoparticles or 2 μM dox, compared to control cells incubated with 2X PBS + 5% dextrose. Error bars represent standard deviation, N=3 (*$p<0.01$).

YopJ-GST nanoparticles caused fragmentation of cells and staining with annexin V, SYTOX® green and propidium iodide (PI) did not indicate apoptosis or necrosis as the cause of death (Figure 6.9). Flow cytometry analysis using annexin V-Alexa 488 and PI was used to characterize cells after 24 hours of treatment. Dox was used as a positive control for apoptosis and necrosis. Dot plots of PI fluorescence versus annexin V fluorescence were used to establish the live/dead status of treated cells (Figure 6.9A). The lower right quadrant (LR) indicates annexin-positive, early apoptotic cells. The cells in the upper right quadrant (UR) are annexin-positive and PI-positive, indicating late apoptotic or necrotic cells. Cells in the upper left quadrant (UL), PI-positive, indicate necrotic cells. Interestingly, cells treated with YopJ-GST nanoparticles appear in the lower left quadrant that indicates live cells, but fewer cells were counted in comparison to

mYopJ and the control. After 72 hours of treatment there were not enough whole cells in the YopJ-GST sample to establish mechanism of cell death. Since these observations indicate that cells fragment during or after YopJ-induced death, shorter periods of time, lower doses and other dyes (Sytox green) were used. Nonetheless, similar results were obtained and no indication of apoptosis or necrosis was observed.

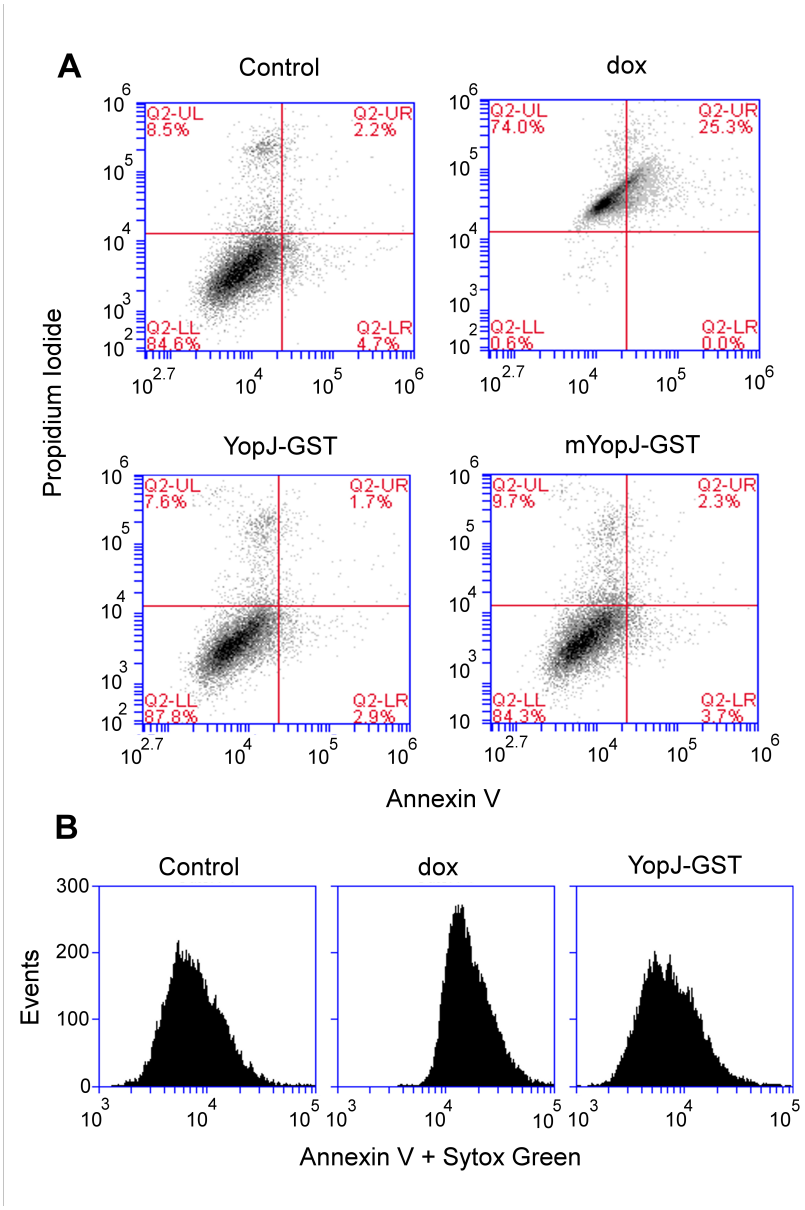

Figure 6.9. *In vitro* assessment of apoptosis in SKBR- 3 breast cancer cells treated with YopJ-GST. *(A)* Flow cytometry analysis using annexin V-Alexa 488 and PI was used to observe the induction of apoptosis or necrosis. Doxorubicin was used as a positive control for annexin-V and PI staining. *(B)* Flow cytometry analysis using annexin V-

Alexa 488 and Sytox green. An increase in population fluorescence intensity indicates the presence of apoptotic or necrotic cells.

6-4-3 Effect of YopJ-GST nanoparticles on MAPK ERK1/2 activity

In an effort to establish if the observed cytotoxicity was the result of the biochemical activity of YopJ on cellular signaling, the effect of YopJ-GST nanoparticles on the ERK 1/2 pathway activity was measured. YopJ is known to irreversibly acetylate the serine and threonine residues of Mitogen/Extracellular signal-regulated Kinase 1/2 (MEK 1/2), directly preventing phosphorylation of MEK 1/2 and subsequently inhibiting ERK 1/2 phosphorylation and activation of the pathway [41]. Levels of phosphorylated ERK 1/2 were measured following incubation with a sub-lethal dose of YopJ-GST nanoparticles (0.16 μM) for 24 hours and stimulation of the pathway with epidermal growth factor (EGF). Phosphorylated ERK 1/2 in cells was fluorescently immunolabeled and quantified by flow cytometry. Figure 6.10 shows lower fluorescence intensity, representing lower levels of phosphorylated ERK 1/2, for stimulated cells pretreated with YopJ-GST nanoparticles compared to cells pre-treated with mYopJ-GST or untreated. This suggests that YopJ-GST nanoparticles block the ERK 1/2 pathway in breast cancer cells, as was expected.

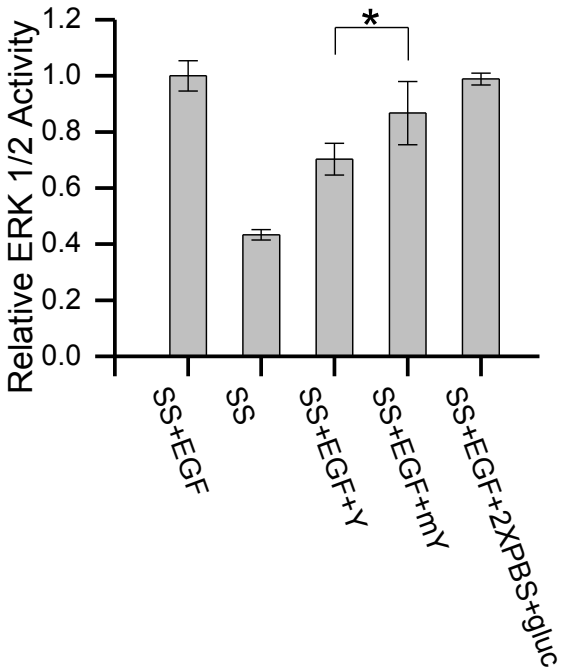

Figure 6.10. Phosphorylation of ERK 1/2 pathway measured as relative fluorescence intensity of cells treated with sub-lethal doses (0.16 μM) of nanoparticles in serum-free media and stimulated with 20 ng/ml EGF for 15 min, compared to stimulated control. Error bars represent standard deviation, N=3 (*$p<0.05$).

6-4-4 Effect of YopJ-GST on NF-κB activity

In addition to its effect on MAPK signaling, YopJ is also known to exert inhibitory activity on NF-κB signaling [8]. Thus, the effect of YopJ on the NF-κB pathway was also examined. In inactivated cells, NF-κB is complexed with its inhibitor IκB and retained in the cytoplasm. When the pathway is activated IκB is phosphorylated, ubiquitinated and degraded, freeing NF-κB to enter the nucleus and affect transcription [41]. To evaluate pathway activation IκB degradation was assessed.

Western blot analysis of cell lysates showed that stimulation with TNF-α caused IκBα degradation, even for cells pretreated with sublethal doses of YopJ-GST nanoparticles (Figure 6.11). Nonetheless, bands for cells pretreated with YopJ-GST and mYopJ-GST nanoparticles appear to have slightly higher intensities. In order to quantify

NF-κB pathway activation the phosphorylation of IκBα was quantified using a phospho-IκBα ELISA.

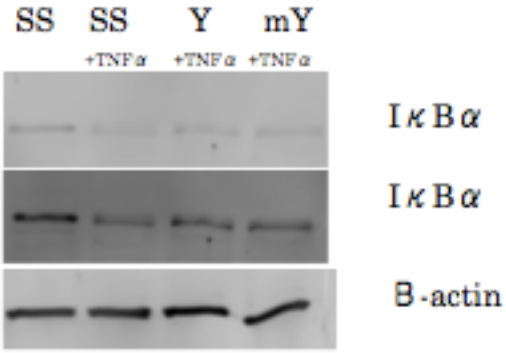

Figure 6.11. Effect of YopJ-GST nanoparticles on IκBα degradation. Western blot on cell lysates probed with anti-IκBα antibody. NFκB pathway was stimulated with 20 ng/ml TNFα in Hank's buffer and basal pathway levels were accomplished by incubating the cells in Hank's buffer for 24h.

Given the inhibition of ERK 1/2 signaling observed in cell pretreated with YopJ-GST nanoparticles, it was hypothesized that delivered YopJ would also inhibit NF-κB signaling in breast cancer cells. Nevertheless, the results of the phospho-IκBα ELISA indicate that YopJ-GST nanoparticles do not prevent phosphorylation of IκBα or that other factors involved in the process upregulate signaling (Figure 6.12). These results were also confirmed in additional studies conducted using flowcytometry with phospho-IκBα antibodies.

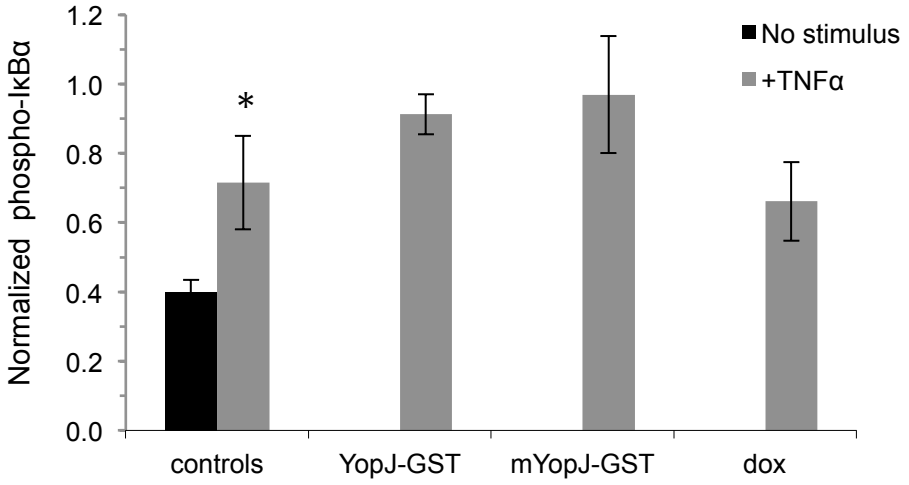

Figure 6.12. Effect of YopJ-GST nanoparticles on phosphorylation of IκBα. Results shown here represent measured phospho-IκBα normalized with GADPH. Cells were serum starved and incubated with YopJ or mYopJ for 24 hours, then stimulated with 20 ng/ml of TNFα for 15 minutes.

6-4-5 Effect of YopJ-GST nanoparticles on cell migration

Since the ERK 1/2 pathway has been correlated to cancer cell migration, invasion and metastasis [42], the effect of YopJ-GST nanoparticles on SKBR-3 cell migration and invasion was evaluated. Cell motility was measured using a transwell assay, with FBS as the attractant and a sub-lethal dose (0.16 μM) of YopJ-GST nanoparticles. The number of cells that migrated to the lower chamber was quantified after 48 hours of treatment. Decreased cell migration was observed in the presence of YopJ-GST nanoparticles but not in the presence of equimolar concentrations of mYopJ-GST nanoparticles or dox (Figure 6.13). Similarly, a scratch assay showed that the invasive capacity of SKBR-3 cells is lower after treatment with YopJ-GST nanoparticles than with dox (Figure 6.14).

Inhibition of the ERK 1/2 pathway by YopJ decreased the migration and invasion capabilities of SKBR-3 cells, while dox did not. This suggests that surviving cells, or those receiving a sub-lethal dose of YopJ-GST nanoparticles, are less likely to migrate and metastasize. This is very important for breast cancer treatment, where metastasis

correlates with mortality [43]. Though most studies focus on cell death, the "state" of surviving cells is just as critical for long-term remission. During treatment, not all cancer cells within a tumor or in the surrounding area will receive the same dose, due to transport limitations in avascular spaces and concentration gradients that develop. It is essential that cells receiving sub-lethal doses do not develop the characteristics necessary to metastasize. It has been demonstrated that many chemotherapeutic agents, including dox, activate ERK 1/2 and related pathways, thus, increasing cell motility and the likelihood of metastasis in surviving cells [44].

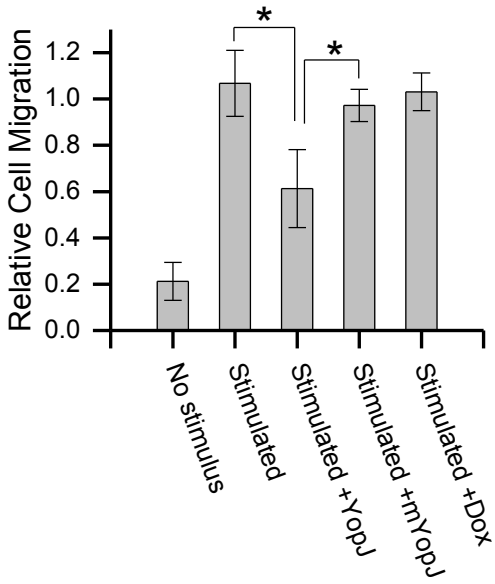

Figure 6.13. Cell migration of treated SKBR-3 cells. Migration of cells treated for 24 hours with sub-lethal doses of nanoparticles in Boyden chambers, stimulated with 10% FBS as a chemoattractant. Migration of samples is normalized to migration of stimulated control. Error bars represent standard deviation for N=3 (*$p<0.05$).

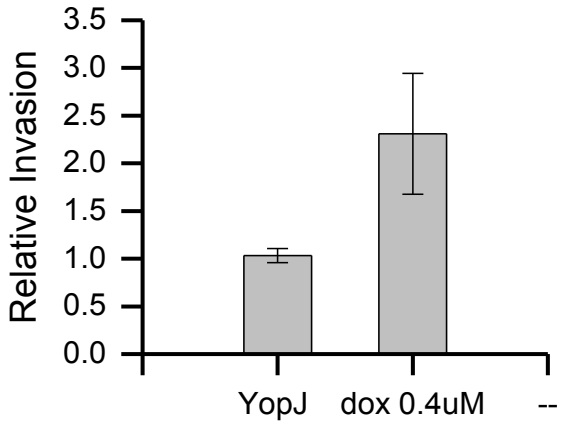

Figure 6.14. Relative cell invasion of SKBR-3 cells treated with YopJ-GST and dox. Invasion was measured in a wound healing assay. Wounds were created at t=0 and cells were treated with 0.4 μM nanoparticles or 0.4 μM dox for 24 hours. Error bars represent standard deviation, N=3 (*$p<0.05$).

6-4-6 Cytotoxic effect of YopJ-GST nanoparticles on doxorubicin resistant cells

Resistance to chemotherapy has also been correlated to ERK 1/2 activation [40] and thus, the response of dox resistant cells to YopJ-GST nanoparticle treatment was evaluated. Through repeated exposure cycles, SKBR-3 cells were made dox resistant at 0.4 μM. The resistant cells were treated with 0.4 μM YopJ-GST particles or dox for 72 hours, immediately after dox exposure and recovery. SKBR-3 resistant cells treated with YopJ-GST nanoparticles showed low viability, 3.5%, similar to normal SKBR-3 cells (Figure 6.15). Conversely, dox treatment showed approximately 30% cell viability, about 3 times that for normal SKBR-3 cells. This data suggests that YopJ-GST nanoparticles could be used not only as a primary adjuvant therapeutic, but also for patients who have previously received dox, to overcome resistance and inhibit metastasis-related pathways immediately after treatment.

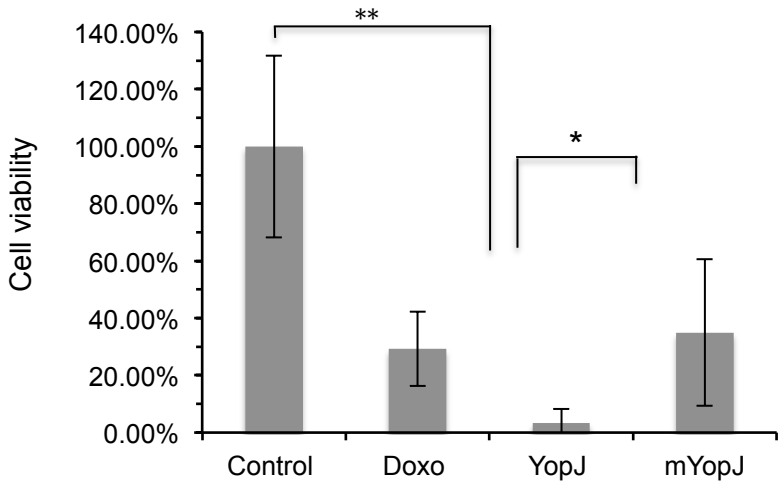

Figure 6.15. Cytotoxic effect of YopJ-GST nanoparticles on SKBR-3 doxorubicin resistant cells. Relative cell viability after 72 hours of treatment with 0.4 μM nanoparticle or dox, measured as number of live cells in sample relative to control. Error bars represent standard deviation for N=3 (* $p<0.05$, ** $p<0.01$).

Further studies performed with SKBR-3 dox resistant cells demonstrated that after three or more passages without exposure to dox, the cells recovered and dox resistance levels doubled (Figure 6.16). Furthermore, cells no longer responded to YopJ-GST or mYopJ-GST nanoparticle treatment. Additional studies in which cells were incubated with a combination of dox and YopJ-GST did not show higher cytotoxicity levels or synergistic activity. Similarly, step treatment studies in which cells were first treated with YopJ-GST nanoparticles for 72 hours and then with dox for 72 more hours, showed there was no improvement in cell death.

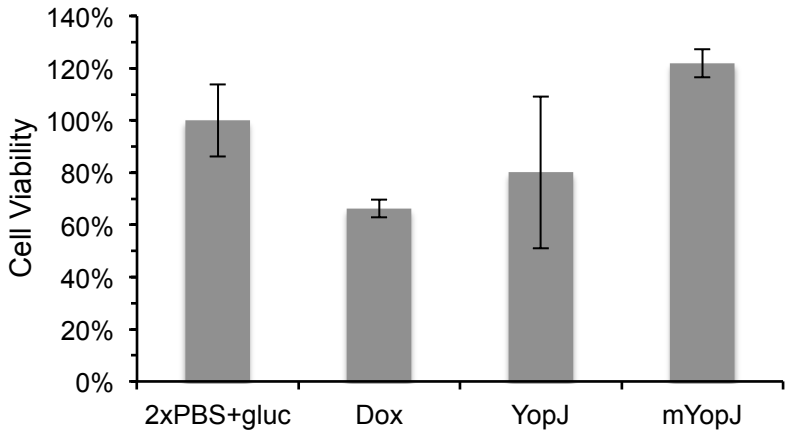

Figure 6.16. Cytotoxic effect of YopJ-GST nanoparticles on SKBR-3 doxorubicin resistant cells after several passages. Relative cell viability after 72 hours of treatment with 0.4 μM nanoparticle or dox, measured as number of live cells in sample relative to control. Error bars represent standard deviation for N=3 (* $p<0.05$, ** $p<0.01$).

6-5 Effect of YopJ-GST nanoparticles on a breast cancer cell line panel

The cytotoxicity of YopJ-GST nanoparticles on other breast cancer cell lines was also investigated. A panel of breast cancer cell lines (MCF-7, MDA-MB-231, and MDA-MB-468) belonging to different molecular subclasses of breast cancer was used. MCF-7 cells are Luminal A subtype, ER and PR positive, and HER2 negative. MDA-MB-468 is a basal cell line that is negative for ER, PR and HER2. MDA-MB-231 is claudin-low subtype and is ER, PR and HER2 negative. Despite the molecular variations among these cell lines, response to YopJ-GST nanoparticles was observed in all of them. SKBR-3 cells were the most responsive breast cancer cell line, followed by MCF-7 with 90% cell death (Figure 6.17A). The viability of MCF-7 cell after 72 hours of treatment was comparable to that induced by a 5 times higher molar dose of dox. MDA-MB-468 and MDA-MB-231 cells were less responsive, with 83% and 65% cell death, respectively (Figure 6.17C,E). In these cells YopJ-induced cytotoxicity was comparable to dox at the same molar concentration. Results were confirmed using MTT assay (Figure 6.18).

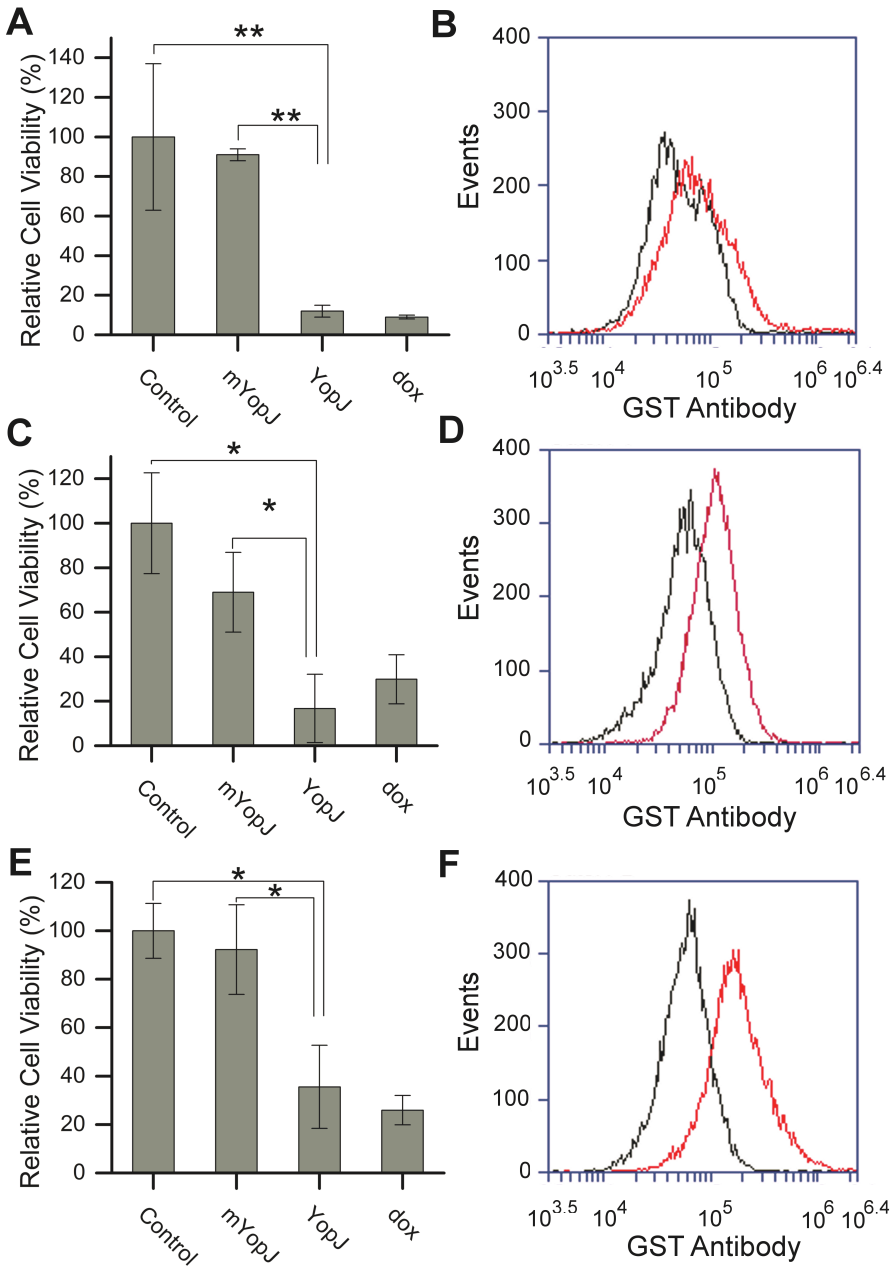

Figure 6.17. Effect of YopJ-GST nanoparticles on a breast cancer cell line panel. *(A, C, E)* Relative cell viability after 72 hours of treatment with 0.4 μM nanoparticle or dox, unless otherwise indicated, for (*A*) MCF-7 (dox 2 μM), (*C*) MDA-MB-468, and (*E*) MDA-MB-231, measured as number of live cells in sample relative to control. *(B, D, F)* Flow cytometry analysis of particle internalization comparing untreated (black) or 0.4 μM mYopJ-GST nanoparticle-treated cells for 72 hours (red) using anti-GST Dylight

488, for (*B*) MCF-7, (*D*) MDA-MB-468, and (*F*) MDA-MB-231. Error bars represent standard deviation for N=3 (*p<0.05, **p<0.01).

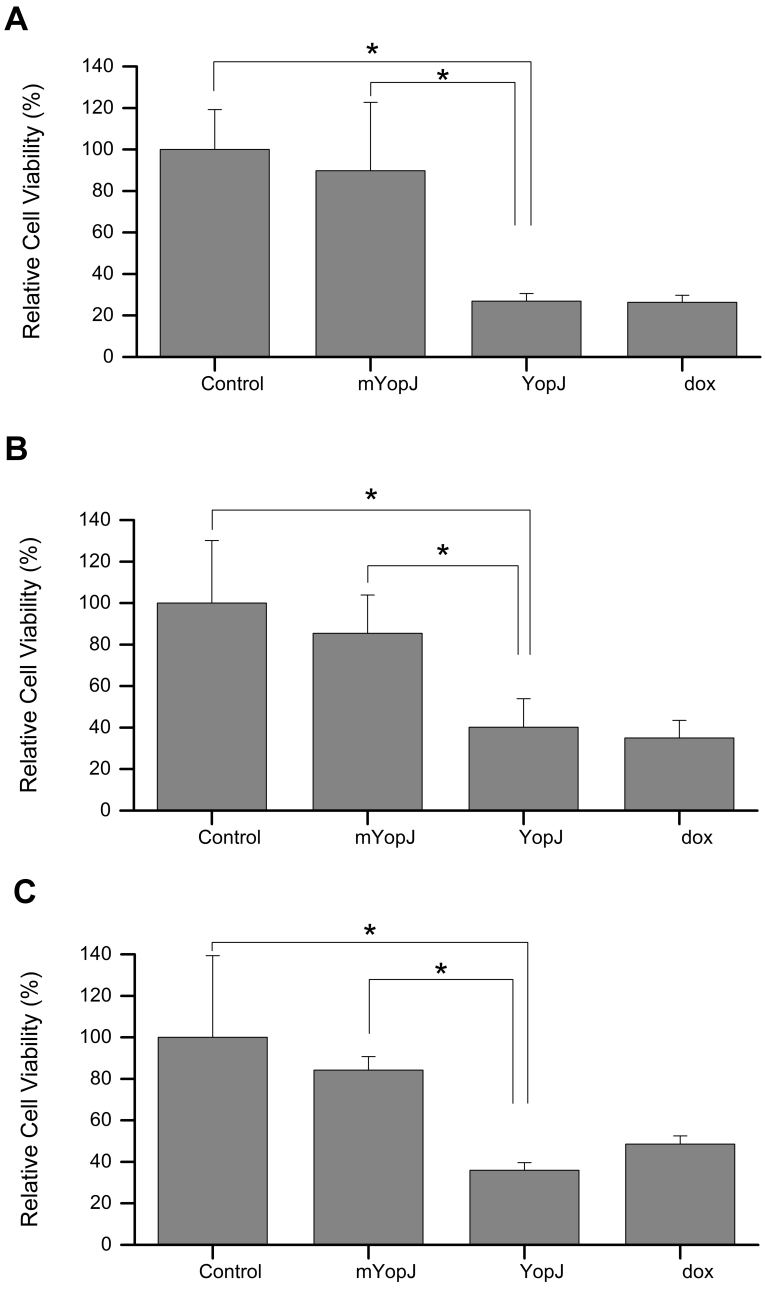

Figure 6.18. Cytotoxicity of a panel of breast cancer cell lines treated with YopJ-GST. *(A*) MCF-7, *(B)* MDA-MB-468, and *(C) MDA-MB-231* cells were assessed by MTT

assay and reported as percentage MTT-positive cells in sample relative to control. Cells were treated for 72 hours with 0.4 μM YopJ-GST or mYopJ-GST nanoparticles, or 2 μM dox. Control cells were treated with 2X PBS + 5% dextrose. Error bars represent standard deviation, N=3 (*$p<0.05$).

Particle internalization by the different cell lines was measured to identify any correlation with the viability trends (Figure 6.17B,D,F). After 72 hours of incubation with mYopJ-GST nanoparticles, MCF-7, MDA-MB-468 and MDA-MB-231 cells showed a 1.3, 2 and 1.8-fold increase in median fluorescence intensity, respectively (Figure 6.19). MDA-MB-468 cells showed the highest level of uptake, indicating there was no correlation between particle internalization and viability. Interestingly, SKBR-3 and MCF-7 cells internalized less particles than the other cell types but higher levels of cell death were observed. This suggests that these cell lines could be more sensitive to the acetylation effect of YopJ, potentially due either to aberrations in the MAPK and NF-κB pathway targets of YopJ, or to higher nanoparticle disassembly efficiency. SKBR-3 cells have shown higher NF-κB expression and activity than MCF-7 cells, but less than MDA-MB-231 and MDA-MB-468 [45]. However, SKBR-3 cells have shown greater MAPK activity and dependence than all the other cell lines, due to the relationship of HER2 with MAPK signaling [39]. Similarly, in MCF-7 cells the MAPK pathway has been found to be central to cell survival and proliferation due to the connection with ER [46, 47]. The importance of these pathways to particular breast cancer subtypes may be the cause of the greater sensitivity to YopJ-GST nanoparticles.

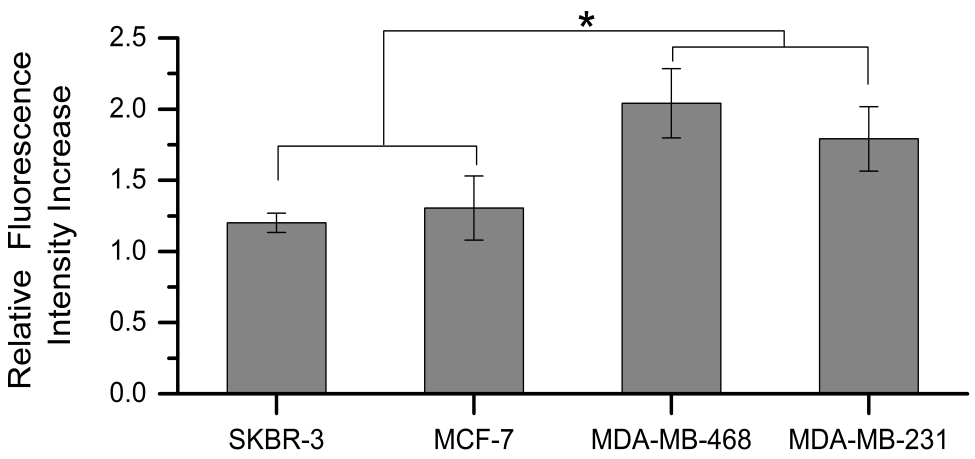

Figure 6.19. Relative median fluorescence intensity increase for breast cancer cell lines treated with 0.4 μM mYopJ-GST nanoparticles. Error bars represent standard deviation for N=3 (*p<0.05, **p<0.01).

6-6 Cytotoxic effect of YopJ-GST nanoparticles on other cell lines

The reported cell-type selectivity of YopJ cytotoxicity suggests that YopJ-GST nanoparticles could also exhibit cell-type selectivity. HeLa cells, a cervical cancer cell line, and NIH/3T3 cells, healthy non-cancerous murine fibroblasts, were used to establish if YopJ-GST nanoparticles display such cell selectivity. HeLa cells treated with 0.4 μM YopJ-GST nanoparticles for 72 hours exhibited no significant cytotoxicity (Figure 6.20A). However, treatment with 0.4 μM dox resulted in high cytotoxicity, with 5% viability. Similarly, 0.4 μM YopJ-GST nanoparticles did not show significant cytotoxic effects on NIH/3T3 fibroblasts (Figure 6.20C). The same dose of dox reduced viability by more than 75%. Results were confirmed using MTT assay (Figure 6.21). Interestingly, particle internalization studies showed that HeLa cells internalize mYopJ-GST nanoparticles but that NIH/3T3 cells do not (Figure 6.20B,D). The median fluorescence intensity increased by 1.75-fold in HeLa cells while there was no significant increase in NIH/3T3 cells.

These results suggest that YopJ-GST nanoparticles have an additional benefit: cell-type selectivity. Lack of cytotoxicity in NIH/3T3 cells could be attributed to low

nanoparticle uptake. Our previous work showed a 33% reduction in uptake for NIH/3T3 cells compared to SKBR-3 for green fluorescent protein nanoparticles [48]. However, we observed that statistically insignificant quantities of internalized YopJ-GST nanoparticles induced 86% cell death in SKBR-3 cells so internalization may not be the only factor. HeLa cells, which internalized more YopJ-GST nanoparticles than SKBR-3 cells, did not respond. It has been reported that inhibition of MAPK pathways in HeLa cells is not sufficient for induction of apoptosis, but that inhibition of ERK 1/2 does sensitize the cells to chemotherapy and radiotherapy [49].

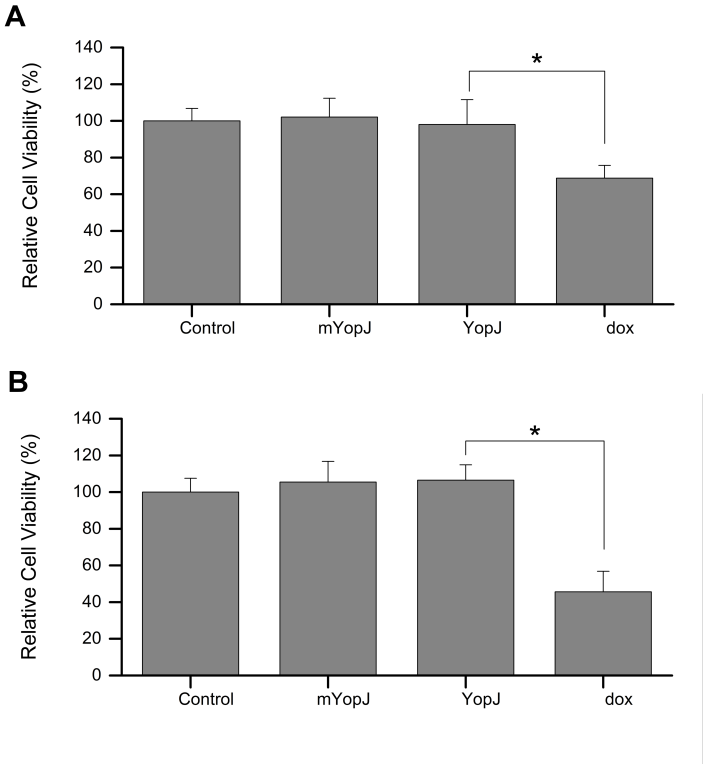

Figure 6.20. Cytotoxicity of other cell lines treated with YopJ-GST. *(A*) HeLa and *(B)* NIH/3T3 cells were assessed by MTT assay and reported as MTT-positive cells in sample relative to control. Cells were treated for 72 hours with 0.4 μM YopJ-GST or mYopJ-GST nanoparticles, or 2 μM dox. Control cells were treated with 2X PBS + 5% dextrose. Error bars represent standard deviation, N=3 (*$p<0.05$).

6-7 Modification of YopJ-GST for improved intracellular delivery

Cell penetrating peptides (CPP) are a group of short 10-30-mer peptides that possess the ability to cross cell membranes either alone or carrying a cargo [50]. Chemical ligation, fusion and physical assembly of CPPs with peptides, proteins, oligonucleotides, and nanoparticles has been shown to increase rate and efficiency of intracellular delivery and endosomal escape [51]. YopJ-GST nanoparticle internalization was shown to be time dependent and small amounts of particles are internalized in the first 24 hours. In order to improve internalization of these particles, YopJ-GST fusion were modified to include a C-terminal CPP.

A histidine modified version of the well-characterized TAT peptide, an arginine rich CPP from HIV, was selected for its ability to promote intracellular delivery and endosomal escape of its cargoes [52]. The 6xHis-TAT-6xHis CPP was fused to YopJ-GST proteins to produce a larger fusion protein YopJ-HIS-TAT with encoded abilities to facilitate the cellular internalization process. Fusion of this peptide to YopJ-GST prevented the self-assembly of the protein into the previously observed nanoparticles. DLS measurements indicate that YopJ-HIS-TAT is soluble in saline buffers (Figure 6.22). However, YopJ-HIS-TAT was fou nd to exhibit low solubilities in water-based buffers.

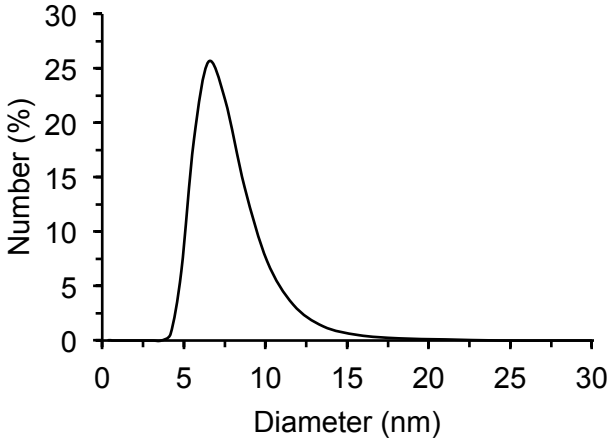

Figure 6.21. Size distribution of purified YopJ-HIS-Tat fusion proteins in saline buffer.

The monomeric state of YopJ-HIS-TAT allowed fine tuning of YopJ dosing to cells in soluble delivery and carrier+YopJ-HIS-TAT nanoparticles, similar to eGFP+AvrA nanoparticles presented in Chapter 5. Fabrication of YopJ nanoparticles using monomeric red fluorescent protein (mRFP) as a carrier protein was performed following the desolvation method used to produce eGFP+AvrA nanoparticles. Different amounts of YopJ-HIS-TAT were included in the particles and nanoparticle size was found to increase as YopJ content increases(Figure 6.23). Average particle diameter varied between 80-120 nm and increased as YopJ content increased from 0.7-2.2% of the total protein content.

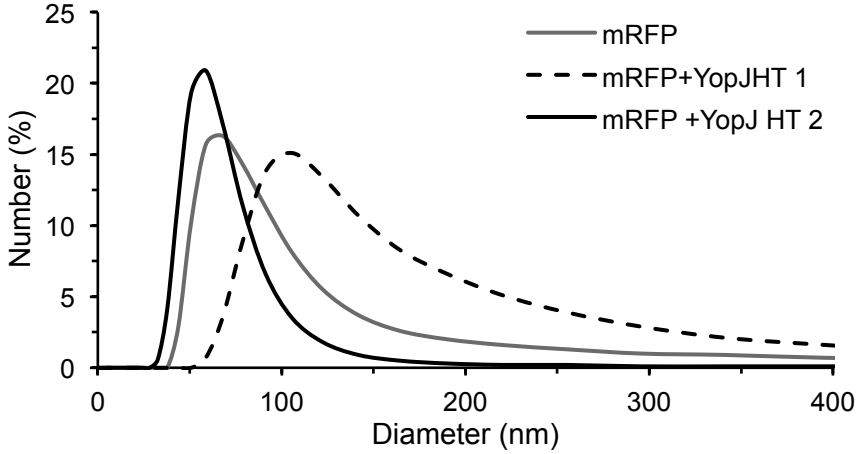

Figure 6.22. Effect of YopJ-HIS-TAT on mRFP+YopJ-HIS-TAT particle size distribution in saline buffer. Nanoparticles made of pure mRFP, mRFP and 2.2% YopJ-HIS-TAT (mRFP+YopJHT1), and mRFP with 0.7% YopJ-HIS-TAT (mRFP+YopJHT2).

Figure 6.24 shows the effect of 0.4 μM soluble YopJ-HIS-TAT on SKBR-3 and MDA-MB-231 cells after 72 hours of incubation. Not surprisingly, the cytotoxicity of soluble YopJ-HIS-TAT was found to be lower than that of YopJ-GST nanoparticles. This

is likely the result of higher internalization in particle form than soluble form, as established in Chapter 4. Therefore, the effect of mRFP+YopJ-HIS-TAT nanoparticles on SKBR-3 cell viability was measured. Particles with different YopJ-HIS-TAT contents were used to vary effector dosage. Due to the limited solubility of the modified effector fusion protein the maximum dose that was accomplished was 0.1 μM YopJ-HIS-TAT. Therefore, the cytotoxic of effect of mRFP+YopJ-HIS-TAT nanoparticles was 70% lower than that of YopJ-GST nanoparticles of the same dose?

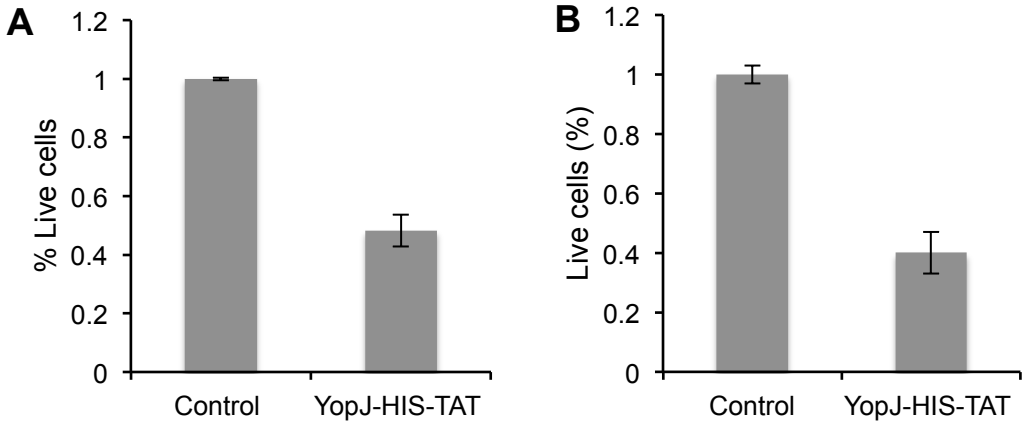

Figure 6.23. Effect of soluble YopJ-HIS-TAT on breast cancer cells. Cells were incubated for 72 hours with 0.4 μM YopJ-HIS-TAT or 2X PBS+5% dextrose (*A*) SKBR-3 cells and (*B*) MDA-MB-231. Error bars represent standard deviation, N=3.

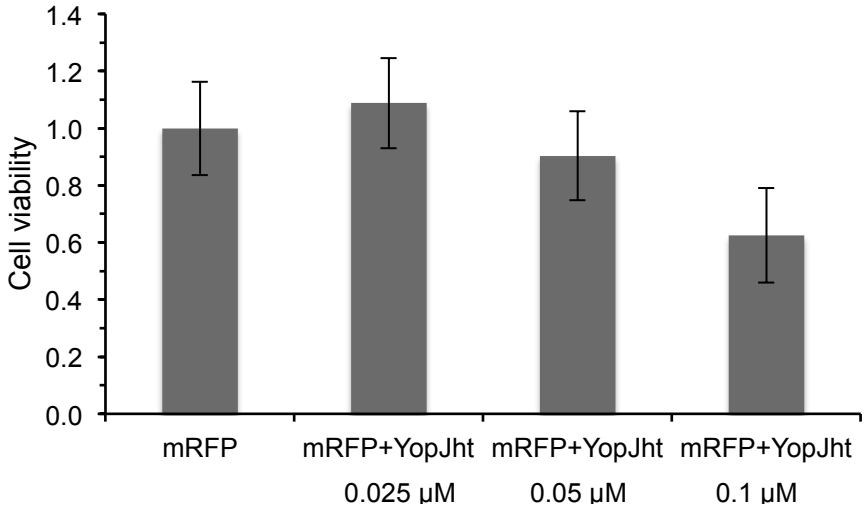

Figure 6.24. Effect of mRFP+YopJ-HIS-TAT nanoparticles on SKBR3 cell viability after 72h of incubation. Error bars represent standard deviation, N=3.

6-8 Summary

The results presented in this chapter illustrate the potential of protein nanoparticles and bacterial proteins as therapeutic agents for cancer. A second method for production of protein nanoparticles was presented, fusion of YopJ to GST for assembly into stable nanoparticles during protein production, removing the need for additional delivery vehicle synthesis steps and materials. The self-assembled nanoparticles induce cell death in multiple breast cancer cell lines with different molecular profiles. Despite variations among cell lines, YopJ performed as well as dox or better in inducing cell death. In addition, YopJ-GST nanoparticles decrease the migration and invasive nature of surviving cancer cells, due to down-regulation of the ERK 1/2 pathway, which has been correlated to metastatic pathology. Though downregulation of NF-κB was not established, the observed biochemical activity of YopJ on MAPK and the strong relationship of MAPK signaling with several of the hallmarks of cancer (including proliferation, chemotherapy resistance and metastasis)[42, 53], grant YopJ-GST nanoparticles a clear advantage over dox or similar chemotherapeutics.

Clinical trials have demonstrated that MAPK targeted therapeutics have more tolerable side effects than traditional chemotherapeutics. Common side effects of ERK 1/2 pathways inhibition are rash, edema and transient blurred vision[54]. Therefore, the observed cell-type cytotoxic selectivity and the mechanism of action of YopJ-GST nanoparticles, compared to dox, suggests that this type of therapy could potentially have less side effects than traditional chemotherapeutics. We expect YopJ-GST nanoparticles and other bacterial effector constructs to be potent cytotoxic agents that have molecular specificity, and control key signaling pathways associated with cancer pathogenesis.

6-9 References

1. Lancellotti, M., M. Brocchi, and W.D. da Silveira, *Bacteria-induced apoptosis: an approach to bacterial pathogenesis.* Braz J Morphol Sci, 2006. **23**(1): p. 75-86.

2. Mattoo, S., Y.M. Lee, and J.E. Dixon, *Interaction of bacterial effector proteins with host proteins.* Curr Opin Immunol, 2007. **19**: p. 392-401.

3. Shames, S.R., S.D. Auweter, and B.B. Finlay, *Co-evolution and exploitation of host cell signaling pathways by bacterial pathogens.* Int J Biochem Cell Biol, 2009. **41**: p. 380-389.

4. Yoshida, S. and C. Sasakawa, *Exploting host microtubule dynamics: a new aspect of bacterial invasion.* TRENDS Microb., 2003. **11**(3): p. 139-143.

5. Lubran, M.M., *Bacterial toxins.* Ann Clin Lab Sci, 1988. **18**(1): p. 58-71.

6. Grassme, H., V. Jendrossek, and E. Gulbins, *Molecular mechanisms of bacteria induced apoptosis.* Apoptosis, 2001. **6**: p. 441-445.

7. Hao, Y., et al., *Structural Requirements for Yersinia YopJ inhibition of MAP kinase pathways.* Plos One, 2008(1): p. 1-9.

8. Mukherjee, S., et al., *Yersinia YopJ acetylates and inhibits kinase activation by blocking phosphorylation.* Science, 2006. **312**: p. 1211-1214.

9. Ward, Y., et al., *Signal pathways which promote invasion and metastasis: critical and distinct contributions of extracellular signal-regulated kinase and Ral-specific guanine factor pathways.* Mol Cell Biol, 2001. **21**(17): p. 5958-5969.

10. Spinner, J.L., et al., *Neutrophils are resistant to Yersinia YopJ/P-induced apoptosis and are protected from ROS-mediated cell death by the type III secretion system.* Plos One, 2010. **5**(2): p. 1-9.

11. Monack, D.M., et al., *Yersinia signals macrophages to undergo apoptosis and YopJ is necessary for this cell death.* Proc Natl Acad Sci, 1997. **94**: p. 10385-10390.

12. Valster, A., et al., *Cell migrasion and invasion assays.* Methods, 2005. **337**: p. 208-215.

13. Weigelt, B., J.L. Peterse, and L.J. van 't Veer, *Breast cancer metastasis markers and models.* Nat Rev Cancer, 2005. **5**: p. 591-602.

14. Malam, Y., M. Loizidou, and A.M. Seifalian, *Liposomes and nanoparticles: nanosized vehicles for drug delivery in cancer.* Trends Pharm Sci, 2009. **30**(11): p. 592-599.

15. Carter, P.J., *Introduction to current and future protein therapeutics: A protein engineering perspective.* Exp Cell Res, 2011. **317**: p. 1261-1269.

16. Holcenberg, J.S., *Enzyme therapy: problems and solutions.* Ann. Rev. Biochem., 1982. **51**: p. 795-812.

17. Schlumberger, M.C., et al., *Real-time imaging of type III secretion: Salmonella SipA injection into host cells.* Proc Natl Acad Sci 2005. **102**(35): p. 12548-53.

18. Gu, F.X., et al., *Targeted nanoparticles for cancer therapy.* Nanotoday, 2007. **2**(3): p. 14-21.

19. Honary, S. and F. Zahir, *Effect of zeta potential on the properties of nano-drug delivery systems- A review (Part 2).* Trop. J. Pharm. Res. , 2013. **12**(2): p. 265-273.

20. Dellian, M., et al., *Vascular permeability in a human tumor xenograft: molecular charge dependence.* Br. J. Cancer, 2000. **82**: p. 1513-1518.

21. Jain, R.K. and T. Stylianopoulos, *Delivering nanomedicine to solid tumors.* Nat. Rev. Clin. Oncol., 2010. **7**(11): p. 653-664.

22. Wang, G., et al., *Preparation of BMP-2 containing bovine serum albumin (BSA) nanoparticles stabilized by polymer coating.* Pharm. Res., 2008. **25**(12): p. 2896-2909.

23. Fang, J., H. Nakamura, and H. Maeda, Adv. Drug Deliv. Rev., 2011. **63**(136-151).
24. Jain, R.K., *Transport of molecules, particles, and cell in solid tumors.* Annu. Rev. Biomed. Eng. , 1999. **1**: p. 241-263.
25. Hagendoorn, J., et al., *Onset of abnormal blood and lymphatic vessel function and interstitial hypertension in early stages of carcinogenesis.* Cancer Res., 2006. **66**(7): p. 3360-3364.
26. Ramanujan, S., et al., *Diffusion and convection in collagen gels: implications for transport in the tumor interstitium.* Biophys. J. , 2002. **83**(3): p. 1650-1660.
27. Pluen, A., et al., *Diffusion of macromoles in agarose gels: comparison of linear and globular configurations.* Biophys. J., 1999. **77**: p. 542-552.
28. Nugent, L.J. and R.K. Jain, *Extravascular diffusion in normal and neoplastic tissues.* Cancer Res., 1984. **44**: p. 238-244.
29. Weissleder, R., M. Nahrendorf, and M.J. Pittet, *Imaging macrophages with nanoparticles.* Nature Materials, 2014. **13**: p. 125-138.
30. Rejman, J., et al., *Size-dependent internalization of particles via the pathways of clathrin- and caveolae-mediated endocytosis.* Biochem. J., 2004. **377**: p. 159-169.
31. Mittal, R., et al., *The acetyltransferase activity of the bacterial toxin YopJ of Yersinia is activated by eukaryotic host cell inositol hexakisphophate.* J Biol Chem, 2010. **285**(26): p. 19927-19934.
32. Hanahan, D. and R.A. Weinberg, *Hallmarks of cancer: The next generation.* Cell, 2011. **144**: p. 646-674.
33. Bhavsar, A.P., J.A. Guttman, and B.B. Finlay, *Manipulation of host-cell pathways by bacterial pathogens.* Nature, 2007. **449**(827-834).
34. Bamrungzap, S., et al., *Nanotechnology in therapeutics.* Nanomedicine, 2012. **7**(8): p. 1253-1271.
35. Kaplan, W., et al., *Conformational stability of pGEX-expressed Schistosoma japonicum glutathione S-transferase: A detoxification enzyme and fusion-protein affinity tag.* Protein Sci, 1996. **6**: p. 399-406.
36. McTigue, M.A., D.R. Williams, and J.A. Tainer, *Crystal structures of a Schistosomal drug and vaccine target: glutathione S-transferase from Schitosoma japonica and its complex with the leading antischistosomal drug praziquantel.* J Mol Biol, 1995. **246**: p. 21-27.

37. Sorg, J.A., et al., *Rejection of impassable substrates by Yersinia type III secretion machines.* J Bacteriol, 2005. **187**(20): p. 7090-7102.

38. Holliday, D.L. and V. Speirs, *Choosing the right cell line for breast cancer research.* Breast Cancer Res, 2011. **13**(215-222).

39. Reddy, K.B., et al., *Mitogen-activated protein kinase (MAPK) regulates the expression of progelatinase B (MMP-9) in breast epithelial cells.* Int J Cancer, 1999. **82**(2): p. 268-273.

40. McCubrey, J.A., et al., *Targeting signal transduction pathways to eliminate chemotherapeutic drug resistance and cancer stem cells.* Adv Enzyme Regul, 2010. **50**(1): p. 285-307.

41. Mittal, R., S.Y. Peak-Chew, and H.T. McMahon, *Acetylation of MEK2 and IκB kinase (IKK) ctivation loop residues by YopJ inhibits signaling.* Proc Natl Acad Sci, 2006. **103**(49): p. 18574-18579.

42. Reddy, K.B., S.M. Nabha, and N. Atanaskova, *Role of MAP kinase in tumor progression and invasion.* Cancer Metastasis Rev, 2003. **22**: p. 395-403.

43. Irvin, W.J., H.B. Muss, and D.K. Mayer, *Symptom management in metastatic breast cancer.* Oncologist, 2011. **16**(9): p. 1203-1214.

44. Boldt, S., U.H. Werdle, and W. Kolch, *The role of MAPK pathways in the action of chemotherapeutic drugs.* Carcinogenesis, 2002. **23**(11): p. 1831-1838.

45. Zhou, J., et al., *The NFkB pathway and endocrine-resistant breast cancer*, in *Endocrine-Related Cancer*. 2005, Soc. Endocrinology. p. S37-S-46.

46. Bacus, S.S., et al., *Taxol-induced apoptosis depends on MAP kinase pathways (ERK and p38) and is independent of p53.* Oncogene, 2001. **20**(2): p. 147-155.

47. Weldon, C.B., et al., *Identification of mitogen-activated protein kinase kinase as a chemoresistant pathway in MCF-7 cells by using gene expression microarray.* Surgery, 2002. **132**(2): p. 293-301.

48. Herrera Estrada, L., S. Chu, and J.A. Champion, *Protein nanoparticles for intracellular delivery of therapeutic enzymes.* J Pharm Sci, 2014. **103**: p. 1863-1871.

49. Zhang, X.D., et al., *Activation of ERK1/2 protects melanoma cells from TRAIL-induced apoptosis by inhibiting Smac/DIABLO release from mitochondria.* Oncogene, 2003. **22**: p. 2869-2881.

50. El-Sayed, A., et al., *Octaarginine-and octalysine-modified nanoparticles have different model of endosomal escape.* J. Biol. Chem., 2008. **283**(34): p. 23450-23461.

51. Foerg, C., et al., *Deconding the entry of two novel cell-penetrating peptides in HeLa cells: Lipid Raft-mediated endocytosis and endosomal escape.* . Biochemistry, 2005. **44**: p. 72-81.

52. Lo, S.L. and S. Wang, *An endosomolytic Tat peptide produced by incorporation of histidine and cysteine residues as a nonviral vector for DNA transfection.* Biomaterials, 2008. **29**(15): p. 2408-14.

53. Chang, L. and M. Karin, *Mammalian MAP kinase signalling cascades.* Nature, 2001. **410**: p. 37-40.

54. Santarpia, L., S.L. Lippman, and A.K. El-Naggar, *Targeting the Mitogen-Activated Protein Kinase RAS-RAF signaling pathway in cancer therapy.* Expert Opin Ther Targets, 2012. **16**(1): p. 103-119.

CHAPTER 7: CONCLUSIONS AND OUTLOOK

As protein therapeutics have increased dramatically in number and frequency of use, it has become essential to improve current techniques and explore the development of new techniques for effective delivery. The work contained in this thesis focuses on the creation of protein-based vehicles for intracellular delivery of therapeutic proteins and enzymes. Various aspects of engineering and production of protein nanoparticles via covalent bonds or strong protein-protein interactions are explored.

This work presents and establishes two distinct particle production methods: desolvation and self-assembly. Nanoparticles produced using the desolvation method require stabilization with environment-responsive cross-linkers for release of soluble active protein inside the cells. The desolvation method is optimized using β-galactosidase as a model enzyme and then applied to a bacterial effector protein, AvrA, a potential therapeutic enzyme for inflammatory bowel disease. Particles produced by self-assembly with GST are held together by strong hydrophobic interactions and disulfide bonds. The self-assembly method was applied to YopJ, another bacterial effector protein and potential therapeutic candidate for breast cancer.

Both methods are optimized to control nanoparticle properties and accomplish intracellular delivery and release of active therapeutic proteins or enzymes. The effectiveness of therapeutic protein nanoparticles is evaluated in two different disease models. The key findings in this work are:

1. Fabrication of protein enzyme delivery vehicles via the desolvation method requires the use of a carrier protein. Particles produced directly from enzymes exhibit high loss of enzymatic activity due to desolvation and cross-linking. Incorporation of a carrier protein decreases loss of enzymatic activity. Highly

soluble and stable proteins such as eGFP, mRFP and BSA are effective carrier proteins. However, fluorescent proteins present the added advantage of easy particle detection and tracking.

2. The size of protein nanoparticles produced by the desolvation method can be tuned by adjusting a variety of parameters. Concentration of imidazole decreases particle size of 6xHis tag proteins. Highly reactive cross-linkers like GTA produce larger particles than less reactive cross-linkers like DTSSP. Cross-linking time also affects particle size, shorter cross-linking times decrease particle diameter. The presence of salts in initial protein solutions is necessary for particle formation via the desolvation method at low protein concentrations.

3. Protein particles stabilized with a reducing environment-responsive cross-linker, DTSSP, release their therapeutic protein/enzyme cargo inside of cells.

4. Fusion of GST to YopJ was necessary for recombinant protein expression and leads to self-assembly of stable nanoparticles during the production process. This self-assembly removes the need for additional delivery vehicle synthesis steps. Self-assembled YopJ-GST nanoparticles are held together by disulfide bonds and strong protein-protein interactions.

5. Bacterial protein effector nanoparticles control key intracellular pathways and retain the biochemical activity and effect of the original effector protein.

6. Bacterial protein effector nanoparticles are promising and highly innovative alternatives to current therapies. eGFP+AvrA nanoparticles successfully

delivered AvrA to intestinal cells, disassembled inside cells, downregulated NF-κB and MAPK signaling and reduced inflammation in IBD models. YopJ-GST nanoparticles effectively delivered YopJ to cancer cells and performed as well as a common therapeutic agent, dox, or better for the treatment of breast cancer. YopJ-GST nanoparticles decreased metastatic markers and were only cytotoxic to breast cancer cells.

These findings illustrate the feasibility of producing and using protein nanoparticles for intracellular delivery of therapeutic enzymes. This work helps bridge the divide between the well-established potential of protein/enzyme therapeutics and their effective delivery to intracellular spaces. The two particle production methods presented in this work are simple, fast and cost-effective. Most importantly, these methods are versatile and can be adapted for particle production with many therapeutic proteins and enzymes.

Evidence presented in this thesis points to the importance of using delivery vehicles to increase and enhance intracellular protein or enzyme delivery. Designed and produced therapeutic protein nanoparticles shown in this work are capable of effectively penetrating mucosal layers, tissue and cell membranes *in vitro* and *in vivo*. In addition, these particles deliver more active protein to multiple types of cells than soluble protein formulations. These results are very promising for therapeutic protein and enzyme delivery and provide a new application for protein nanoparticles as drug carriers.

This thesis also explores the potential of bacterial effector proteins for therapeutic purposes. The bacterial effectors evaluated in this work are easily incorporated into protein nanoparticles and are capable of modulating intracellular pathways to control the fate of target cells. YopJ and AvrA are shown to induce cell death and decrease inflammatory signals, respectively, and thus are potential therapeutic agents for breast cancer and IBD.

These findings give future researchers a platform to more deeply explore applications of bacterial effector proteins. This cutting-edge translational approach has the potential to add a new class of biologic drugs to treatment strategies against a wide variety of diseases Additionally, the existing knowledge of the molecular basis of different diseases can be paired with known effector mechanisms and target pathways, to find and formulate new potential therapies.

This research provides a solid foundation for future work centered both on creating bioactive protein-based delivery vehicles and developing new therapeutic alternatives based on bacterial proteins. Potential thrusts for such work are as follows:

1. Particle internalization mechanism.

   Results presented in this thesis suggests that protein nanoparticles are internalized via energy dependent mechanisms. Data on the precise uptake mechanism would provide information on the conditions and environment the particle will be exposed to. This information coupled with knowledge on specific receptors that are overexpressed on the surface of targets cells can be useful to fine tune the particle design to achieve higher internalization rates. By decorating the surface of the particles with specific ligands the rate and path of internalization can be controlled.

2. Subcellular particle localization.

   Data gathered on the localization of protein/enzyme nanoparticles inside the cells would be helpful in establishing the need for additional engineering of the particle. If particles are trapped in endosomes and are routed to lysosomes for degradation, for example, cell penetrating peptides can increase cellular internalization and promote endosomal escape.

3. Particle disassembly characterization.

The disassembly of DTSSP cross-linked particles has been proven but the process and kinetics have not been elucidated. The location within the cell in which particle disassembly occurs, how long the process takes and the extent of particle disassembly remains unknown. The seemingly small amount of YopJ-GST nanoparticles internalized within the first 24 hours shows potent induction of breast cancer cell death. Information on disassembly kinetics would provide information on the amount and state (soluble/particle) of effector proteins within the cell required for biochemical activity.

4. Engineering of protein particles for *in vivo* stability.

The results of stability studies on protein nanoparticles exposed to body fluids and simulated body fluids indicates that these vehicles do not protect their cargo from damage in harsh environments. Engineering the protein particle surface with polymers, peptides or further cross-linking could improve enzyme stability. In addition, YopJ-GST nanoparticles have not been tested in blood serum and little is known about the stability of YopJ in biological fluids.

5. *In vivo* studies of breast cancer treatment.

While the treatment of breast cancer *in vitro* has been proven to be highly successful with YopJ-GST nanoparticles, it remains unclear if these particles will be able to specifically induce cell death of malignant cells, decrease cell migration and reduce side effects *in vivo*. Animal models would provide information on immune response to YopJ-GST nanoparticles and efficacy of YopJ for breast cancer treatment.

6. Application to other diseases

Novel potent molecularly targeted therapies can be formulated by pairing bacterial protein effectors to diseases where their biochemical function can restore cellular functions. For example, neurodegenerative diseases such as Parkinson's and Alzheimer's disease, lung cancer, colorectal cancer and melanoma progression have been linked to de-regulated MAPK activity. In particular, in Alzheimer's and Parkinson's disease the p38 MAPK cascade has been linked to neuronal cell death. OspF, from *Shigella*, irreversibly inactivates this particular pathway and thus, could be studied as a potential therapeutic agent for neurodegenerative disorders. Other potential pairings include NleE from EPEC and OspZ from *Shigella* that block NF-κB activation and decrease aberrant IL-8 production and hence, could be potentially used to treat chronic inflammation such as that observed in rheumatoid arthritis and psoriasis.

In addition, protein particles can be modified to incorporate these or other potential therapeutic proteins and engineered to fit requirements and needs for the treatment of other diseases. Additionally, combination therapies could be formulated in these protein nanoparticles. For example, particles could be formulated to include two or more enzymes with different functions or a mix of enzymes and small molecule drugs in each formulation. These strategies would allow the particles to potentially be multifunctional and could help increase response time or improve outcome.

APPENDIX A: BACTERIAL EFFECTOR SEQUENCES

The DNA sequences of bacterial effector proteins, YopJ and AvrA, used in this work are presented here:

YopJ

ATGATCGGACCAATACCACAAATAAATATCTCCGGTGGCTTATCAGAAAAAGAGACC
AGTTCTTTAATCAGTAATGAAGAGCTTAAAAATATCATAACACAGTTGGAAACTGAT
ATATCGGATGGATCCTGGTTCCATAAAAATTATTCACGTATGGATGTAGAAGTCATG
CCCGCATTGGTAATCCAGGCGAACAATAAATATCCGGAAATGAATCTTAATCTTGTT
ACATCTCCATTGGACCTTTCAATAGAAATAAAAAACGTCATAGAAAATGGAGTTAGA
TCTTCCCGCTTCATAATTAACATGGGGGAAGGTGGAATACATTTCAGTGTAATTGATT
ACAAACATATAAATGGGAAAACATCTCTGATATTGTTTGAACCAGCAAACTTTAACA
GTATGGGGCCAGCGATGCTGGCAATAAGGACAAAAACGGCTATTGAACGTTATCAA
TTACCTGATTGCCATTTCTCCATGGTGGAAATGGATATTCAGCGAAGCTCATCTGAAT
GTGGTATTTTTAGTTTTGCACTGGCAAAAAAACTTTACATCGAGAGAGATAGCCTGTT
GAAAATACATGAAGATAATATAAAAGGTATATTAAGTGATGGTGAAAATCCTTTACC
CCACGATAAGTTGGACCCGTATCTCCCGGTAACTTTTTACAAACATACTCAAGGTAA
AAAACGTCTTAATGAATATTTAAATACTAACCCGCAGGGAGTTGGTACTGTTGTTAA
CAAAAAAAATGAAACCATCGTTAATAGATTTGATAACAATAAATCCATTGTAGATGG
AAAGGAATTATCAGTTTCGGTACATAAAAAGAGAATAGCTGAATATAAAACACTTCT
CAAAGTA

AvrA

ATGATATTTTCGGTGCAGGAGCTATCATGTGGAGGGAAAAGTATGCTAAGTCCTACG

ACTCGTAATATGGGGGCGAGTTTATCGCCTCAGCCTGACGTCAGCGGGGAGCTAAAC

ACCGAAGCATTGACCTGTATTGTTGAGCGTCTGGAAAGTGAAATTATAGATGGCAGC

TGGATTCATATCAGTTACGAGGAAACCGATCTCGAAATGATGCCTTTTCTTGTTGCAC

AGGCCAATAAGAAGTATCCAGAGTTAAATCTTAAATTTGTTATGTCAGTCCATGAGC

TTGTTTCCTCTATAAAGGAGACCAGAATGGAAGGCGTTGAATCTGCCCGATTTCTCGT

AAATATGGGAAGTTCAGGTATCCATATTTCAGTCGTCGATTTTAGAGTTATGGACGG

AAAGACATCGGTGATTTTGTTCGAACCAGCAGCGTGTAGCGCTTTTGGACCTGCACT

GGCGTTGAGGACCAAAGCAGCTCTTGAACGTGAACAACTGCCTGATTGTTATTTTGC

TATGGTCGAGCTGGACATTCAACGAAGCTCTTCTGAATGCGGTATTTTTAGCCTGGCG

CTCGCCAAAAAACTTCAGCTTGAATTTATGAACTTAGTAAAAATTCATGAAGATAAT

ATTTGTGAACGTCTGTGTGGTGAAGAACCTTTTCTCCCGTCCGATAAAGCAGACCGCT

ATCTGCCGGTGAGTTTTTACAAACATACTCAAGGCGCACAACGATTAAATGAATATG

TGGAGGCCAATCCGGCGGCGGGAAGCAGTATAGTAAACAAAAAGAATGAAACGCTT

TATGAGCGATTCGATAACAATGCCGTTATGCTAAACGATAAAAAACTCTCTATATCC

GCTCATAAAAAAAGGATAGCTGAATATAAGTCTTTACTTAAACCGTAA